PATTERNS IN TELEOST PHOTORECEPTOR ORGANIZATION:

A CHARACTERIZATION

OF BASAL BODY POSITIONING IN ZEBRAFISH PHOTORECEPTORS

AND VARIATIONS IN SWORDTAIL PHOTORECEPTOR MOSAICS

A Dissertation

by

MICHELLE BRITTANY RAMSEY

Submitted to the Office of Graduate and Professional Studies of
Texas A&M University
in partial fulfillment of the requirements for the degree of

DOCTOR OF PHILOSOPHY

Chair of Committee,	Gil G. Rosenthal
Committee Members,	Brian D. Perkins
	Hubert O. Amrein
	Michael S. Smotherman
Head of Department,	Thomas D. McKnight

May 2014

Major Subject: Biology

ABSTRACT

Vertebrate vision is enabled by light-sensitive photoreceptors arranged in a plane in the retina. This study investigates two aspects of this arrangement: 1) positioning of basal bodies within photoreceptors, and 2) positioning of photoreceptors themselves. First, the planar cell polarity of basal bodies, and therefore cilia, is often critical for proper cilia function and is controlled by the planar cell polarity (PCP) pathway. Cilia planar positioning in vertebrate photoreceptors, however, has not been characterized. Because zebrafish photoreceptors form an organized, well-characterized mosaic, they are an ideal system to address photoreceptor basal body positioning. Second, swordtail fish are frequently studied to investigate visually-mediated social behaviors such as mate choice and how these influence evolution. However, less is known about the morphology of their photoreceptor mosaic and how this mosaic influences behavior. Therefore, characterization of the swordtail photoreceptor mosaic is an important step in understanding this relationship between physiology and behavior. In this study, immunohistology is used to characterize cryosectioned flatmounted retinas from zebrafish and swordtails with various genetic, behavioral, and environmental backgrounds.

The results of this study reveal that in adult zebrafish retinas, the basal bodies of red-, green-, and blue-sensitive cone photoreceptors localize asymmetrically on the cell edge nearest the optic nerve. In contrast, no patterning is in the basal bodies of ultraviolet-sensitive cones, of rod photoreceptors, or of larval cones. Both rod loss and

UV-light addition do not affect cone basal body patterning. Darkness during development leads to bimodality of basal bodies. These results suggest that, after the transition to the adult mosaic, a cellular mechanism involving cell-cell contact, consistent with the PCP pathway, regulates photoreceptor basal body positioning.

The results of this study also reveal that the swordtails *Xiphophorus malinche*, *Xiphophorus birchmanni*, and their hybrids exhibit an organized square mosaic, although some variations in this pattern exist, including between males and females. As square mosaics have been correlated with sensitivity to changes in light polarization, this warrants future studies in swordtail polarization vision, which may play an important role in visually-mediated behavior. Also, changes in the photoreceptor mosaic might have explanatory power for changes in visually-mediated behavior.

ACKNOWLEDGEMENTS

I am very grateful for the generous support I have received from Gil Rosenthal and from Brian Perkins during my time at Texas A&M. They have each played an important role in my intellectual development. I am thankful for all the opportunities they have given me and everything I have learned from them. I am also thankful for all the other faculty members at A&M, especially for Hubert Amrein, Mike Smotherman, Bruce Riley, Deb Bell-Pedersen, and Arne Lekven, who have guided me at various stages of my dissertation research. I sincerely appreciate all the assistance I have received from lab members, other graduate students, undergraduate students, and staff at Texas A&M. I am thankful for all I have learned from my peers and from my students.

For Chapter II, I thank Brian Perkins for his valuable contributions to study design, to data analysis, and to drafting and revising the manuscript. I thank my committee and anonymous reviewers for their helpful comments. I am very grateful to James Fadool and his group for assistance with observing the photoreceptor mosaic. I also thank James Fadool, Sue Brockerhoff, David Hyde, Ann Morris, and Brian Link for the gifts of animals and reagents. This research was supported by NIH Grant EY017037 to Brian Perkins.

For Chapter III, I thank Gil Rosenthal and Brian Perkins for their valuable contributions to study design and analysis, and I thank them and the rest of my committee for their helpful comments for this chapter. I am grateful to Carmen Montaña, Kirk Winemiller, and Kevin Conway for their assistance catching and

identifying red shiners. This research was supported by NSF Grant IOS-0923825 to Gil Rosenthal and NIH Grant EY017037 to Brian Perkins.

For Chapter IV, I thank Gil Rosenthal for his valuable contributions to study design and analysis, and I thank him and the rest of my committee for their helpful comments for this chapter. I thank Rongfeng Cui and Michael Stanley for their work on the behavioral trials. I thank Pablo Declos for assistance with the statistical analysis. I am grateful to Pablo Delclos, Gastón Jofre, Dan Powell, Mattie Squire, and undergraduates from the Rosenthal lab for fish collection and fish care. I thank Brian Perkins for histology supplies and reagents, and I thank Bruce Riley for cryostat use. This research was supported by NSF Grant IOS-0923825 to Gil Rosenthal.

My accomplishments at Texas A&M would have been impossible without the previous investments others have made in my life for which I will always be grateful. My past teachers and professors have all contributed in a variety of ways to my intellectual growth. Finally, and most importantly, the unwavering support I have received from my husband, parents, family, and friends has been an irreplaceable encouragement to me.

"If I have seen further it is by standing on the shoulders of Giants."

Sir Isaac Newton (1676)

NOMENCLATURE

4C12	antibody that labels zebrafish rod photoreceptors
AOSLO	Adaptive Optics Scanning Laser Ophthalmoscopy
CFP	cyan fluorescent protein
DAPI	nuclear stain 4,6-diamidino-2-phenlindole dihydrochloride
dfp	days post fertilization
DMSO	dimethyl sulfoxide
ERG	electroretinogram
GFP	green fluorescence protein
MSP	microspectrophotometry
OMR	optomotor response
ON	overnight or (in figures) optic nerve
ONL	outer nuclear layer
PBS	phosphate buffered solution
PBSTD	0.1% TWEEN 20 and 0.1% DMSO in PBS
PCP	planar cell polarity
PFA	paraformaldehyde
red shiner	*Cyprinella lutrensis*
RPE	retinal pigment epithelium
RT	room temperature
RT-PCR	reverse transcription polymerase chain reaction

s.d.	standard deviation
swordtail	fish within the genus *Xiphophorus*
TFM	tissue freezing medium
UV	ultraviolet
X. birchmanni	*Xiphophorus birchmanni*
X. malinche	*Xiphophorus malinche*
XOPS-GFP	transgenic zebrafish line *Tg(XlRho:EGFP)*^{fl1}
XOPS-mCFP	transgenic zebrafish line *Tg(XlRho:gap43-CFP)*^{q13}
zebrafish	*Danio rerio*
Zpr-1	antibody that labels zebrafish red-/green-sensitive double cones

TABLE OF CONTENTS

Page

Page

LIST OF FIGURES

Page

Page

Page

LIST OF TABLES

Page

CHAPTER I

INTRODUCTION

The field of vision research is widely applicable to a variety of scientific questions. Developmental biologists can study the ontogeny of the eye, cell biologists can study the attributes and interactions of specialized cells in eyes, neurobiologists can study how the brain interprets signals from the retina, evolutionary biologists can study the evolution of the eye, behavioral biologists can study visually-mediated behaviors, doctors can study eye disorders and diseases, and physicists can study the optical processes behind vision. This study aims to investigate the organization of photoreceptors while integrating several of these different scientific approaches.

Photoreceptors

Vertebrate photoreceptors are elongated cells that include a nucleus, an inner segment, and an outer segment (Figure 1). Primary cilia, which are generally nonmotile and help cells sense signals from other cells and from the environment, are essential components of photoreceptors because the light-sensitive outer segment of each vertebrate photoreceptor is a modified primary cilium (for review, see Ramamurthy and Cayouette 2009). The outer segment is connected to the inner segment via a connecting cilium that is anchored to the inner segment via a basal body. This connecting cilium is the passageway through which cellular components important to the development,

function, and maintenance of the outer segment must pass. The inner segment is where proteins are translated and energy is synthesized while the outer segment is where the phototransduction cascade occurs.

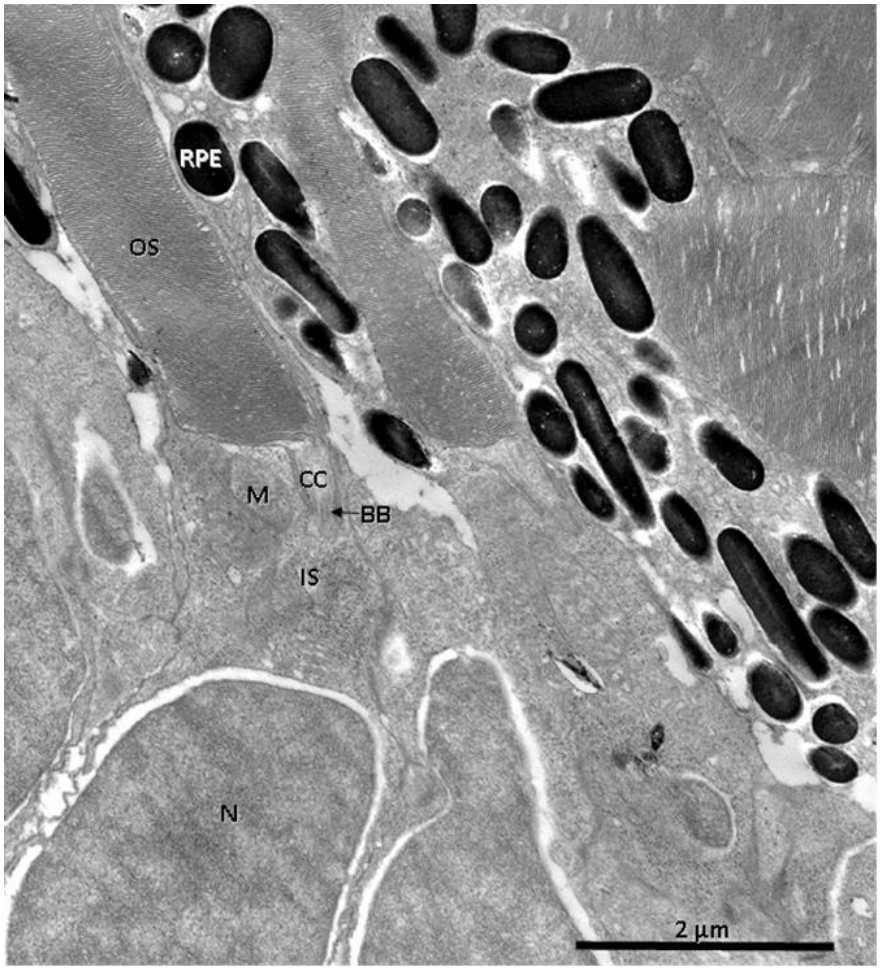

Figure 1. Photoreceptor morphology.
Two photoreceptors can be seen in this electron micrograph. Basal body (BB with arrow); connecting cilium (CC); inner segment (IS); mitochondrium (M); outer segment (OS); nucleus (N); retinal pigment epithelium layer (RPE). x 10,000.

Photoreceptors are neurons that enable vision. The two types of vertebrate photoreceptors are rods and cones. Rods are sensitive to individual photons of light, enabling vision in low light conditions. Cones, though less sensitive, come in different subtypes that differ morphologically and in the type of opsin they produce, which is the protein that absorbs light and triggers the phototransduction cascade. Because cone opsins absorb light at different wavelengths, multiple cone subtypes expressing different opsins enable color vision. Zebrafish have four cone subtypes that are called ultraviolet (UV)-, blue-, green-, and red-sensitive cones (or simply UV, blue, green, and red cones); the UV- and blue-sensitive cones are short single and long single cones, respectively, and the red- and green-sensitive cones are paired together double cones that wind around each other (Raymond, Barthel et al. 1993). These subtypes are similar in humans, who have three cone subtypes called red, green, and blue. In both zebrafish and humans, the names of these cones do not directly match their absorbance maxima; in zebrafish, for example, the cones called UV-, blue-, green-, or red-sensitive have absorbances at 362 nm, 407 nm, 473 nm, and 564 nm, respectively (Robinson, Schmitt et al. 1993; Cameron 2002), which are closer to the colors UV, violet, blue, and green-yellow. Therefore, in humans the designation of long wavelength, middle wavelength, and short wavelength are sometimes used instead of red, green, and blue. However, as the traditionally designated colors for each of these cones are also within their absorption spectra, and as zebrafish have two short wavelength cones (UV and blue) that would make the latter terminology less clear, in this work the terms UV-, blue-, green-, and red-sensitive cones will be used.

Distinct from the ciliary photoreceptors of vertebrates, many invertebrates, including *Drosophila*, have rhabdomeric photoreceptors. In rhabdomeric photoreceptors, rather than light sensitivity occurring in a modified primary cilium, it occurs in specialized microvilli (for review, see Rister and Desplan 2011). Although invertebrate rhabdomeric photoreceptors are morphologically different from vertebrate ciliary photoreceptors, they have some similarities . For example, many similarities exist between the processes and proteins involved in vertebrate and invertebrate photoreceptor development and phototransduction. Additionally, different photoreceptor types which express different opsins enable color vision for both vertebrates and invertebrates. However, in the *Drosophila* eye, a well-studied invertebrate model system, all of the opsins expressed are more similar to rod opsins (rhodopsins) in vertebrates than cone opsins. *Drosophila* photoreceptors nonetheless come in two types that are functionally similar to rods and cones, having six photoreceptor types (R1-6) that express the same opsin and that are highly sensitive to low levels of light like vertebrate rods, and having two photoreceptor types (R7-8) that are used at higher light levels and are involved in color discrimination. Unlike vertebrate cones, however, R7 and R8 vary in spectral sensitivity based on which opsins are expressed, though R7 tends to be sensitive to UV light while R8 tends to be sensitive to relatively longer wavelengths than R7.

Planar cell polarity

The term planar cell polarity (or PCP) describes the positioning of structures within cells and the patterned repetition of this positioning within a field of cells in the same plane (for review, see Wallingford 2010). This pattern often involves the positioning of cilia, and it can influence both their orientation and localization. For example, motile cilia can be oriented in the same angular position to enable them to all beat in the same direction, as in the *Xenopus laevis* embryonic epidermis (Park, Mitchell et al. 2008). Rotational polarity refers to when all of the motile cilia within one cell are oriented similarly, whereas tissue-level polarity refers to when multiple cells within a field of cells exhibit rotational polarity in the same direction (Wallingford 2010). Alternatively, a single primary cilium or multiple motile cilia can be localized on one side of a cell. This localization can be repeated within a plane of cells to create what is called translational symmetry within the tissue, as in mouse inner ear hair cells (Montcouquiol, Rachel et al. 2003; Wallingford 2010)(see Figure 2).

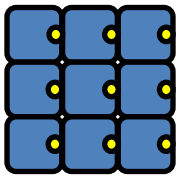

Figure 2. An illustration of translational symmetry of primary cilia.
A field of nine generic cells (blue) and the locations of their cilia (yellow) are shown.

The ependymal cells in mice, which are multiciliated epithelial glial cells in the brain and spinal cord, possess both rotational and translational polarity (Mirzadeh, Han et al. 2010). The current study focuseson the localization of the primary cilium within each photoreceptor and investigates the possibility of translational polarization of these cilia.

While recent work has developed our understanding of the signals that control PCP, questions still remain regarding the initial establishment of PCP and the different roles it plays in different tissues. The genetic pathway that has been shown to control PCP in many cell types is a non-canonical Wnt pathway called the planar cell polarity (PCP) pathway (for review, see Vladar, Antic et al. 2009; Singh and Mlodzik 2012). As described in these reviews, the initial characterization of this pathway involved the study of *Drosophila* structures such as the translationally symmetrical wing bristles and the more complex patterning in the eye's ommatidia. The core PCP proteins that were discovered are Frizzled (Fz), Flamingo (Fmi), Van Gogh (Vang), Prickle (Pk), Dishevelled (Dsh), and Diego (Dgo), with their respective vertebrate homologs Fz1/2/3/6/7, Celsr1/2/3, Vangl1/2, Pk1/2, Dsh1/2/3, and Inversin (Inv). Fz and Dsh are also involved in the canonical Wnt pathway. The polarization of the core PCP proteins themselves is thought to establish a polarity within the cell that allows the positioning of cellular structures (Figure 3). Vang, a transmembrane protein, recruits the cytoplasmic Pk to form a complex; and Fz, another transmembrane protein, recruits the cytoplasmic Dsh and Dgo form a complex. These complexes are mutually inhibitory within the same cell, which establishes their polarized localizations. The polarization of these complexes varies; for example, these two complexes localize to opposite sides of the cells

themselves in inner ear hair cells while they localize to opposite sides of each motile cilia in multiciliated epidermal cells. Fmi, a transmembrane protein, localizes to both sides of the cells and interacts with Fmi in neighboring cells. Downstream effectors include Inturned (In) and Fuzzy (Fy). Four-jointed (Fj), Fat (Ft), and Dachsous (Ds) appear to be involved in upstream processes that establish the initial polarization. Furthermore, Fj, Ft, and Ds may sometimes act as an alternate, parallel PCP pathway.

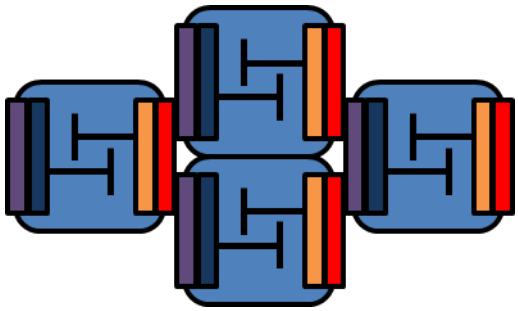

Figure 3. Illustration of one example of PCP protein localization.
Generic cells (light blue) showing transmembrane localization of Fz (red) and Vang (purple) and cytoplasmic localization of the recruited Dsh and Dgo (orange) and Pk (dark blue). Adapted from the protein localization in the *Drosophila* wing as illustrated and reviewed by Vladar, Antic et al. (2009) and Singh and Mlodzik (2012).

Evidence suggests that the Pk/Vang complex and the Fz/Dsh/Dgo complex in opposing cells directly interact at the neighboring cell membranes to allow propagation of the signal and of the planar polarity. For example, Fz and Vang exhibit opposite non-cell autonomous effects on PCP patterning in *Drosophila* wing bristles (Vinson and Adler 1987; Taylor, Abramova et al. 1998). Also, Fz is capable of pulling down Vang

in a pulldown assay (Wu and Mlodzik 2008). Furthermore, Fmi is involved in this recruiting of Fz and Vang in neighboring cells (Chen, Antic et al. 2008).

Although PCP has not been previously established in vertebrate photoreceptors, it is well established in the *Drosophila* photoreceptors (for review, see Jenny 2010). However, the unique arrangement and morphology of these rhabdomeric photoreceptors leads to these photoreceptors being a unique example of PCP, both in the protein localization and in the pattern created by these cells. In each *Drosophila* eye, hundreds of units called ommatidia contain eight photoreceptors each (R1-8). In each ommatidium, the arrangement of each of these eight photoreceptors the same, creating a striking pattern of ommatidia that is mirrored between dorsal and ventral regions of the eye. The morphological similarities between vertebrate ciliary photoreceptors and mouse inner ear hair cells, both in utilizing a primary cilia for sensory function and in the general arrangement of these fields of cells, suggest that PCP in vertebrate photoreceptors, if present, might more closely represent PCP in vertebrate inner ears than invertebrate eyes, Nonetheless, the similarities between vertebrate and invertebrate vision and the conservation of PCP pathway within many cell types support the potential for PCP to exist in vertebrate photoreceptors.

Planar cell polarity defects and ciliopathies

Disruption of PCP leads to various phenotypes. The loss of Vangl2 in the mouse inner ear leads to a loss of translational polarity in the kinocilia and, consequentially, in the stereociliary bundles of these single-ciliated cells (Montcouquiol, Rachel et al.

2003). While neural tube defects prevent the analysis of hearing in these embryonic lethal mutants (for review, see Petit and Richardson 2009), other studies have linked stereociliary bundle misorientation to hearing loss (Ross, May-Simera et al. 2005; Li, Zhang et al. 2008). The loss of Vangl2 in the zebrafish floor plate (Borovina, Superina et al. 2010) and the loss of Dvl in the mouse node cilia (Hashimoto, Shinohara et al. 2010) also lead to a loss of translational polarity in these single-ciliated cells. In the multi-ciliated *Xenopus laevis* epidermis, loss of Dvl leads to the failure of basal bodies to dock apically and the failure of ciliogenesis, and the expression of a dominant-negative Dsh allows ciliogenesis but leads to misorientation of these motile cilia and consequentially disrupted directional fluid flow (Park, Mitchell et al. 2008). Other phenotypes of PCP mutants include left-right asymmetry defects (Borovina, Superina et al. 2010), renal cysts (Simons, Gloy et al. 2005), and convergent extension defects (Park and Moon 2002; Park, Gray et al. 2005; Wang, Hamblet et al. 2006).

Ciliopathies, which are diseases caused by dysfunctional cilia, have diverse symptoms due to the prevalence of cilia throughout the body. Photoreceptor degeneration is a symptom frequently found alongside renal disease, neural defects, obesity, and/or polydactyly in genetic disorders such as Joubert syndrome (JBTS), Meckel-Gruber syndrome (MKS), Jeune syndrome (Asphyxiating thoracic dystrophy, ATD), Senior–Løken syndrome (SLSN), Alström syndrome (ALMS), and Bardet-Biedl syndrome (BBS) (for review, see Sharma, Berbari et al. 2008; Bergmann 2012). Most ciliopathies are considered rare diseases, for example both BBS and JBTS occur in approximately 1 in 100,000 births (Beales, Warner et al. 1997; Kroes, van Zon et al.

2008). However, one form of polycystic kidney disease (PKD) is estimated to occur in 1 in 1,000 births (Sharma, Berbari et al. 2008). Understanding how cilia function will lead to a more complete understanding of the causes of these diseases.

PCP mutant phenotypes found in vertebrate animal models are also found in some human ciliopathies. For example, ALMS includes the symptoms retinitis pigmentosa (retinal degeneration), hearing loss, and renal disease; and renal disease is a PCP mutant phenotype in mice (Jagger, Collin et al. 2011). Furthermore, mice lacking the gene *ALMS1*, which, when mutated, has been shown to cause ALMS in humans, show misoriented stereociliary bundles in the inner ear outer hair cells, similar to this PCP phenotype (Jagger, Collin et al. 2011). In a second example, BBS, a syndrome caused by mutations in *BBS1-BBS8*, includes the symptoms of photoreceptor degeneration, obesity, polydactyly, and, like ALMS, renal disease (Ross, May-Simera et al. 2005). Also, *Bbs1*, *Bbs4*, and *Bbs6* mutant mice have misoriented or abnormal stereociliary bundles; *Bbs4* mutant embryos have exencephaly and open eyelids; and *Bbs6* mutants have hearing loss(Ross, May-Simera et al. 2005). Because of the hearing loss discovered in *Bbs6* mice mutants, BBS patients were evaluated, and subclinical hearing loss in these patients was found (Ross, May-Simera et al. 2005). Although the shared characteristics between animals with PCP mutations and humans with ciliopathies do not prove a direct link between failure of the PCP pathway and these diseases, they do support the importance of further study into this possibility.

In addition to some PCP mutant phenotypes matching symptoms of ciliopathies, genes known to be involved in PCP have been shown to contribute to ciliopathies. For

example, nephronopthisis (NPHP), a form of kidney disease, has been shown to be caused by a mutation in *INVERSIN*, a core PCP gene (Otto, Schermer et al. 2003). This study revealed that symptoms in these patients include kidney cysts and can include situs inversus, which are common PCP phenotypes and were phenocopied in this study in zebrafish inversin morphants. A later study confirmed the mutation of *INVERSIN* in a patient with Senior–Løken syndrome (SLSN), which is a disease that combines NPHP with retinitis pigmentosa (O'Toole, Otto et al. 2006). In a second example, zebrafish *vangl2* mutants showed a more severe convergent extension phenotype when injected with a sub-phenotypic amount of bbs4 or bbs6 morpholinos, indicating a genetic interaction between Vangl2 and these BBS-related proteins (Ross, May-Simera et al. 2005). Recent unpublished work has shown a similar interaction between Vangl2 and Arl13b, a protein known to cause JBTS when mutated (Dudinsky and Perkins 2011). Ift88 and Kif3a, although not known to cause human ciliopathies, are necessary for ciliogenesis; mouse hair cells lacking either of these proteins have misoriented stereociliary bundles, and this misorientation also occurs in mice heterozygous for both *ift88* and *vangl2*, indicating again a genetic interaction between these two proteins (Jones, Roper et al. 2008).

In summary, many similarities exist between symptoms of both ciliopathies and disrupted PCP. Interestingly, retinal degeneration, a common symptom in ciliopathies, has not been shown to be a phenotype of vertebrate PCP mutants. Establishing a role for the PCP pathway in photoreceptors could not only increase our understanding of retinal

degeneration, but it would establish a novel model to further test the PCP pathway itself.

Retinomotor movements

Retinomotor movements are a critical part of the vertebrate retina's ability to adjust to different levels of light (for review, see Burnside and Nagle 1983). Adult zebrafish exhibit typical retinomotor movements, which include the lengthening of rods and the shortening of cones in the light, and vice versa in the dark (Hodel, Neuhauss et al. 2006). Simultaneous movements occur in the retinal pigment epithelium (RPE) (Hodel, Neuhauss et al. 2006). Because of the change in cell contact that occurs in different light adapted states, retinomotor movements may have the potential to influence cell signaling. In the light, the RPE surrounds the rod inner and outer segments, and the pigments of the RPE travel to the ends towards the outer nuclear layer, serving to block light from the rods. The extensions of the RPE extend between the cones ending approximately midway into the inner segments. In contrast, in darker environments, the RPE pigments move away from the photoreceptors, and the cones are surrounded by the RPE while the rods are exposed to the limited available light.

Retinomotor movements are controlled directly by the light on a specific region of the retina (Easter and Macy 1978). Intermediate light leads to an intermediate dark adaptation state (Engström and Rosstorp 1963; Easter and Macy 1978; Case and Plummer 1993). Although retinomotor movements will occur at any time in response to changes in light levels, fullest light and dark adaptation occur when the light level corresponds with the circadian clock (Levinson and Burnside 1981).

Several studies suggest that different cone subtypes move independently based on their own stimulation. Burnside and Nagle describe a German study (Weidemann 1966) where three cone types in guppies exhibit different retinomotor movements when exposed to different colored lights (Burnside and Nagle 1983). They also describe an unreferenced study by Glicksteinand others in 1969 where only one third of the cones in goldfish contract in response to long-wavelength light. Also, disassociated green sunfish (*Lepomis cyanellus*) cones will undergo appropriate elongation or contraction in response to dark and light (Burnside, Wang et al. 1993).

However, other studies suggest that the retinomotor movements in cones are not directly triggered by stimulation of individual cone types. In the cichlid *Aequidens pulcher* and in the frog *Xenopus laevis,* the action spectra necessary to elicit cone contraction matched the absorption spectrum of the rods, not of the cones, suggesting that rods may play a role in eliciting cone light adaptation (Kirsch, Wagner et al. 1989; Besharse and Witkovsky 1992). In the both the blue acara (*Aequidens pulcher*) and the Red Sea bream (*Pagrus major*), when monochromatic stimuli were used, all cones contracted together, rather than different cones moving independently depending on the wavelength used (Wagner, Kath et al. 1993; Kawamura, Miyagi et al. 1997).

Because retinomotor movements lead to changes in the cell-cell contact between photoreceptors, it is important to consider the effect that changes in the light environment could have on cell signaling in photoreceptors. Under normal cyclic lighting conditions, these contacts will vary. However, variations in the light cycle, light intensity, or light wavelengths that fish are exposed to over extended periods of

development could lead to changes in cell contacts. If these changes are dramatic enough to alter cell signaling, this has the potential to effect photoreceptor development, particularly for those photoreceptors which are formed during the time that the lighting conditions are altered.

Zebrafish model system

Among the retinas that have been histologically observed from numerous vertebrate species (for review, see Ahnelt and Kolb 2000), what these retinas have in common is their photoreceptor mosaic: that is, they have a variety of photoreceptor cell types that are arranged in a plane. Often, the distribution of different cell types within this mosaic is non-random. In the case of zebrafish, the distribution is crystalline—the cells are neatly arranged in rows, and the cell types are arranged into a predictable, well-characterized pattern that radiates out from the optic nerve where the oldest cones are near the center (see Figure 4)(Engström 1960; Raymond, Barthel et al. 1993; Allison, Barthel et al. 2010). Therefore, if planar cell polarity controls cilia localization in vertebrate photoreceptors, the strikingly organized zebrafish photoreceptor mosaic is an excellent system to first look for it since each cell's identity and orientation in relation to the surrounding cells is easily identified.

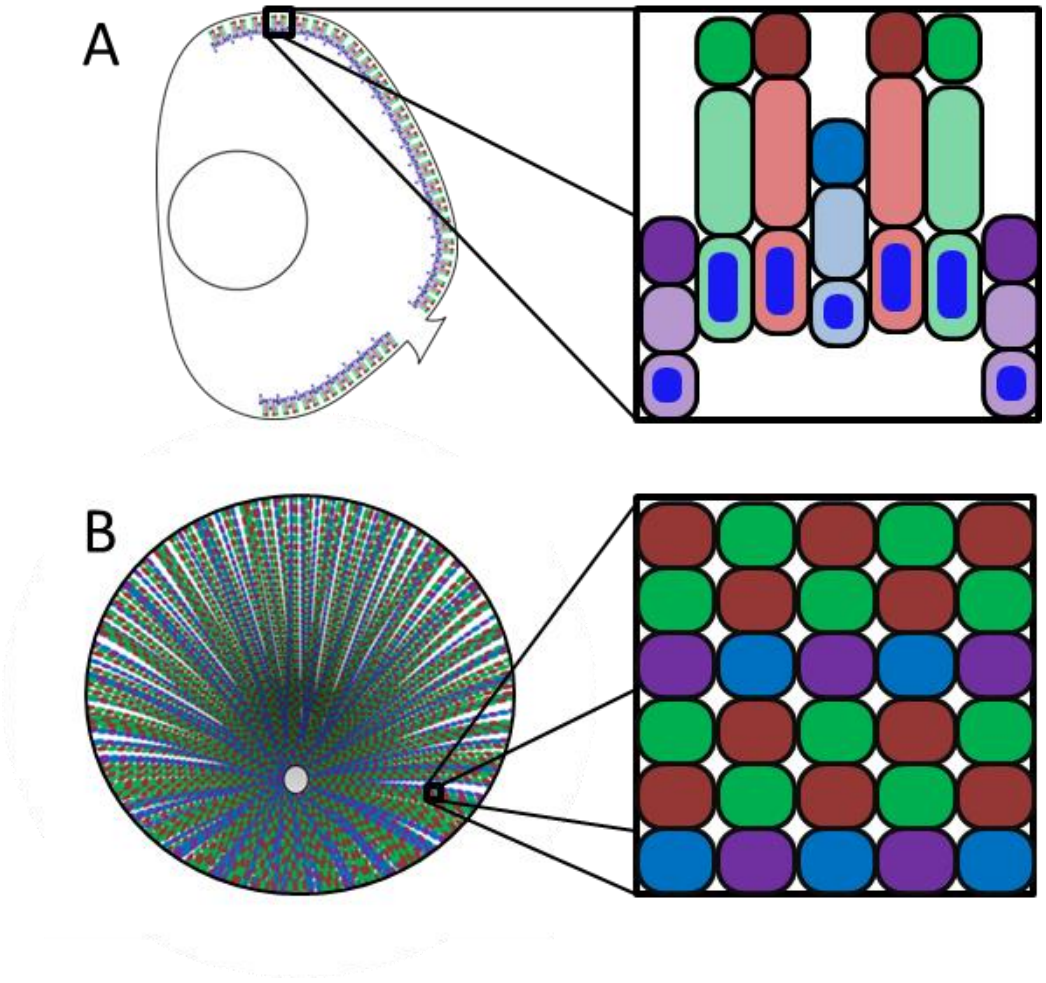

Figure 4. The arrangement of photoreceptors in the adult zebrafish retina.
A: Illustration of a transverse section through the eye with the lens and photoreceptors shown (not to scale). Inset shows the tiered red-, green-, blue-, and UV-sensitive cone types. Each cone is divided from bottom to top into a nucleus, inner segment, and outer segment. **B:** Illustration of a flatmounted retina to show the cone mosaic radiating out from the optic nerve (not to scale). Inset shows the pattern of the red-, green-, blue-, and UV-sensitive cone mosaic.

Discovering a PCP model in zebrafish photoreceptors would be useful because, whereas the PCP pathway has been shown to affect zebrafish developmental processes, such as convergent extension, the only known zebrafish model of the PCP pathway leading to translationally polarized large fields of cells within the same plane is the organization of cilia in the neural tube (Borovina, Superina et al. 2010). Zebrafish have many advantages as a model organism: they can serve as a vertebrate model for human disease, they can generate hundreds of transparent embryos that are not dependent on their mothers, and they are economically maintained for adult analysis. Therefore, it would be useful to find another system similar to the hair cells in a mouse cochlea or the bristles on a fly wing to expand our ability to study PCP in zebrafish.

Teleost photoreceptor mosaics

As previously described, the arrangement of different types of photoreceptors within a plane is called a photoreceptor mosaic. These mosaics vary between vertebrates, with photoreceptors being arranged in a variety of patterns, and with these patterns ranging from extremely well organized to disorganized. Across teleosts, there are two basic mosaic patterns: the row mosaic (Figure 5A), made of double cones arranged parallel to one another (and, often, alternating with rows of single cones that align with the double cones, as in the previously described zebrafish mosaic), and the square mosaic (Figure 5B), made of double cones that are angled in respect to neighboring double cones (and alternating with rows of single cones that are offset from the double cones) (Engström 1963). Variations on these two mosaics are observed among different species, which sometimes have different numbers of cone subtypes

(Reckel and Melzer 2003). Interestingly, Kjell Engström concludes that these two mosaics can "be considered as two different stages of transformation" with the row mosaic preceding the square mosaic (Engström 1963). Evidence for this includes A. H. Lyall's observation that the row mosaic was most common in the periphery of the trout retina, where the most newly formed cones exist, which progressively become a stronger square mosaic towards the central retina (Lyall 1957). Additional examples of square and row mosaics being present in the same retinas have since been reported (Wan and Stenkamp 2000; Reckel and Melzer 2003).

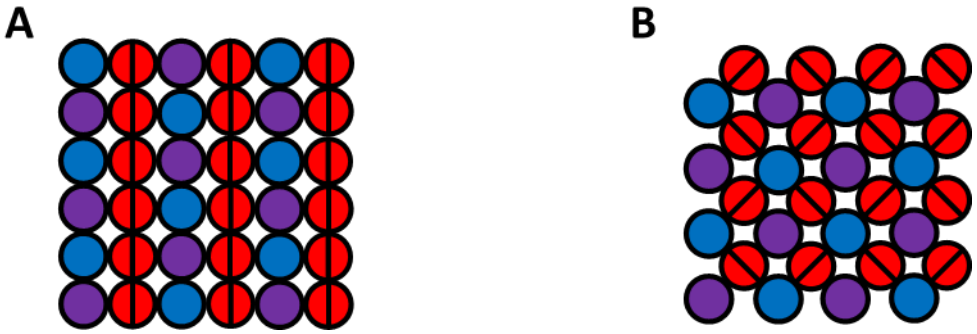

Figure 5. The row and square photoreceptor mosaics.
A: Illustration of a row mosaic. **B:** Illustration of a square mosaic. Blue and purple circles represent two subtypes of single cones and red circles represent double cones with each half of the red circle representing one of the cones in the double cone.

A model was developed to determine whether a row or square mosaic would form based on adhesive forces between neighboring cells (Tohya, Mochizuki et al. 2003). The zebrafish row mosaic and the medaka square mosaic were analyzed. Both of these species have red-, green-, blue-, and UV-sensitive cones; morphologically, the

former two form double cones and the latter two are long single and short single cones, respectively. The authors note that any pattern should be advantageous over none—this allows cones to be evenly distributed to increase resolution for all wavelengths. Interestingly, their model produced irregular patterns when parameters were set to in-between the cell adhesions necessary to produce either of the organized mosaics. They predict that this could lead to stabilizing selection for regular mosaics. Others have similarly hypothesized that organized mosaics could improve motion detection and contrast (Reckel and Melzer 2003)

Behavioral evidence also exists that an organized mosaic—be it a row or square mosaic—confers visual advantages. Lyall hypothesizes that since patterned teleost cone mosaics are so common, they may have a functional significance, particularly for detecting motion, since these patterns are more common in fish that feed on fast-moving prey (Lyall 1957). Engström hypothesizes the same, finding the same trend in predatory fish and also finding that the most disorganized mosaics were found in bottom-dwelling and nocturnal fish whose behavior was not highly visually-oriented (Engström 1963). Not observing behavioral differences between individuals with row or square mosaics, but instead observing more closely related species being more likely to exhibit the same type of mosaic, he concludes that phylogeny more than function determines the square versus row mosaic, while the function determines how crystalline that mosaic form appears in a given fish species. The correlation between species exhibiting visually-mediated behavior and an organized mosaic does not indicate that an organized mosaic is necessary for any functional vision; however, the conservation of organized mosaics

among many teleosts suggests that an organized mosaic confers some advantage, potentially an advantage that involves optimizing visual function.

Swordtail model system

Swordtail fish (members of the genus *Xiphophorus*), due to their mating preferences that are strongly influenced by visual cues and olfactory cues and their diverse, sexually dimorphic phenotypes, are an excellent system for studying mate choice, which is one form of pre-copulatory sexual selection. Mate choice must start with a perception of potential mates. For each individual of every species, perception of the external world is dependent on the ability to detect and interpret various signals from the environment (for review, see Ryan and Cummings 2013). For example, sensitivity to lightis dependent on the specific light wavelengths that photoreceptors can absorb and by how this information is organized and interpreted by other neurons in the retina and brain. These differences can be tailored to a specific environment; for example, an animal might have opsins that are maximally sensitive to an important light wavelength in that animal's environment. In models of the evolution of sensory systems, such as the retina, this is driven by the role of that system in preserving the individual in their own environment, such as in mating, predator avoidance, and feeding (for review, see Coleman 2011). Most sensory research in poeciliids has focused on mating behavior itself, particularly on the visual and olfactory cues that drive female preference, while the fewest studies have been done on the physiology behind these preferences or cues (Coleman 2011).

Mate preference in swordtails is a very complex phenotype that involves interactions between many factors. Increased association time of females with males has been shown to correspond with decreased time to spawning in fish (Wong 2004) and is commonly used to assess preference in swordtails. Sometimes preferences, which are often visual, vary greatly among species. For example, *X. helleri* females prefer sworded over non-sworded males (Rosenthal and Evans 1998). On the other hand, *X. birchmanni* females prefer *X. birchmanni* males without swords over *X. malinche* males or over *X. birchmanni* males with swords (Wong and Rosenthal 2006). *Xiphophorus nigrensis* females show no preference for long swords (Rosenthal, Wagner Jr et al. 2002). *X. cortezi* females prefer males with the same number of vertical bars on their left and right sides over males with different numbers of bars (Morris and Casey 1998).

The olfactory system has also been shown to be important for swordtails, both in mate choice and predator avoidance. While visual cues alone will keep *X. birchmanni* fry away from predators, both visual and olfactory cues leads to fry getting closer to conspecifics than visual cues alone (Coleman and Rosenthal 2006). In polluted waters, *X. birchmanni* females failed to show an olfactory preference for *X. birchmanni* males over *X. malinche* males (unlike in fresh water or when a visual cue was also present, where they preferred conspecifics) which supports the hypothesis that a recent hybridization event in Río Calnali between *X. birchmanni* and *X. malinche* was a consequence of pollution's disturbance of the olfactory cues that these species use to differentiate each other (Fisher, Wong et al. 2006). Male *X. birchmanni* exhibit a preference for olfactory cues from female conspecifics or from the closely related

heterospecific *X. malinche*, but not for the more distantly related heterospecific *Xiphophorus variatus* (Wong, Fisher et al. 2005). However, when given the choice between *X. birchmanni* or *X. malinche*, they prefer *X. malinche* (Wong, Fisher et al. 2005).

Multivariate naturally occurring traits do not necessarily correspond with multivariate preferences; in other words, females may prefer a combination of individual traits that does not naturally occur in males of their species. For example, *X. birchmanni* females prefer males with small dorsal fins but large body size, whereas *X. birchmanni* males have larger dorsal fins as their body size increases (Fisher, Mascuch et al. 2009). Furthermore, evidence that learning plays a role in mate preference is found in *X. birchmanni* females, which show a preference for the visual and olfactory cues of the species they are reared with (conspecific *X. birchmanni* or heterospecific *X. malinche*) (Verzijden and Rosenthal 2011).

Increased sword length and, perhaps more relevantly, increased body size of male swordtails have both been shown to be preferred by female swordtails in various species; however, the swordtail predator Mexican tetra (*A. mexicanus*) has also been shown to spend more time near swordtails expressing these same traits, which is likely due to these traits leading to these swordtails being more conspicuous and potentially could indicate they are more likely to be attacked (Rosenthal, Flores Martinez et al. 2001). Not surprisingly, then, predation risk plays a role in mate choice. For example, *X. birchmanni* females prefer conspecifics over *X. malinche* males, but only when predation risk (measured by distance to a shelter) is equal; when predation risk is greater

for conspecifics, they show a preference for heterospecifics (Willis, Rosenthal et al. 2012). In *Xiphophorus pygmaeus* females, behavorial trials suggest an aversion to the gold coloring of some males, but only in areas with low predation (Kingston, Rosenthal et al. 2003).

Vision in swordtails

Visual communication is a complex process that involves the physics of light and the processes that influence it, the production of messages, the perception and interpretation of these signals, the physiological mechanisms behind these behaviors, the development of these mechanisms, and the evolution of these mechanisms (for review, see Rosenthal 2007). The visual system is important in swordtails. As previously described, many of the preferences demonstrated in mate choice experiments have been visually-based preferences. One such preference highlights the interactions between mate choice visual communication and predator avoidance: *X. nigrensis* males reflect more UV light than *X. nigrensis* females or *X. malinche* fish, which is important because, unlike female *X. malinche*, female *X. nigrensis* show a preference for male *X. nigrensis* in the presence of UV light (Cummings, Rosenthal et al. 2003). This same study shows that this visual communication is advantageous for *X. nigrensis*, who have high predation from tetras (*A. mexicanus*), since the tetras did not change their association time with *X. nigrensis* in the presence or absence of UV light; similarly, this communication is not important among *X. malinche*, which do not have tetra predation. Beyond mate choice, in *X. birchmanni*, fry shoal more tightly when presented with

chemical or visual predator stimuli than when presented with conspecific stimuli (Coleman and Rosenthal 2006). Additionally, there is evidence that *X. helleri* exhibit light-based circadian rhythms (Rajchard, Hajek et al. 2000).

Despite all that is known about visual behavior in swordtails, little is known about their retina morphology or how this might play a role in their diverse preferences. In a study of a teleost retinas, Engström briefly mentions a single *Xiphophorus helleri* specimen he observed as having square photoreceptor mosaic consisting of double, long single, and short single cones (Engström 1963). The precise appearance of this mosaic is unknown. If this mosaic is consistent within this species, among different swordtail species, and among swordtails with different visual preferences is also unknown.

Hybridization and hybrid breakdown

Hybridization has been linked to various causes (for review, see Rosenthal 2013). In closely related species, individuals are likely to share similar mating signals and preferences, which may lead to hybridization. Furthermore, hybridization may occur due to changes in the environment that minimize the ability for individuals to detect differences between species as previously described in the hybridization in polluted waters of *X. malinche* and *X. birchmanni*. Reduction in the abundance of conspecifics can lead to increased familiarity with heterospecifics and increased cost to finding a conspecific, both which may increase the probability of hybridization.

Hybrid breakdown, a term describing the phenomenon whereby a hybrid individual with parents from two different species is less fit than either of the original

species, is a process that helps different species remain distinct. This can occur in many different ways with varying severity. The original construction of this idea is referred to as the Dobzhansky-Muller model. Dobzhansky specifically studied hybrid sterility, which he proposed might be caused by chromosomal differences that prohibited meiosis or by incompatibility between the alleles of certain genes from each of the parent species (Dobzhansky 1936). More recent studies have indicated that these incompatibilities may occur not only between different alleles of nuclear genes but also between different alleles in mitochondrial genes and between the interactions between mitochondrial and nuclear genes (for review, see Burton and Barreto 2012).

The problems that Dobzhansky and Muller observed caused hybrids to be sterile. However, hybrids could also fail to reproduce due to behavioral isolation. In sexual selection, traits can be selected against within a species due to pre-copulatory selection (e.g., mate choice) or post-copulatory selection (e.g. sperm competition) (for reviews, see Eberhard 2009; Jones and Ratterman 2009). Similarly, hybrids of two species could possess traits that minimized further hybridization if their fitness was limited due to incompatibilities pre- or post-copulation.

Sensory dysfunction

Sensory dysfunction occurs when hybrid breakdown specifically disrupts a sensory system, potentially leading to disrupted mate choice or decreased ability to perform necessary functions. Of interest here is the possibility of the loss of spectral tuning in photoreceptors. Changes in opsin structure or expression can change the light

wavelengths that an organism can best detect; when these changes are selected for in response to the environment, this is called spectral tuning (for review, see Coleman 2011). An ideal spectral tuning for, the ability to forage, for example, might consequentially lead to mating preferences that can in turn drive changes in the traits preferred within the population. Changes in the expression of opsin genes may be an early selectable trait that influences visual function; in cave-dwelling Atlantic mollies (*Poecilia mexicana*), while their eyes are still functional, opsins are downregulated (Tobler, Coleman et al. 2010). Beyond just sensitivity, acuity can also be selected for. Acuity can increase when eye size increases and when the photoreceptor density increases.

In one study, the histology of a variety of cyprinid retinas was characterized (Zaunreiter, Junger et al. 1991). These authors chose five species based on different behaviors and brain morphologies, from the predatory *Aspius aspius* (asp) to the benthivorous *Cyprinus carpio* (common carp). They found a great variation in cone and rod density, resolving power, and sensitivity in the different fish, which they corresponded with distinct behaviors in the fish. For example, the asp has a greater cone density in the retinal region used looking upward, which is important as this fish generally locates its prey from below. Other hypotheses include that increased photoreceptor density leads to increased visual acuity that improves motion detection and therefore predation and predator avoidance (Reckel and Melzer 2003).

In humans with diseases that lead to photoreceptor degeneration, decreased visual function has also been correlated with decreased photoreceptor density and

changes in the photoreceptor mosaic. Adaptive Optics Scanning Laser Ophthalmoscopy (AOSLO) allows doctors and scientists to observe differences and changes in the photoreceptor mosaic in living patients. For example, patients with retinitis pigmentosa, a disease involving progressive degeneration of photoreceptors and eventual vision loss, may maintain normal central vision for some time, yet nonetheless their cone photoreceptor mosaics are commonly less regularly organized than the photoreceptor mosaics of volunteers with healthy eyes (Makiyama, Ooto et al. 2013). Furthermore, in this same study, decreased cone density was seen in eyes with retinitis pigmentosa, and this decrease in cone density corresponded with a thinner outer nuclear layer and thinner inner and outer segment layer. In a similar study, AOSLO was used to observe the retinas of five patients with fundus albipunctatus, a form of inherited night blindness that can progress to cone dystrophy (Makiyama, Ooto et al. 2013). These authors found reduced cone density and reduced regularity of the cone mosaic in the macula of these patients when compared to healthy individuals. In another study, AOSLO was used to observe the retinas of patients with late age-related macular degeneration, and again a large reduction, over 20%, of cone density was found in diseased retinas (Mrejen, Sato et al. 2013). Furthermore, a positive correlation has been shown between decreased contrast sensitivity and decreased cone density in patients with various retinal degenerative diseases (Choi, Doble et al. 2006). In patients with retinitis pigmentosa or Usher syndrome, another disease involving retinal degeneration, cone density was shown to decrease over time (Talcott, Ratnam et al. 2011). Combined, these studies in both fish and humans indicate that decreased photoreceptor density is one potential

indicator of visual sensory dysfunction. Measuring photoreceptor density in swordtail hybrids could therefore be one way to test for evidence of hybrid breakdown.

Summary

First, because 1) photoreceptors have a sensory cilium that is critical for their function, 2) many types of cilia are organized by the PCP pathway, 3) many symptoms of ciliopathies overlap with symptoms of disrupted PCP, 4) photoreceptor degeneration is a common symptom of ciliopathies, and 5) genetic interactions have been shown between proteins involved in the PCP pathway and proteins that, when mutated, cause retinal degeneration, I have characterized cilia positioning in zebrafish photoreceptors. The phenotypes of cilia positioning in different photoreceptor cell types under different conditions, including under different lighting in rearing conditions, will provide insights into the processes controlling this localization.

Second, because 1) teleost mosaics vary among species, 2) differences in teleost mosaics suggest differences in visual function, 3) diverse visual preferences exist among swordtails, and 4) little is known about the swordtail photoreceptor mosaic, I have characterized the swordtail photoreceptor mosaic in several swordtail species. By characterizing this mosaic, I take a necessary early step in understanding the mechanisms behind the visual behavior of swordtails. This also introduces a potentially new opportunity to study hybrid breakdown in the form of visual sensory dysfunction.

CHAPTER II

BASAL BODIES EXHIBIT POLARIZED POSITIONING IN ZEBRAFISH CONE PHOTORECEPTORS*

Overview

The asymmetric positioning of basal bodies, and therefore cilia, is often critical for proper cilia function. This planar polarity is critical for motile cilia function but has not been extensively investigated for nonmotile cilia or for sensory cilia such as vertebrate photoreceptors. Zebrafish photoreceptors form an organized mosaic ideal for investigating cilia positioning. I report that in the adult retina, the basal bodies of red-, green-, and blue-sensitive cone photoreceptors localized asymmetrically on the cell edge nearest the optic nerve. In contrast, no patterning was seen in the basal bodies of ultraviolet-sensitive cones or in rod photoreceptors. The asymmetric localization of basal bodies was consistent in all regions of the adult retina. Basal body patterning was unaffected in the cones of the XOPS-mCFP transgenic line, which lacks rod photoreceptors. Finally, the adult pattern was not seen in 7 days-post-fertilization (dpf) larvae; basal bodies were randomly distributed in all the photoreceptor subtypes. These results establish the asymmetrical localization of basal bodies in red-, green-, and blue-sensitive cones in adult zebrafish retinas but not in larvae. This pattern suggests an active

* This chapter has been previously published as "Basal bodies exhibit polarized positioning in zebrafish cone photoreceptors." Michelle Ramsey and Brian D. Perkins. *Journal of Comparative Neurology*. 2013 Jun 1;521(8):1803-16. DOI: 10.1002/cne.23260.

cellular mechanism regulated the positioning of basal bodies after the transition to the adult mosaic and that rods do not seem to be necessary for the patterning of cone basal bodies.

Introduction

The light-sensitive outer segment of vertebrate photoreceptors develops from a primary cilium, which is anchored to the apical surface of the inner segment by the basal body (De Robertis 1956; De Robertis 1960). The connecting cilium also serves as the only conduit for transporting proteins involved in phototransduction from the inner segment to the outer segment. As such, defects in cilia formation or maintenance often lead to photoreceptor degeneration, a common symptom of ciliopathies (Adams, Awadein et al. 2007). Anatomical studies of outer segment morphogenesis over several decades have primarily focused on cilia growth and disc membrane formation (De Robertis 1956; Steinberg, Fisher et al. 1980; Besharse, Forestner et al. 1985; Knabe and Kuhn 1997). Very little is known, however, about the initial steps leading to cilia formation in photoreceptors or subsequent changes in cilia structure during photoreceptor maturation.

One of the earliest steps in cilia formation is the migration and docking of the basal body at the apical cell surface. Once the basal body docks, it extends microtubules to form the axoneme of the cilium (Dawe, Farr et al. 2007). Although recent studies have provided some insight on the molecular mechanisms governing these processes, the results often appear context-specific, or even contradictory, and no consensus model on

cilia formation exists (for review, see Wallingford and Mitchell 2011). For example, basal body docking requires the organization of the apical actin cytoskeleton (Boisvieux-Ulrich, Laine et al. 1990), a process involving the RhoA GTPase (Pan, You et al. 2007). Studies of zebrafish motile cilia revealed that RhoA activation requires the forkhead box (F-box) transcription factor Foxj1 (Yu, Ng et al. 2008) and loss of Foxj1 resulted in actin cytoskeleton defects and a failure to properly dock basal bodies (Gomperts, Gong-Cooper et al. 2004). Although Foxj1 factors serve as "master regulators" for genes essential for motile cilia, primary (9+0) and sensory cilia are unaffected by loss of Foxj1 (Brody, Yan et al. 2000; Yu, Ng et al. 2008), indicating that other factors likely govern actin assembly and/or RhoA activation. Additional evidence suggests that basal body docking and ciliogenesis also requires planar cell polarity (PCP) signaling.

PCP refers to the ability of cells or cellular structures (e.g. cilia) to orient within a plane of a tissue and this phenomenon is controlled by the PCP signaling cascade (for recent reviews see (Simons and Mlodzik 2008; Goodrich and Strutt 2011; Gray, Roszko et al. 2011). Early studies in *Drosophila* elucidated a core group of proteins responsible for PCP signaling activity. The pathway includes the transmembrane proteins Van Gogh (Vangl), Flamingo (Fmi), and Frizzled (Fz) and the cytoplasmic proteins Dishevelled (Dsh), Diego (Dgo), and Prickle (Pk). This group of core proteins subsequently signals through downstream effectors, such as Inturned and Fuzzy. Subsequent analyses in *Xenopus* (Wallingford, Rowning et al. 2000), zebrafish (Heisenberg, Tada et al. 2000; Jessen, Topczewski et al. 2002), and mice (Montcouquiol, Rachel et al. 2003) demonstrated that the pathway is evolutionarily conserved in vertebrates, and multiple

homologs have been identified for each of these proteins (Simons and Mlodzik 2008). Somewhat unexpectedly, PCP has now been linked to defects in cilia, although the exact nature of this relationship is not entirely clear.

In multiciliated cells of the *Xenopus* epidermis, the cytoplasmic protein Dishevelled, a core component of the PCP pathway, mediated activation of RhoA and basal bodies failed to dock in the absence of Dishevelled (Park, Mitchell et al. 2008). Studies in *Xenopus* and mouse also found actin cytoskeleton and cilia defects following the loss of downstream PCP effectors Inturned and Fuzzy (Park, Haigo et al. 2006; Gray, Abitua et al. 2009). Thus, components of the PCP pathway can function in cilia formation, but reports detailing the precise roles for specific proteins are often contradictory. For example, formation of primary cilia was not affected by the loss of the core PCP gene *vangl2* in zebrafish (Borovina, Superina et al. 2010), but basal body docking and cilia formation were perturbed by morpholino knockdown of Vangl2 in multiciliated epidermal cells of *Xenopus* (Mitchell, Stubbs et al. 2009). Nevertheless, after the loss of Vangl2, both motile primary cilia and motile epidermal cilia exhibited defects in planar orientation and asymmetric tilting, characteristics that are necessary to produce directional fluid flow (Mitchell, Stubbs et al. 2009; Borovina, Superina et al. 2010). Taken together, these results indicate that PCP components in motile cilia function in basal body docking and/or planar orientation of cilia, which coordinates cilia beating to create directional fluid flow. Current data do not suggest, however, that primary or sensory cilia universally require planar polarization across a tissue. Such

cilia are nonmotile and the need for ciliary polarization has not been thoroughly investigated, particularly in vertebrate photoreceptors.

In this study, I investigated planar positioning of basal bodies and cilia within zebrafish photoreceptors. The zebrafish retina is ideal for these studies because the photoreceptors are arranged into a precise, geometric lattice known as the row mosaic (Engström 1960; Larison and Bremiller 1990; Raymond, Barthel et al. 1993). This mosaic provides an ideal background to identify planar polarization of individual cilia within the plane of the epithelia (Figure 6A). Zebrafish possess four distinct cone subtypes, which I will refer to as ultraviolet (UV)-, blue-, red-, and green-sensitive cones (Branchek and Bremiller 1984). Morphologically, the UV- and blue-sensitive cones exist as single cones, while the red- and green-sensitive cones form a double-cone pair (Branchek and Bremiller 1984; Raymond, Barthel et al. 1993). UV- and blue-sensitive cones alternate with rows of red- and green-sensitive cones (Figure 6A). These rows radiate out from the optic nerve with the oldest cones being near the center (Allison, Barthel et al. 2010). The rods are arranged in squares surrounding the UV-sensitive cones (Fadool 2003).

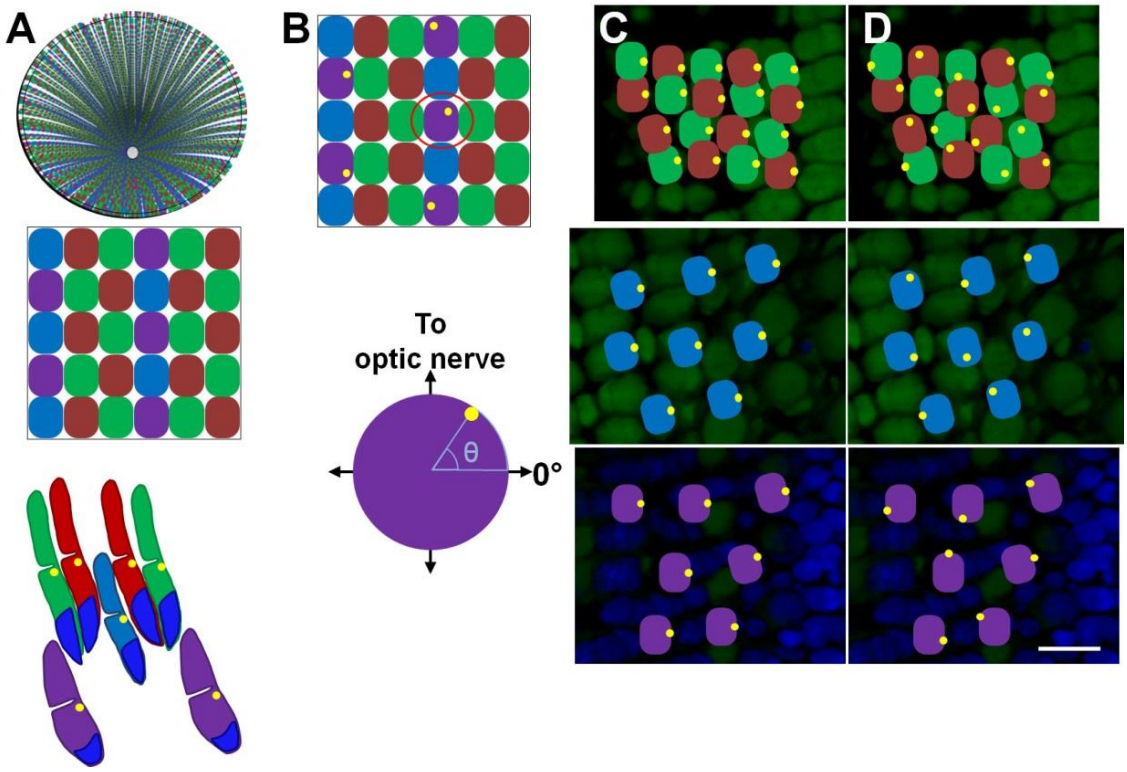

Figure 6. Basal body positioning within the zebrafish cone mosaic.
A: Top: Schematic of an adult retina showing the cone row mosaic radiating out from the optic nerve. Middle: Magnification shows the mosaic pattern of the red (R)-, green (G)-, blue (B)-, and UV (U)-sensitive cones. Bottom: Schematic of the vertical tiering of cones within the photoreceptor layer. Basal bodies (yellow dots) are located in the ellipsoids at the base of the outer segments. Nuclei are labeled in blue. **B:** Top: Schematic with basal bodies in the UV-sensitive cones adopting a random distribution around the perimeter of the cell. Bottom: The angular position of a basal body in one selected UV-sensitive cone (below) is determined as shown. **C:** Fluorescent image of an oblique cryosection through a retinal flat mount. Photoreceptor nuclei were stained with DAPI (blue). Autofluorescence (green) from excitation with 488-nm light shows inner and outer segments. **D:** Potential basal body arrangements for red-/green-sensitive cones (top), blue-sensitive cones (middle), and UV-sensitive cones (bottom) at their appropriate depths in the retina are illustrated. Basal bodies may be asymmetrically polarized and similarly positioned or are randomly positioned at the apical end of the inner segment. Basal bodies are illustrated in yellow. A magenta-green version of this figure is provided in the Appendix. Scale bar = 10 μm.

Cone photoreceptors in the adult zebrafish retina are also tiered within the photoreceptor layer. UV-sensitive cones are located most vitreally, followed (moving in the scleral direction) by blue-sensitive cones and red-/green-sensitive double cones (Branchek and Bremiller 1984; Raymond, Barthel et al. 1993). This vertical tiering dramatically separates the ellipsoids and outer segments of different cone types. The ellipsoids and outer segments of UV-sensitive cones lie below the ellipsoid region of blue-sensitive cones, whereas the blue-sensitive cone outer segments terminate near the base of the double-cone outer segments. This tiering predicts a similar tiering of the basal bodies in photoreceptors, which anchor the connecting cilia to the apical surface of the inner segments (Figure 6A, bottom). Each cell in relation to the surrounding cells is easily identified, based on both the mosaic pattern and the tiering of the cone subtypes, so the zebrafish photoreceptor mosaic is an excellent system to search for planar polarization of basal bodies.

Larval zebrafish lack the highly patterned row mosaic of cone photoreceptors seen in adults, but they do exhibit a nonrandom mosaic array of cones (Allison, Barthel et al. 2010). A transition occurs between 20-36 days post fertilization (dpf), whereby cones born after this time are arranged in the adult row mosaic. Cones generated during embryonic and larval stages remain as a distinct larval remnant surrounding the optic nerve in the adult retina. As the adult retina grows, new cones are produced at the margins and adopt the row mosaic. I have identified a pattern of basal body positioning in zebrafish red-, green-, and blue-sensitive cones. At the apical surface of the inner segment of these cones, the basal bodies are positioned asymmetrically on the cell edge

nearest to the optic nerve. This pattern is seen throughout the adult mosaic. In contrast, the basal bodies of UV-sensitive cones and rods are not patterned. In 7 day-old larval retinas no pattern is evident. I also report that in a transgenic line that undergoes early degeneration of rod photoreceptors, no change in the patterning of cone basal bodies was observed, suggesting that rods are not necessary for establishing the pattern of the cone basal bodies.

Materials and methods

Zebrafish care and maintenance

Zebrafish (*Danio rerio*) were maintained according to standard procedures (Westerfield 1995). Light-adapted wild-type AB/Ekkwill hybrids, *Tg(TαC:GFP)*^{ucd1} (Kennedy, Alvarez et al. 2007), and *Tg(-5actb2:cetn2-GFP)*^{cu6} (Randlett, Poggi et al. 2011) fish were used for quantification of wild-type cone basal body positioning. Dark-adapted *Tg(XlRho:EGFP)*^{fl1} fish (referred to here as XOPS-GFP) utilize the *Xenopus* opsin promoter to drive GFP in rod photoreceptors and were used to analyze rod basal bodies (Fadool 2003). The *Tg(XlRho:gap43-CFP)*^{q13} transgenic line, which is referred to here as XOPS-mCFP, expresses a membrane-targeted cyan fluorescent protein (CFP) in rod photoreceptors that causes degeneration of rods without affecting cones (Morris, Schroeter et al. 2005).

Immunohistochemistry and imaging

Adult light-adapted fish were sacrificed, and their eyes were enucleated. The retinas were removed and four or five incisions were made so that they could subsequently be laid flat. The retinas were fixed 3 hours to overnight (ON) in 4% paraformaldehyde in phosphate buffered solution (PBS: 137 mM NaCl, 2.7 mM KCl, 10 mM Na_2HPO_4, 1.76 mM KH_2PO_4, pH 7.4) at 4°C. Alternatively, dark-adapted fish were killed and their heads were fixed ON as described above. After fixation, their eyes were enucleated, and their retinas were prepared as described above. Retinas were infiltrated with 30% sucrose in PBS at 4 °C until they sank and with tissue freezing medium (TFM; Triangle Biomedical Sciences, Durham, N.C.) at room temperature (RT) for 20 minutes. Retinas were flat-mounted in TFM between two coverslips spaced with No.1 coverslips prior to freezing. The flat-mounted retinas were cryosectioned such that each tangential section (10 μm) was slightly oblique and off-parallel to the outer limiting membrane. Cryosections were mounted on gelatin-coated slides and dried overnight at room temperature. The sections were rehydrated and washed in 0.1% Tween 20 and 0.1% dimethyl sulfoxide (DMSO) in PBS (PBSTD). To detect γ-tubulin in the basal bodies, sodium citrate antigen retrieval (adapted from Jiao, Sun et al. 1999) was performed by maintaining slides at 70-90°C for 30 minutes while they were submerged in 10 mM sodium citrate. The slides were cooled at RT while submerged in sodium citrate solution. Slides were blocked for 1–2 hours at RT in 5% normal goat serum in PBSTD and incubated overnight at 4°C in primary antibody diluted in blocking solution. After being washed in PBSTD, slides were incubated for 1 hour at RT in the appropriate

AlexaFluor secondary antibodies (Invitrogen, Eugene, OR; 1:500) and in the fluorescent nuclear stain 4,6-diamidino-2-phenlindole dihydrochloride (DAPI, Invitrogen; 1:10,000). Larval zebrafish (7 dpf) were prepared as described for adult retinas, except that sodium citrate antigen retrieval was not used. Sagittal sections of whole larvae were taken, and photoreceptors perpendicular to the visible optical plane were analyzed.

Antibody characterization

Antibodies used in this study are summarized in Table 1. The mouse monoclonal anti-γ-tubulin antibody (Sigma-Aldrich, St. Louis, MO; T6557; mouse IgG1 isotype) is a well-established marker for basal bodies. The antibody was raised against a synthetic γ-tubulin peptide (N-terminal amino acids 38-53) conjugated to keyhole limpet hemocyanin (KLH) and was derived from the GTU-88 hybridoma produced by the fusion of mouse myeloma cells and splenocytes from an immunized mouse. It recognizes a 48 kDa epitope located in the N-terminal amino acids 38-53 of γ-tubulin (manufacturer's data sheet).

Table 1. Primary Antibodies

Antibody	Antigen	Dilution/species	Immunizing antigen	Source and catalog number
Gamma-tubulin	γ-tubulin	1:5000 Mouse, monoclonal	Synthetic peptide corresponding to amino acids 38-53 and conjugated to KLH	Sigma-Aldrich, St. Louis, MO Cat. No. T6557 Clone GTU-88
GFP	Green fluorescent protein (GFP)	1:500 Rabbit, polyclonal	Green fluorescent protein purified from *Aequorea Victoria*	Invitrogen, Life Technologies, Grand Island, NY Cat. No. A-111-22 Lot Nos. 1141866 and 632116
Green opsin	Zebrafish green opsin	1:200 Rabbit, polyclonal	C-terminal fragment	D. Hyde, University of Notre Dame, South Bend, IN, USA
Blue opsin	Zebrafish blue opsin	1:200 Rabbit, polyclonal	N-terminal fragment	D. Hyde, University of Notre Dame, South Bend, IN, USA
Ultraviolet opsin	Zebrafish ultraviolet opsin	1:200 Rabbit, polyclonal	N-terminal fragment	D. Hyde, University of Notre Dame, South Bend, IN, USA
Zpr-1	Arrestin 3-like	1:200 Mouse, monoclonal	Whole adult zebrafish retinal cells	Zebrafish International Resource Center (ZIRC), Eugene, OR. Cat. No. Zpr-1
4C12	Rod photoreceptors	1:150 Mouse, monoclonal	Whole zebrafish retina	J. Fadool, Florida State University, Tallahassee, FL, USA

The rabbit polyclonal anti-green fluorescence protein (GFP) antibody (Invitrogen; A-111-22, IgG isotype) was raised against GFP isolated directly from the jellyfish *Aequorea victoria* and the IgG fraction was purified by ion-exchange chromatography (manufacturer's data sheet). This antibody was used to identify the centrin-GFP fusion protein as well as enhanced GFP (eGFP) in the XOPS-GFP line. In centrin-GFP transgenic animals, staining with this antibody gave a pattern identical to that of anti-γ-tubulin, another marker for basal bodies. Furthermore, no staining was observed when the antibody was used to stain tissue from zebrafish lacking the centrin-GFP transgene.

Rabbit polyclonal antibodies against the zebrafish opsin proteins were a generous gift of Dr. David Hyde (University of Notre Dame). A carboxyl terminal polypeptide generated from the amplified cDNA template for zebrafish green opsin (5'-GAATTCAGCTTTGCTGCCTGGATCTTCT-3' and 5'-CTCGAGCAGATCTATGCAGGGAACAGAGGA-3') was used to generate polyclonal antibodies against zebrafish green opsin. Amino terminal polypeptides were generated from the amplified cDNA templates for zebrafish blue opsin (5'-GAATTCGAAGCAACAACAGCAAACGC-3' and 5'-CTCGAGGGTAAGAACGTTGATGGCAG-3') and ultraviolet opsin (5'-GAATTCGCGTGGGCCGTTCAATT-3' and 5'-CTCGAGTTCATCGTGACGAAGAGGACG-3') to generate polyclonal antibodies against the zebrafish blue and ultraviolet opsins, respectively. All antibodies detected single bands that were near the expected sizes of the individual opsin proteins (~38 kDa)

and labeled the outer segments of the appropriate cone subtypes (Vihtelic, Doro et al. 1999).

The mouse monoclonal antibody Zpr-1 (Fret-43; Zebrafish International Resource Center, Eugene, OR) recognizes the arrestin 3-like (*arr3l*) protein in the red/green-sensitive double cones (Ile, Kassen et al. 2010). The Zpr-1 antibody recognized a single 45-kDa protein in Western blots of zebrafish retinal lysates and was confirmed as *arr3l* by MALDI-TOF mass spectrometric analysis and by loss of Zpr-1 immunofluorescence in *arr3l* morphant retinas (Ile, Kassen et al. 2010). Stained cells were identified as red-/green-sensitive double cones on the basis of anatomical location and morphological features such as outer segments and synaptic terminals (Larison and Bremiller 1990).

The mouse monoclonal antibody 4C12 was a gift from Dr. James Fadool (Florida State University) and was generated by immunizing mice with homogenized zebrafish retinal extracts (Fadool, Fadool et al. 1999). Hybridomas were screened for antibodies that labeled the zebrafish retina, and 4C12 specifically recognized cells within the outer nuclear layer. Based on the morphology of the outer segments and the tiering within the outer nuclear layer, 4C12 labels an uncharacterized epitope on rod photoreceptors. Additional evidence that 4C12 labels rods is that only 4C12 staining of regenerating rod photoreceptors is seen in the rod degeneration XOPS-mCFP line along with the increase in 4C12 staining in *tbx2b* mutants, which show increased numbers of rod photoreceptors (Morris, Schroeter et al. 2005; Alvarez-Delfin, Morris et al. 2009).

Sections were imaged by taking z-stacks of approximately 12-20 optical sections at 0.5-0.8 μm steps with a Zeiss ImagerZ1 fluorescence microscope with an ApoTome. The location of each field in relation to the optic nerve (near the optic nerve, in the middle of the retina, or in the peripheral retina) was recorded when each field was imaged. The larval remnant was identified by the lack of organized adult cone mosaic in cells nearest the optic nerve. To define the other areas of the retina, the radius of the retina was visually divided into one-thirds, the first starting immediately outside the larval remnant and the third ending at the retinal margin (see the figure on page 50). Fields that were very close to the boundaries between the different regions were not analyzed. All images shown consist of either a single plane or multiple optical sections from one z-stack obtained in AxioVision or ZEN (blue edition; v. 4.8.2 or v. 1.0.0.0, respectively; Zeiss, Thornwood, NY). The RGB and CMYK levels of fully assembled figures were adjusted in Adobe Photoshop.

Quantification of basal body localization

Basal body positions were determined from images of adult retinas stained with γ-tubulin as described above. Each optical section of the z-stack was analyzed individually, and all data for a given cone subtype within a z-stack were combined to form one data set. Each data set contains the positions of basal bodies from red-/green-sensitive cones, blue-sensitive cones, UV-sensitive cones, or rods within one z-stack. Each basal body was located along the periphery of the apical side of the inner segment, and the angular position was quantified using AxioVision or ZEN. As rows of cells

radiate outward from the optic nerve (Allison, Barthel et al. 2010)(Figure 6A), the angular position of a basal body was defined by the direction of the row within the field relative to the optic nerve (Figure 6B). The direction of the optic nerve was arbitrarily defined as an angular vector of 90° (Figure 6B). All subsequent calculations and graphs were completed in Excel 2010 using standard statistical methods (Batschelet 1981; Fisher 1993; Zar 1996). Formulas, when possible, were confirmed in StatistiXL (v. 1.8). The angular positions of all the basal bodies from one data set were plotted around a unit circle with the point (1,0) corresponding with 0°. The Rayleigh test was used to determine the probability that the mean position represented a true mean position of the population. I calculated the circular 95% confidence interval for the mean position of each data set. To calculate the mean position of multiple data sets (i.e., the grand mean position) and the corresponding 95% confidence interval, all data sets to be combined were represented by their mean vectors and the angular position of the grand mean vector was calculated. The circular 95% confidence intervals for the grand mean position were calculated as for a second-order mean angle (Zar 1996). If the strength of the trend was very weak, then no circular confidence interval could be calculated. Finally, positions from red- and green-sensitive cones were combined because the double cones and their basal bodies are found at very similar depths in the retina.

Results

To analyze the positioning of basal bodies in zebrafish photoreceptors, I labeled cryosections of flat-mounted adult retinas with γ-tubulin, a specific marker for basal

bodies (Stearns, Evans et al. 1991). I hypothesized that, if an active signaling mechanism controlled cilia positioning in photoreceptors, then the basal bodies within a plane of cells would align in a reproducible pattern, which would be propagated within each subtype (Figure 6C, D). Alternatively, in the absence of an active signaling mechanism, basal bodies would be distributed randomly on the apical surface of the inner segment of the photoreceptors (Figure 6E). In either scenario, the photoreceptor positioning within the mosaic remains unaffected. I first identified individual cell types by their vertical tiering position within the outer nuclear layer, by their position within the row mosaic, and by staining with individual opsin antibodies to label outer segments (Figure 7).

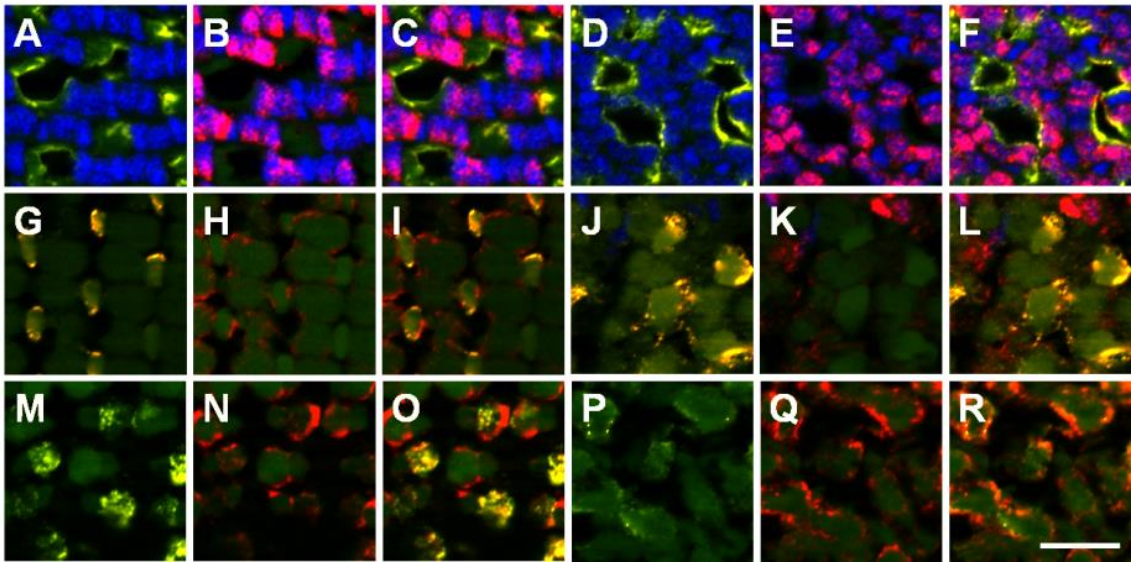

Figure 7. Cone subtypes can be identified by the vertical tiering distribution. **A-F:** UV opsin (yellow) marks UV-sensitive cones, and zpr-1 staining (red) marks the cell bodies of the red-/green-sensitive double cones in the adult mosaic (A-C) and the larval remnant (D-F) at the vertical location of the basal body. **G-L:** Blue opsin (yellow) labels blue-sensitive cones and zpr-1 staining (red) labels red-/green-double cones in the adult mosaic (G-I) and the larval remnant (J-L) at the vertical location of the basal bodies. **M-R:** Green cone opsin (yellow) labels green-sensitive cones and colocalizes with one member of the double-cone pair labeled by zpr-1 staining (red) in the adult mosaic (M-O) and the larval remnant (P-R). A magenta-green version of this figure is provided in the Appendix. Scale bar = 10 μm.

Within the adult row mosaic, basal bodies of the red-, green-, and blue-sensitive cones appear to be located at the same position along the periphery of most cells within a single field (Figure 8A, B, D, E). The angular positions of basal bodies within a single field of cells were combined into a unique data set. Each data set was then quantified in relation to the direction of the optic nerve and graphed on a circular plot (Figure 8G, H). The position of the optic nerve was determined from low-magnification views of the field of cells and from the orientation of cell rows. Red- and green-sensitive cones form a double cone pair and the basal bodies within each pair appeared to be similarly aligned. As such, the angular positions reflect the combined data from both subtypes. Within individual data sets, basal bodies of the red-/green-sensitive cones exhibited a strong polarization toward the optic nerve (Figure 8G, Table 2). Basal bodies of the blue-sensitive cones also aligned preferentially on the leading edge with a low angular deviation (Figure 8H, Table 2). The mean angular position for all basal bodies within a data set was calculated and graphed as the mean vector (Figure 8G, H, black arrows). The length of this vector corresponds to the strength of the trend. In contrast to the other cone subtypes, the basal bodies of UV-sensitive cones appeared randomly distributed around the edge at the apical inner segment (Figure 8C, F, I).

Figure 8. Basal body positioning is strongly patterned in individual fields of red-/green- and blue-sensitive cones.
Sample portions of fields of cells at the depths of the basal bodies of (**A**) red-/green-sensitive cones, (**B**) blue-sensitive cones, and (**C**) UV-sensitive cones, along with their respective magnified subsets of cells (**D-F**), in adult light-adapted zebrafish retinas. γ-tubulin localized to basal bodies (yellow), whereas nuclei were counterstained with DAPI (blue). Autofluorescence (green) from 488-nm excitation shows inner and outer segments. Some red-, green-, blue-, and UV-sensitive cones are labeled as R, G, B, and U, respectively. **G-I:** Graphs of the positions of basal bodies from fields A-C in which the positions of all the basal bodies of red-/green-, blue-, or UV-sensitive cones were plotted around a unit circle (red, blue, or purple lozenges, respectively), and the mean vector is indicated (black arrow). The angular position of each mean vector indicates the basal bodies' mean position around the periphery of the cell, and the distance of each mean vector from the origin indicates the strength of the trend. Optic nerve is upward in all panels. A magenta-green version of this figure is provided in the Appendix. Scale bars = 10 μm in C (applies to A–C); 10 μm in F (applies to D–F).

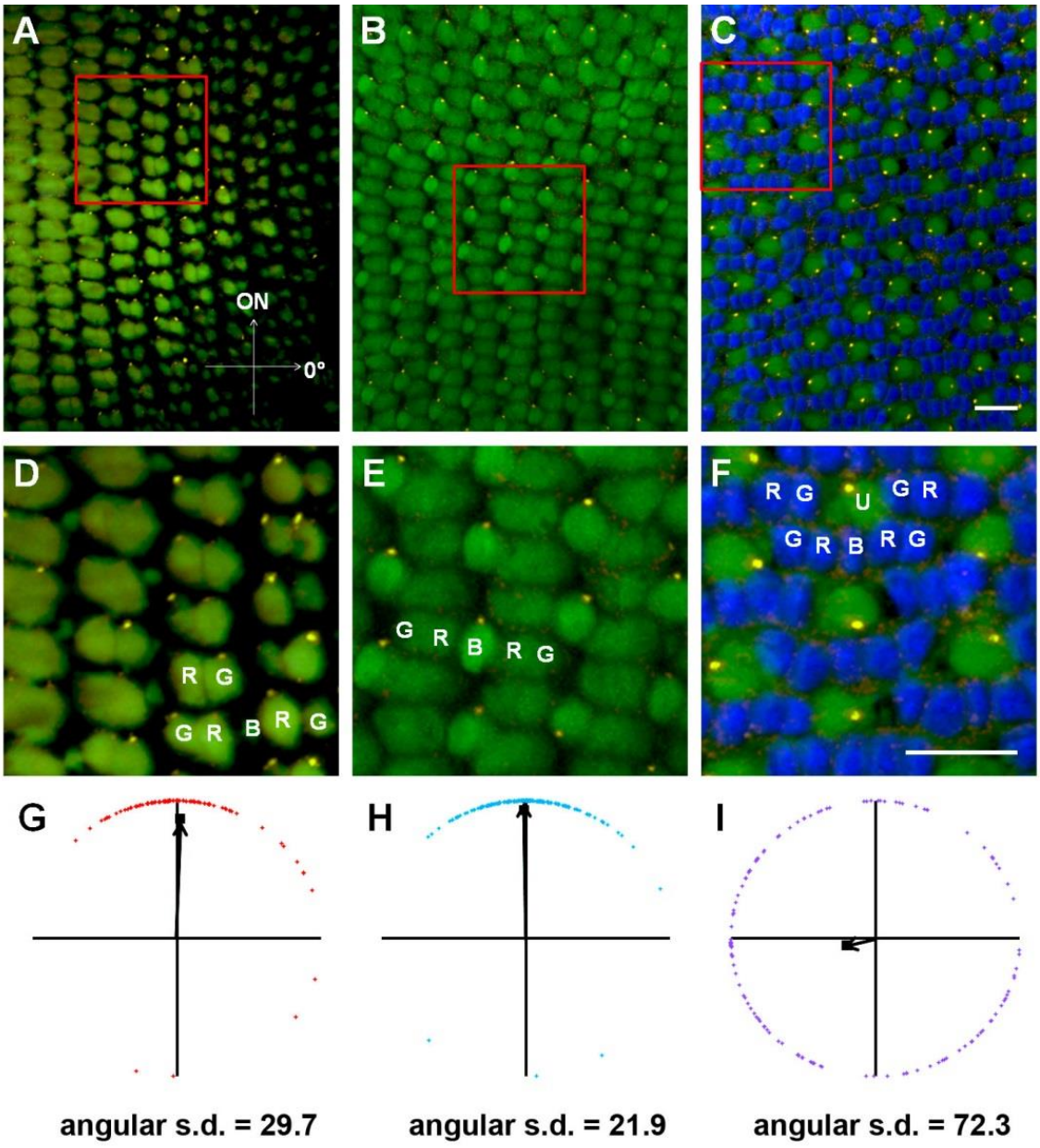
A
ON
0°
B
C
D
R G
G R B R G
E
G R B R G
F
R G U G R
G R B R G
G
H
I
angular s.d. = 29.7
angular s.d. = 21.9
angular s.d. = 72.3

Table 2. Numerical Analysis of Basal Body Position (1)

Sample	Photoreceptor Subtype	Field Location	Mean Angular Position (0-360°)	95% Confidence Interval (°)	Circular Standard Deviation	Avg. # cells/field	# Fields	# Retinas	# Fish
Wild-type	Red/green	Near optic nerve	94	76-107	43.1	133	6	3	3
Wild-type		Middle retina	92	79-134	40.1	121	6	2	2
Wild-type		Peripheral retina	85	76-96	23.9	87	4	3	3
Wild type		Grand Mean	91	85-98	34.8	117	**Total = 16**	**3**	**3**
Wild-type	Blue	Near optic nerve	83	53-96	40.1	60	8	4	3
Wild-type		Middle retina	87	81-94	32.2	77	9	3	3
Wild-type		Peripheral retina	90	82-98	27.9	55	6	4	3
Wild-type		Grand Mean	87	82-91	32.5	65	**Total = 23**	**5**	**4**
Wild-type	UV	Near optic nerve	168	ND	73.9	72	3	3	2
Wild-type		Middle retina	209	ND	73.1	86	3	2	2
Wild-type		Peripheral retina	119	ND	74.5	63	3	3	2
Wild-type		Grand Mean	151	99-235	73.2	74	**Total = 9**	**5**	**4**
Wild-type	Rods	Middle and peripheral retina	58	ND	72.5	115	7	6	4
XOPS-mCFP	Red/green	Middle retina	81	58-91	56.3	119	11	6	3
XOPS-mCFP	Blue	Middle retina	88	76-95	34.0	78	10	6	3
XOPS-mCFP	UV	Middle retina	278	204-313	68.4	85	9	6	3
							Total = 30	**6**	**3**
Larvae (7 dpf)	Red/green	n/a	115	ND	74.5	66	4	4	4
Larvae (7 dpf)	Blue	n/a	60	ND	70.9	39	4	4	4
Larvae (7 dpf)	UV	n/a	100	ND	74.5	111	4	4	4
Larvae (7 dpf)	Rods	n/a	28	ND	68.1	34	4	4	4
							Total = 16	**9**	**9**

For each cone subtype, the mean angular positions of basal bodies from several data sets were graphed on circular plots and used to calculate a grand mean angular position (Figure 9A-D; Table 2). The basal bodies of the red-/green-sensitive double cones and blue-sensitive cones were strongly polarized toward the optic nerve in almost all fields, although a few data sets were less polarized. The grand mean angular position of all basal bodies in the red-/green-sensitive cones and the blue-sensitive cones was 91º and 87°, respectively, whereas that of the UV-sensitive cones was 151° (Figure 9D). As cone organization transitions into the row mosaic during metamorphosis (Allison, Barthel et al. 2010), which is a time of significant morphological and hormonal changes (Brown 1997; Parichy, Elizondo et al. 2009), I next addressed whether basal body patterning may be influenced by developmental changes. Basal body positioning was analyzed in multiple fields near the optic nerve, near the middle of the retina, and near the peripheral retina (Figure 9E; for details see Materials and Methods). For the red-/green-sensitive cones and the blue-sensitive cones, no deviation existed in the average angular position of basal bodies in various regions of the retina (Figure 9F; Table 2). The mean angular position of basal bodies for the UV-sensitive cones remained highly variable across the adult retina. Taken together, these results show that in the adult retina basal bodies of the blue-sensitive cones and the red-/green-sensitive double cones strongly polarize toward the optic nerve, whereas basal bodies of the UV-sensitive cones do not organize in a polarized fashion.

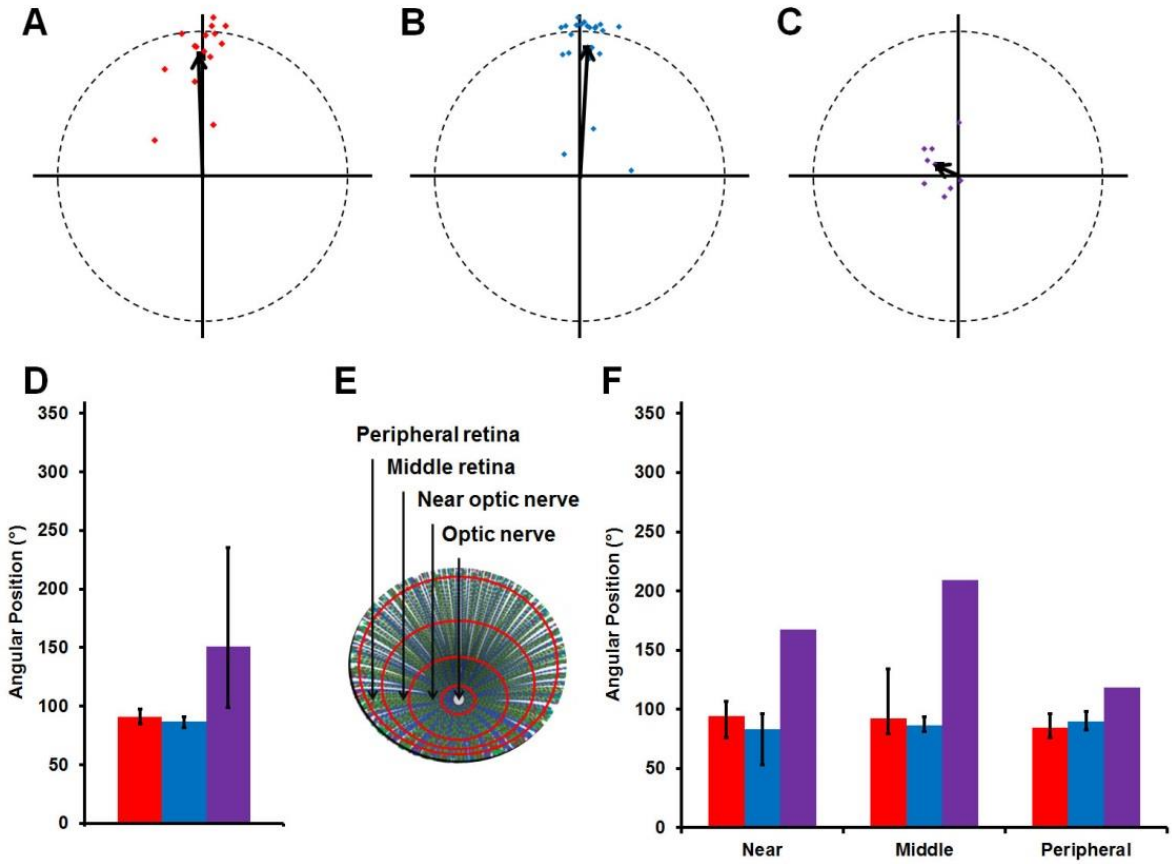

Figure 9. Basal body positioning is consistent throughout the adult retina.
A–C: Mean vectors from individual fields of red-/green-, blue-, or UV-sensitive cone are plotted (red, blue, or purple lozenges, respectively). The grand mean vectors are also plotted (black arrows). Optic nerve is upward. **D:** The grand mean angular position of basal bodies is plotted for each subtype of cones. **E:** Schematic of a flat-mounted retina showing the different regions where fields of cells were analyzed. **F:** The mean position of basal bodies is shown for each subtype of cones in regions of the retina near the optic nerve, in the middle of the retina, and in the peripheral retina. Red-/green-, blue-, and UV-sensitive cones are shown in red, blue, and purple, respectively. Error bars represent the confidence intervals that are calculated to 95% confidence. The lack of error bars for UV-sensitive cones indicates the strength of the trend was too weak to calculate a confidence interval. A magenta-green version of this figure is provided in the Appendix.

I next asked whether basal bodies in adult rod photoreceptors were polarized. Although cone subtypes are tiered within the outer nuclear layer (ONL), the cell bodies and ellipsoids remain in close proximity to each other (Figure 6A). In contrast, the rod nuclei and cell bodies are located on the most vitreal portion of the ONL, whereas the slender rod inner segments project past the cones such that the rod ellipsoids and outer segments cluster above the cone outer segments. To follow rods clearly from the cell body to the ellipsoid, I used the *Tg(XlRho:EGFP)*^{fl1} transgenic line, which expresses a soluble eGFP throughout the rods but not in cones (Fadool 2003). Tangential cryosections were stained with antibodies against γ-tubulin and GFP to label basal bodies within the rods. Rod basal bodies were identified in cells immunopositive for GFP (Figure 10A). Although the transgene expresses a soluble GFP that extends throughout the cytoplasm, the GFP immunoreactivity was limited to the periphery of the rods (Figure 10A). This may reflect reduced antigen accessibility resulting from the sodium citrate treatment required to label with γ-tubulin or by the exclusion of GFP from the mitochondria within the ellipsoids (Fadool 2003). Similar to the UV-sensitive cones, rod basal bodies were randomly oriented in all fields analyzed (Figure 10B, C).

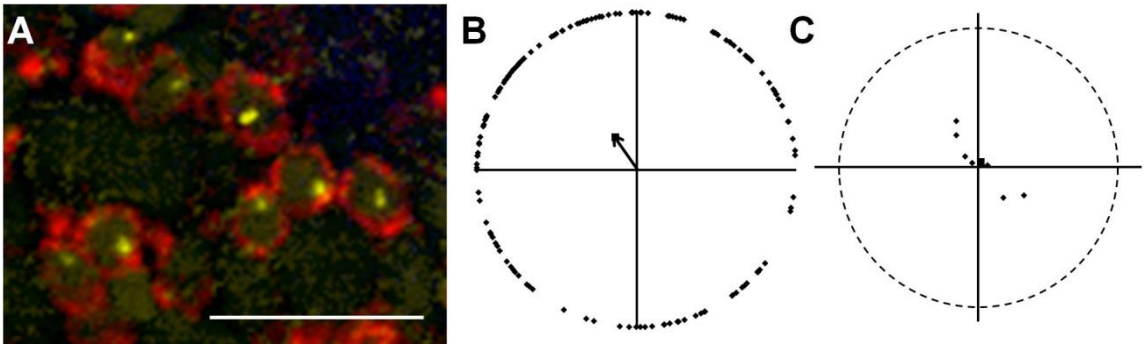

Figure 10. Rod basal bodies are randomly positioned.
A: Basal bodies of rod photoreceptors within the mosaic of a dark-adapted retina. GFP immunoreactivity (red) labels rods in the XOPS-GFP line. γ-Tubulin (yellow) localizes to basal bodies. Nuclei were stained with DAPI (blue). Autofluorescence at 488 nm (green) shows inner and outer segments. **B:** Graphic analysis of rod basal bodies from an individual field of cells. The mean vector is indicated as a black arrow. **C:** Plot showing the mean vectors from several individual fields of rods (lozenges) and the grand mean vector of these mean vectors (square). The optic nerve is upward in all panels, and all fields analyzed were from the middle or peripheral retina. A magenta-green version of this figure is provided in the Appendix. Scale bar = 10 μm.

The random positioning of basal bodies in the UV-sensitive cones suggests that the mechanisms guiding basal body polarization in the other cone subtypes are missing from UV-sensitive cones or that a nonpermissive signal from neighboring cells may be present. As the cell bodies of UV-sensitive cones largely contact only rods, I asked whether the absence of rods would permit the polarized organization of basal bodies with the UV-sensitive cones. Toward this end, I analyzed basal body positioning in cones from the XOPS-mCFP transgenic line (Morris, Schroeter et al. 2005). This line expresses a membrane-targeted cyan fluorescence protein (CFP) that selectively kills rods beginning at 3.5 dpf, with an almost complete absence of rods by 5 dpf (Morris, Schroeter et al. 2005). The adults completely lack rods outside the retinal margin

(Morris, Schroeter et al. 2005). I did not detect any effects of rod degeneration on the cone row mosaic and individual subtypes were located in the normal tiering patterns. As with wild-type retinas, I found that the basal bodies of red-/green- and blue-sensitive cones in the adult XOPS-mCFP mosaic remained strongly oriented toward the optic nerve, whereas UV-sensitive cones had randomly oriented basal bodies (Figure 11, Table 2). The average angular positions of the red-/green-sensitive cones and blue-sensitive cones were 81° and 88°, respectively. There appeared to be more deviation in basal body positioning in the red-/green-sensitive cones of XOPS-mCFP fish than in wild-type adults, but the overall trend remained nonrandom (Table 2). In contrast, the basal bodies of UV-sensitive cones remained randomly positioned. These results suggest that rod photoreceptors do not negatively affect the arrangement of basal bodies in UV-sensitive cones. Furthermore, rod degeneration in XOPS-mCFP transgenic zebrafish does not dramatically alter the intrinsic pattern observed in red-/green-sensitive and blue-sensitive cones.

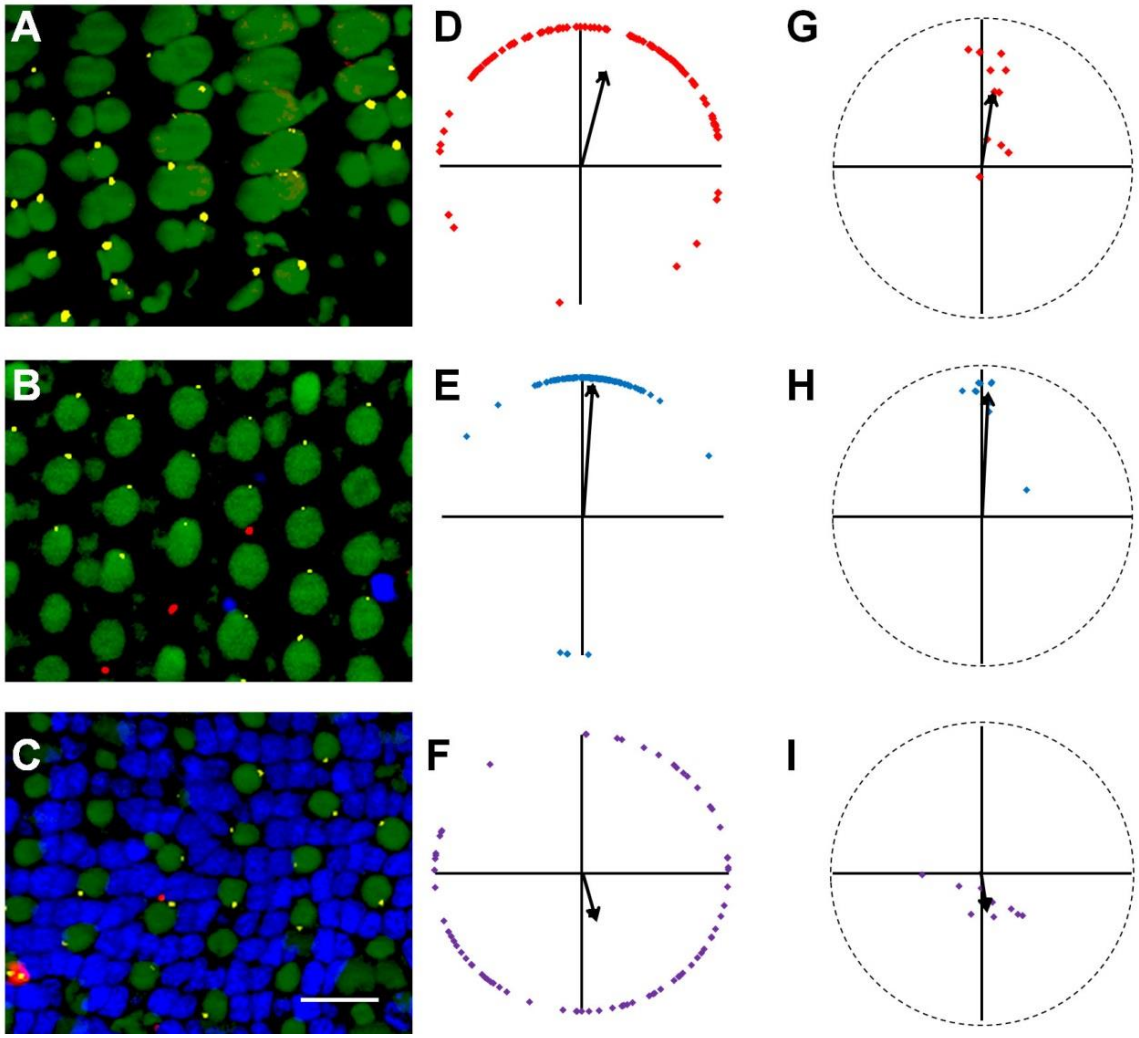

Figure 11. Loss of rods does not affect basal body positioning in cones.
Sample portions of fields of cells at the depths of the basal bodies of red-/green-sensitive cones (**A**), blue-sensitive cones (**B**), and UV-sensitive cones (**C**) show basal body positioning in adult light-adapted XOPS-mCFP zebrafish retinas. **D–F**: Graphs of the positions of basal bodies from fields A–C in which the positions of all the basal bodies of red-/green-, blue-, or UV-sensitive cones were plotted around a unit circle (red, blue, or purple lozenges, respectively), and the mean vector is indicated (arrow). **G–I**: Mean vectors of basal bodies from individual fields of red-/green-, blue-, and UV-sensitive cones are plotted (red, blue, and purple lozenges, respectively). The grand mean vector of these mean vectors is indicated (arrow). Optic nerve is upward in all panels. Small numbers of remaining rods are occasionally visible (red). γ-Tubulin (yellow) localizes to basal bodies. Nuclei were stained with DAPI (blue). Autofluorescence at 488 nm (green) shows inner and outer segments. All fields analyzed were from the middle retina. A magenta-green version of this figure is provided in the Appendix.

I next asked whether the basal body position that I observed also appeared in the larval retina. I used the *Tg(-5actb2:cetn2-GFP)*^{cu6} line to identify basal bodies with a centrin-GFP transgene (Randlett, Poggi et al. 2011). Centrins are Ca^{2+} binding proteins that localize to basal bodies (Wolfrum 1995), and the centrin-GFP transgene is a viable marker for centrioles and basal bodies (Borovina, Superina et al. 2010). Basal body position was quantified by using the *Tg(-5actb2:cetn2-GFP)*^{cu6} line and the results were similar to those obtained from immunostaining with γ-tubulin (Figure 12). Transgenic larvae were analyzed at 7 dfp when photoreceptor outer segments were present and the animals exhibited robust visual behaviors (Brockerhoff, Hurley et al. 1995).Unlike the adult retina, the larval retina lacks the crystalline row mosaic, which prevents identification of cone subtypes simply by position within the mosaic (Allison, Barthel et al. 2010). I therefore analyzed sagittal sections of 7-dpf wild-type zebrafish retinas labeled with polyclonal antibodies against cone opsins, which label outer segments, and with monoclonal antibodies that label entire red-/green-sensitive cones and rods. Serial sections could then be labeled with GFP antibodies to identify centrin-GFP. Fields of cells that contained the optic nerve also contained photoreceptors that were perpendicular to the optical plane of the image and could be viewed head-on as in a flat-mounted retina. The basal bodies of red-/green- and blue-sensitive cones were located at similar optical depths within the retina, whereas the basal bodies of the UV-sensitive cones were located more vitreally. Consistent with previous reports (Vihtelic, Doro et al. 1999), zpr-1 colabeled the cones labeled with anti-green opsin and did not colocalize with the cones labeled with anti-blue opsin (Figure 7). Basal bodies located within zpr-1

positive red-/green-sensitive cones were randomly positioned (Figure 13C, G). To identify blue-sensitive cones accurately, I immunostained larval sections with both the monoclonal zpr-1, which labels red-/green-sensitive cones, and the rod-specific monoclonal antibody 4C12 (Morris, Schroeter et al. 2005). Basal bodies in cones lacking both zpr-1 and 4C12 staining (i.e., blue-sensitive) were also randomly positioned (Figure 13D, H). The UV-sensitive cones, which did not stain with zpr-1 and could be identified as having wide outer segments and by their vitreally tiered position within the ONL, also possessed randomly positioned basal bodies (Figure 13E, I). Rods were identified by staining sections with only 4C12 and the basal bodies within 4C12-positive cells were also randomly positioned (Figure 13F, J). Taken together, these results show that basal bodies and cilia do not polarize in larval animals, suggesting an active mechanism that rearranges cilia polarity after photoreceptor outer segments have formed.

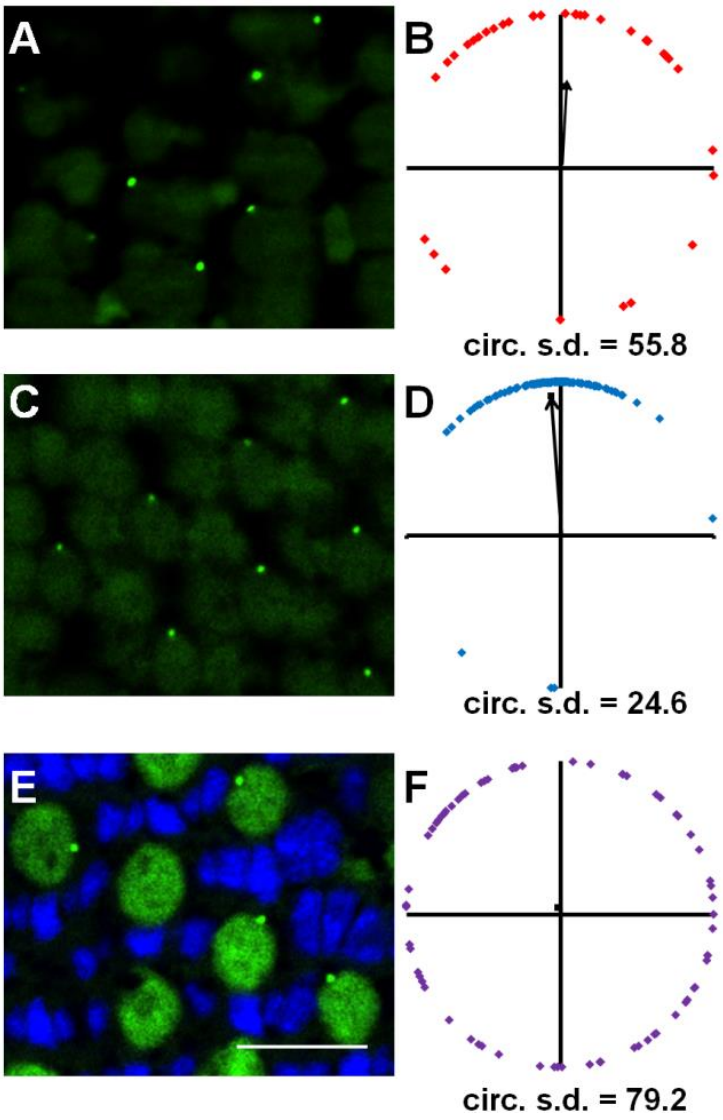

Figure 12. Centrin-GFP labels basal bodies in the retinas of adult *Tg(XlRho:gap43-CFP)*^{ucd1} transgenic zebrafish.
Sample portions of fields of cells at the depths of the basal bodies of red-/green-sensitive cones (**A**), blue-sensitive cones (**C**), and UV-sensitive cones (**E**). GFP fluorescence localized to basal bodies (green), and nuclei were counterstained with DAPI (blue). Autofluorescence (green) from 488-nm excitation shows inner and outer segments. **B,D,F:** Graphs of the positions of basal bodies from fields A,C,E in which the positions of all the basal bodies of red-/green-, blue-, or UV-sensitive cones were plotted around a unit circle (red, blue, or purple lozenges, respectively), and the mean vector is indicated (arrow). Optic nerve is upward in all panels. A magenta-green version of this figure is provided in the Appendix. Scale bar = 10 μm.

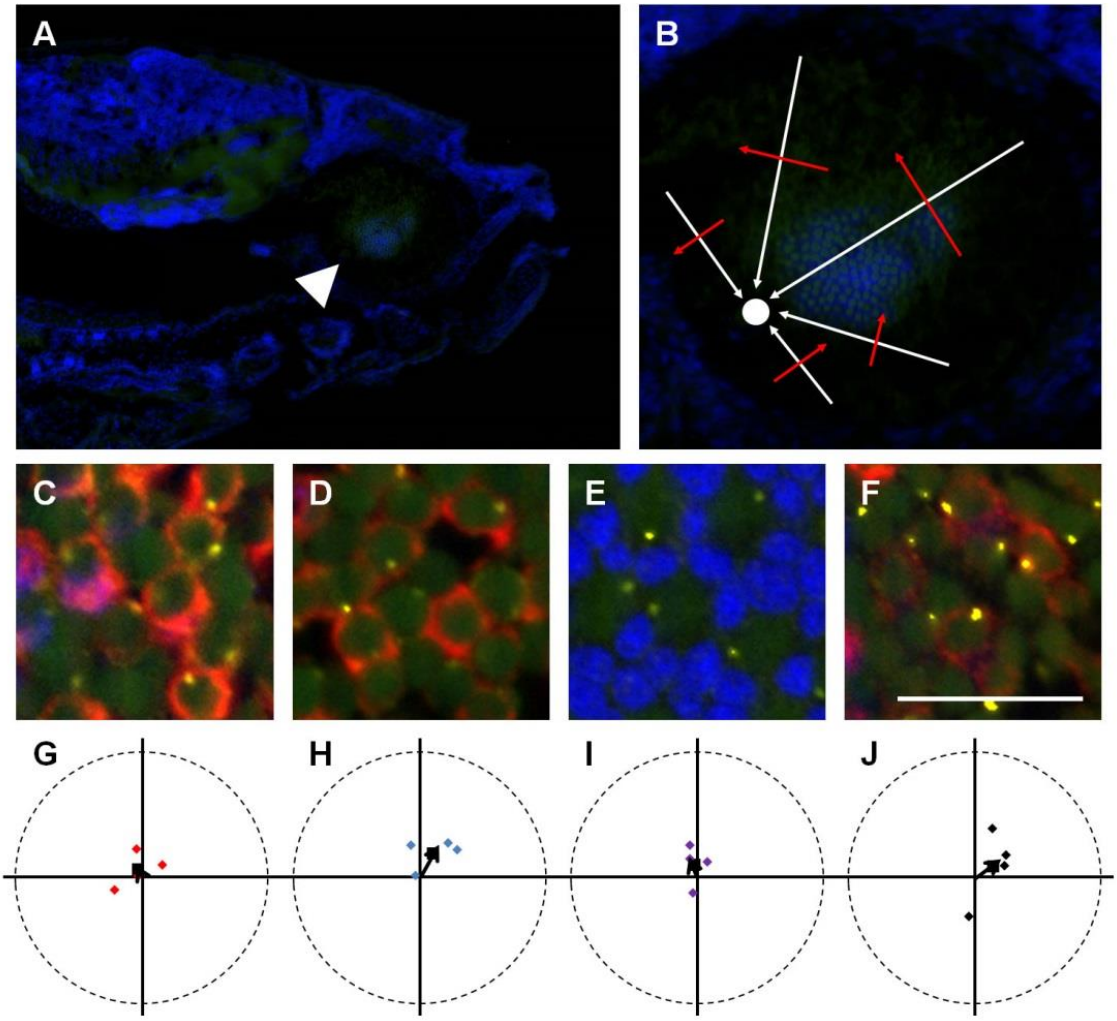

Figure 13. Larval photoreceptor basal bodies are randomly positioned.
A: Sagittal section through a 7-dpf Tg(-5actb2:cetn2-GFP)cu6 larvae shows the optic nerve (arrowhead) and larval retinal mosaic (arrow). **B:** Enlarged view of sectioned retina shows how to determine the orientation of cells relative to the optic nerve (circle). White arrows indicate the direction of the optic nerve, whereas red arrows indicate the 90° perpendicular angle. **C,D:** Immunostaining with zpr-1 (red) and GFP (yellow) antibodies identifies basal bodies in red-/green-sensitive cones. Blue-sensitive cones were negative for zpr-1 and 4C12 immunoreactivity (arrows). **E:** Inner and outer segments (autofluorescence from excitation with 488-nm light) and basal bodies (yellow) of UV-sensitive cones. **F:** Basal bodies (yellow) and 4C12 (red)-immunopositive rods. **G–J:** Mean angular positions of individual fields of red-/green-, blue-, and UV-sensitive cones and rods are plotted on circular graphs. Grand mean angular positions are shown as black squares. In all images, nuclei are counterstained with DAPI (blue). A magenta-green version of this figure is provided in the Appendix. Scale bar = 10 μm (C–F).

Discussion

In this article, I identify and provide an initial description of the planar polarization of basal bodies within adult zebrafish photoreceptors. The data show for the first time that basal bodies of red-/green-sensitive and blue-sensitive cones preferentially align on the edge of the ellipsoid directed toward the optic nerve. UV-sensitive cones and rod photoreceptors do not, however, exhibit this polarized positioning. Furthermore, because this pattern does not exist in the larval retina, the mechanisms driving this polarization do not occur during photoreceptor differentiation. Finally, basal body positioning within the cones was not disrupted by early-onset rod degeneration. Because basal bodies anchor the cilium within the cell body, I conclude that cilia within specific cone subtypes become asymmetrically positioned in an age-dependent manner.

Planar polarization of basal bodies and cilia has been described for multiciliated cells, as well as primary motile cilia of the embryonic node (Park, Mitchell et al. 2008; Mitchell, Stubbs et al. 2009; Borovina, Superina et al. 2010; Mirzadeh, Han et al. 2010), but the polarization of nonmotile cilia and sensory cilia remains poorly understood. The asymmetric localization of cilia to one side of the apical cell surface has been termed *translational planar polarity* (Mirzadeh, Han et al. 2010) and is observed for ependymal cilia (Mirzadeh, Han et al. 2010), kinocilia of the vertebrate inner ear (Jones, Roper et al. 2008), and in lens fiber cells (Sugiyama, Stump et al. 2010). Such nonrandom arrangements clearly argue for active signaling mechanisms to regulate basal body placement. However, although components of the PCP pathway govern the planar polarization of basal bodies in both motile and nonmotile cilia, reports differ on whether

an intact PCP pathway is necessary (for review see Wallingford and Mitchell 2011). For motile cilia, planar polarization of basal bodies coordinates the beating by multiple cilia on a single cell, as well as coordinating ciliary beating across a plane of cells (Wallingford 2010). In contrast, it is not immediately obvious why the nonmotile cilia of photoreceptors would require polarized positioning. Photoreceptor packing should not depend on cilia position, since the diameter of the cilium is considerably smaller than that of the outer segment, and cilia placement would not influence outer segment location. Consistent with this, the placement of UV-sensitive cones and rods into the photoreceptor mosaic occurs without cilia adopting any translational polarity. In a similar fashion, the loss of PCP signaling disrupted the hexagonal cell packing of lens fiber cells, but the planar polarization of primary cilia was unaffected. This suggests that translational polarity of cilia and cellular packing are independent, at least in some cell types (Sugiyama, Stump et al. 2010).

Why do the basal bodies exhibit translational polarity in red-/green-sensitive and blue-sensitive cones, but not in the UV-sensitive cones and rods? One possibility is that basal body positioning is a cone-specific phenomenon. The UV-sensitive cones and rods share a number of similarities not shared by other cones. It has been suggested that rods and UV-sensitive cones, the likely S-cone homolog, share a common multipotent progenitor in teleosts (Alvarez-Delfin, Morris et al. 2009), and this may skew UV-sensitive photoreceptors into a more "rod-like" cell. The lack of planar polarity in rod basal bodies could explain why this phenomenon was not observed earlier, insofar as the rod-dominated mouse retina remains the favored model of study. It is important to note,

however, that an examination of adult retinas from the cone-dominated tree shrew, *Tupaia*, showed that cilia were "located eccentrically on the same side of the inner segments in hundreds of neighbouring cones," but such a phenomenon was rarely seen in younger animals (Knabe and Kuhn 1998). An alternative, though not mutually exclusive, explanation is that the signaling mechanism required to position the basal bodies must operate through specific contacts at the level of the myoid or ellipsoid. The ellipsoids of the UV-cones are located below those of the other cones, whereas rod ellipsoids are more scleral than the other cones. Thus, neither the UV-sensitive cones nor the rods make contact with other cells at the level of the ellipsoids to propagate a signal (Figure 6A). The lack of cell-cell contact between ellipsoids would likely prevent any kind of planar signaling from neighboring cones to the UV-cones, and even rods. This may also explain why basal bodies in UV-sensitive cones failed to polarize in the XOPS-mCFP line, insofar as the absence of rods does not affect the ellipsoid position of UV-sensitive cones or the ability of these cells to receive a polarizing signal.

It is interesting to note that basal bodies become polarized after the larval stage, likely during the metamorphic changes into adulthood. This suggests that the mechanisms governing basal body polarization are not required for photoreceptor development but may serve critical functions later in photoreceptor maturation or maintenance. The lack of an observable basal body pattern in larvae precludes the analysis of most zebrafish mutants to search for candidate signaling pathways because these mutants are typically lethal prior to metamorphosis. Creating genetically mosaic animals by blastula transplantation (Moens and Fritz 1999) may allow examination of

cells lacking key genes, as long as these genes are not essential for photoreceptor differentiation. Previous studies have noted that the larval mosaic also transitions into the adult row mosaic at metamorphosis and may reflect a change in visually mediated behaviors such as feeding and mating (Allison, Barthel et al. 2010). It is unclear whether basal body polarization simply correlates temporally with this anatomical rearrangement or whether these processes share similar molecular mechanisms.

In summary, I provide the first detailed evidence that basal bodies in vertebrate photoreceptors show planar polarity. A similar phenomenon was briefly mentioned for tree shrews (Knabe and Kuhn 1998), suggesting that basal body polarity can also occur in mammals, including primate-like animals. Such planar polarity is critical for motile cilia function but the importance for primary cilia and sensory cilia is unknown.

CHAPTER III

POSITIONING OF BASAL BODIES IN CYPRINID CONE PHOTORECEPTORS MAY BE INFLUENCED BY LIGHT EXPOSURE DURING RETINA DEVELOPMENT AND BY CELL-CELL CONTACT

Overview

Basal bodies in zebrafish red-, green-, and blue-sensitive photoreceptors exhibit translational planar polarity, but the basal bodies of ultraviolet (UV)-sensitive cones are disorganized. I investigate three potential mechanisms behind this disorganization: 1) UV light absence, 2) reduced selective pressure, and 3) lack of adequate cell-cell contact. While the lack of UV light exposure in lab-reared zebrafish does not appear to affect their photoreceptor mosaic, I show that limited light during development corresponds with some changes in basal body positioning, including increased bimodality, and in visually-mediated behavior. Wild-caught zebrafish, which do not have the reduced selective pressure of lab-reared zebrafish, do not show evidence of changes in their basal body positioning. Wild-caught specimens of another cyprinid, the red shiner (*Cyprinella lutrensis*), have a similar photoreceptor row mosaic but different tiering of the photoreceptors and their cell bodies. This change in cell body tiering corresponds with a change in basal body positioning and suggests that cell-cell contact, consistent with that necessary for the planar cell polarity (PCP) pathway, is important for positioning photoreceptor basal bodies. Also consistent with the PCP pathway's

potential involvement in photoreceptor basal body patterning, I found that genes involved in this pathway are expressed in the zebrafish retina.

Introduction

Translational polarity of cilia, characterized by patterned, asymmetrical localization of cilia within cells via the planar cell polarity (PCP) pathway, has been established in several vertebrate model systems, for example in the mouse inner ear (Montcouquiol, Rachel et al. 2003), in the *Xenopus laevis* gastrocoel roof plate (Antic, Stubbs et al. 2010), and in the zebrafish embryonic floorplate (Borovina, Superina et al. 2010). Important to the asymmetrical localization of cilia is the asymmetrical localization of the core PCP proteins Frizzled, Dishevelled, Van Gogh, and Prickle (for review, see Wallingford 2010). Recently, I described a similar localization of basal bodies, which orient and localize to the base of cilia, in the cone photoreceptors of adult zebrafish (Ramsey and Perkins 2013). We showed that the basal bodies of red-, green-, and blue-sensitive cones are positioned on the side of the cell that is closest to the centrally-located optic nerve. The positioning was not disrupted in retinas lacking rods. However, no basal body patterning was observed in UV-sensitive cones.

It is currently unknown if the translational polarity of basal bodies in zebrafish photoreceptors is controlled by the PCP pathway. In addition to the organization of basal bodies, the photoreceptors themselves are arranged in a well-organized row mosaic composed of alternating rows of red-/green-sensitive double cones and blue- and UV-sensitive cones that radiate out from the optic nerve with new columns of cones added to

the peripheral circumference as the retina grows (Engström 1960; Raymond, Barthel et al. 1993; Allison, Barthel et al. 2010). A recently proposed mathematical model of how this cell mosaic forms integrates the potential roles of the PCP pathway and mechanical forces (Salbreux, Barthel et al. 2012). Consistent with this model, proteins in the Crumbs complex, which are involved in maintaining cell-cell adhesion between photoreceptors (Wei, Zou et al. 2006), are planar polarized in the inner segments of red-, green-, and blue-sensitive cones but are either not expressed or not polarized in UV-sensitive cones (Zou, Yang et al. 2010; Salbreux, Barthel et al. 2012; Zou, Wang et al. 2012). Although the absence of UV-sensitive cones during mosaic formation disrupts the organization of the photoreceptor mosaic, it does not disrupt this protein polarization in individual cells and in short chains of cells in the remaining cones, albeit long columns of cells are absent (Raymond, Colvin et al. 2014). Together, these data show that UV-sensitive cones fail to exhibit the planar polarity observed in other cone subtypes. Here, I investigate the mechanisms underlying disorganization of the basal bodies of UV-sensitive cones in zebrafish. The cause of basal body disorganization in UV-sensitive cones will give insight into the mechanism controlling basal body orientation in zebrafish photoreceptors. Herein, I test three different hypotheses for the mechanism by which the basal bodies of UV-sensitive cones fail to become organized.

First, since lab-reared zebrafish are not generally exposed to UV light, I tested the hypothesis that lack of UV light inhibits basal body patterning in UV cones. Supporting this, zebrafish larvae raised in long-wavelength (orange) light showed decreased light sensitivity in their blue- and UV-sensitive cones (Dixon, McDowell et al.

2004). This indicates that light deprivation may lead to functional changes in photoreceptors. Furthermore, it is well established that light and dark adaptation in the vertebrate eye includes retinomotor movements of photoreceptors: cones contract and rods elongate in the light, and vice versa in the dark (for review, see Burnside and Nagle 1983). Because cell-cell contact is important to relaying the signal of the core PCP proteins (Wu and Mlodzik 2008), and because the vertical positioning of photoreceptors in relation to each other changes in response to light, constant rearing under different light environments may provide different cell-cell contacts and different cilia arrangements. Therefore, I reared zebrafish under different light wavelengths to determine if the addition of UV light organized UV-sensitive cone basal bodies or if the removal of light from the other cones disorganized their basal bodies. I also assessed visually-mediated behaviors in these fish to determine if any changes in basal body positioning corresponded with functional changes in vision.

Second, I tested if the reduced selective pressure on many generations of lab-reared zebrafish is responsible for the disorganization of UV-sensitive cone basal bodies. While it has been established that lab-reared adult zebrafish have functional UV-sensitive cones (Nava, An et al. 2011), their functionality may not be optimal. Detrimental fitness effects have been shown to occur from both inbreeding and outbreeding laboratory zebrafish stocks (Monson and Sadler 2010). As lab-reared zebrafish are not standardly exposed to UV light, and as these fish also lack predatory and foraging pressures that wild fish would be constrained by, mutations negatively

affecting the UV-sensitive cones might be introduced into these populations. I addressed this possibility by measuring basal body positioning in wild-caught zebrafish.

Third, I investigated the hypothesis that the lack of cell-cell contact of the UV-sensitive cones with the other cone types is responsible for the disorganization of UV-sensitive cone basal bodies. The photoreceptors in the zebrafish retina are tiered, and UV-sensitive cones are located beneath the other cones with UV-sensitive cone outer segments being found at the same retinal depth as the other cone nuclei (Branchek 1984). Even if the lack of exposure to UV light does not contribute to this tiering, this positioning in itself may fail to provide the cell-cell contact necessary to propagate a signal to organize the cilia, such as would be necessary if the PCP pathway patterns the other cones. Besides being lower within the retina relative to the other cones, this position also means that Müller glial processes surround the UV-sensitive cones and may minimize direct contact with other cells, whereas the inner segments of the other cone subtypes are capable of direct cell-cell contact (Salbreux, Barthel et al. 2012; Zou, Wang et al. 2012). Because I am unaware of any zebrafish lines with alternate tiering patterns, I sought out other cyprinids with a similar row mosaic but different tiering. I found the red shiner (*Cyprinella lutrensis*) to be a suitable example of alternate tiering. To directly assess the possibility that the PCP pathway is involved, I also observed the expression of genes involved in the PCP pathway in the adult zebrafish retina.

I have shown that limited light during development corresponds with increased disorganization and bimodality in basal body positioning of red-, green-, and blue-sensitive cones. Limited light during development is correlated with a change in

visually-mediated behavior, but this may be a behavioral rather than visual change. The lack of UV light and the lack of selective pressure do not appear to affect basal body positioning in lab-reared zebrafish. The disorganized basal body positioning in the blue-sensitive-like cones of red shiners and the expression of PCP genes in the zebrafish retina both support the conclusion that cell-cell contact is important for establishing basal body patterning in cyprinids.

Materials and Methods

Animals

Zebrafish (*Danio rerio*) were lab-reared wild type AB/Ekkwill hybrids or wild-caught from rivers in West Bengal or Assam, India. Red shiners (*Cyprinella lutrensis*) were wild-caught from the Brazos River near Navasota, Texas.

Zebrafish were maintained according to standard procedures (Westerfield 1995). For feeding behavior and OMR experiments, rearing conditions were changed as follows. Once zebrafish reach 13 days post fertilization (dfp), they were removed from static nursery tanks and distributed among five tanks in common flow-through systems. Situated approximately 6 inches above the tanks was a UV bulb (32 Watt 11476 48-inch Desert Series 50 UVB T8 fluorescent, Zilla, Franklin, WI) that supplemented standard fluorescent lighting in the room. Lighting followed the normal cyclic conditions (14 hours light, 10 hours dark). Four tanks were placed under this lamp. One (normal light) was a standard polycarbonate tank and lid. The lid served as an effective filter for UV light (<400 nm) and allowed other light through. One (UV light) was a standard tank

with a lid made of a single layer of thin mesh with half-inch-squared holes to allow maximum UV exposure. One (yellow light) was a standard tank covered on all sides by a yellow gel sheet (Rosco Roscolux light filter #312: Canary; Rosco Laboratories, Stamford, Connecticut) with a lid made of the same gel sheet. One (red light) was a standard tank covered on all sides by a red gel sheet (Rosco Roscolux light filter # 19: Fire) with a lid made of the same gel sheet. Further away from the light source, a fifth tank receiving minimal light (dark) was covered with cardboard that blocked light. Dark fish received brief small amounts of light during feedings and health monitoring. The health of all fish was regularly monitored.

Filters were chosen based on their ability to block light to UV- and blue-sensitive cones (yellow filter) and to UV-, blue-, and green-sensitive cones (red filter). Blue cones lose sensitivity to light by 500 nm with minimal light absorbance above 450 nm and maximum absorbance at 407 nm; green cones lose sensitivity by 575 nm with minimal absorbance above 525 nm and maximum absorbance at 473 nm (Cameron 2002). The yellow filter transmits no light through 440 nm, 1% of light at 460 nm, 6% at 480 nm, and 30% at 500 nm. The red filter transmits no light through 540 nm, 1% at 560 nm, and 15% at 580 nm. Transmission spectra of filters are available at www.Rosco.com.

Optomotor response assay

Adult lab-reared wild type zebrafish which had been raised for nine months under different light environments were used for behavioral testing. The number of fish

tested in the behavioral tests was as follows: 2 from UV light, 10 from white light, 4 from yellow light, 6 from red light, and 5 from the dark. One day prior to behavioral testing, zebrafish were moved to individual tanks and allowed to adapt to white light. Fish were maintained in these tanks for the duration of behavioral testing. Optomotor response (OMR) was measured similar to as described in Krauss and Neumeyer (2003). Briefly, it involved placing a fish inside a glass beaker through which they could see black and white stripes lining a larger outside cylinder. When the stripes are rotated, the fish have a tendency to follow the stripes. The outer cylinder was rotated at a rate of 10 rotations per minute and measurements were taken for one minute. During this minute, a count was kept of how many times the fish crossed a reference line at one place along the circumference of the beaker in each direction. The net rotations/minute was calculated by subtracting the net crossings in the least frequent direction from the net crossings in the most common direction. OMR in four light environments was tested: white light, white light with the red filter, white light with the yellow filter, and white light with UV light. Each fish was randomly tested once from 10:00 AM-6:00 PM on the first or second day of behavioral testing. Each test consisted of the following sequence: 1) 1 minute acclimation in white light with no moving stripes followed by 1 minute measurement, 2) 20 seconds acclimation in environment 1 with moving stripes followed by 1 minute measurement, 3) 20 seconds acclimation in environment 1 with moving stripes in the reverse direction followed by 1 minute measurement, 4) 1 minute rest in white light with no moving stripes, 5) Repeat steps 2-4 for environments 2, 3, and

4. Order of environment tested was randomized for each fish. Initial direction of moving stripes was randomized for each environment in each test.

Feeding behavior

Feeding behavior was measured on the second through fifth days of behavioral testing. Lights turned on at 8:00 AM each morning, and fish were allowed to adapt to white light for a minimum of 30 minutes prior to testing. Fish were only fed in the morning for the day subsequent to testing. Tests were performed between 8:30-10:00 AM. When being tested, fish were placed into a chamber that only allowed light through the top of the tank. 20 small (0.5 mm) New Life Spectrum Small Fish Formula sinking pellets (New Life International, Homestead, Florida) were introduced to the tank. These pellets would float throughout the trial unless directly disturbed by a fish. Because the fish would sometimes exhibit a lag period before noticing the food, but would generally begin to eat as fast as they could once food was identified, each fish was observed until it made its first feeding attempt at a floating pellet. When this occurred, the tested light condition was applied (red filter with white light, yellow filter with white light, opaque filter with white light, UV light with white light, or white light). This was maintained for 15 seconds. After 15 seconds, the test condition, if applicable, was removed and the pellets still floating were counted. The fish were given 45 more seconds under white light, and the pellets remaining after every 15 seconds were measured. If fish did not respond to the pellets within 3 minutes, it was not tested that day. This was repeated for

each fish each day. One filter type was tested each day. The order that individual fish were tested was randomized each day. The same fish used in the OMR assay were used for the feeding assay. The following are the fish that were omitted due to not recognizing the food: for the UV trial, one raised in white and one raised in dark; for the white light trial, one raised in white, one raised in yellow, and three raised in dark; for the yellow trial, one raised in white and one raised in dark; for the red trial, two raised in dark; for the dark trial, one raised in white, one raised in red, and four raised in dark. All fish that were unresponsive were unresponsive for only one of the five trials, with the exception of one fish raised in white light (four of five trials) and two fish raised in the dark (three of five and five of five trials).

Histology, microscopy, and image analysis

Retina dissections, immunohistology, microscopy, and measurement of basal body positioning were performed as described by Ramsey and Perkins (2013).

Statistics

For OMR tests, error bars indicate 95% confidence intervals that were calculated by multiplying the standard error of the mean by 1.96. For feeding assays, error bars indicate standard deviation. For the dark raised fish during the dark trial, only one fish was responsive, so no standard deviation could be calculated. Basal body orientation analysis was performed as described by Ramsey and Perkins (2013). Confidence

intervals could not be determined (ND) when positioning was too disorganized and/or sample size was too small. Basal bodies from one field of each cone subtype were quantified from each fish analyzed. Bimodality was assessed using the doubling of angles test, where I multiplied the angle of each basal body position within a field by two after adding 135° to the angle to adjust for the 90° rotation that occurs during the test so that the final plotted orientation of the basal bodies remained comparable (Fisher 1993; Zar 1996).

Reverse transcription polymerase chain reaction (RT-PCR)

TRIzol (Invitrogen, Carlsbad, CA) was used to extract cDNA from 5 samples composed of pooled tissues (from 6 adult zebrafish: 12 lenses, 12 retinas, and 6 hearts, from 1 adult zebrafish: ~50 unfertilized dechorionated eggs, and 20 7-dpf larvae). RT-PCR was performed using Transcriptor First Strand cDNA Synthesis Kit (Roche, Indianapolis, IN).

Results

I tested the hypothesis that cone basal body orientation is influenced by the light environment during development in two ways (Figure 14, Table 3). First, to determine if the addition of UV light led to the polarization of the basal bodies of UV-sensitive cones, I raised zebrafish with UV light added to the normal light environment. Second, to determine if limiting exposure to certain wavelengths of light led to a disruption of the basal body pattern, I minimized exposure to the absorbed wavelengths of light in UV- and blue-sensitive cones (using a yellow filter), in UV-, blue-, and green-sensitive cones (using a red filter), and in all photoreceptors (using an opaque filter). Adding UV light did not lead to a patterning of UV-sensitive cone basal bodies (Figure 14K). Although removing light from the blue cones alone did not lead to any change in basal body patterning for any cone type (Figure 14C,H,M), removing light from all cones but the red (Figure 14D,L) and, more dramatically, from all cones (Figure 14E,J), led to a decreased organization of basal bodies in previously organized cones. I did not observe any change in the organization of photoreceptor mosaic itself.

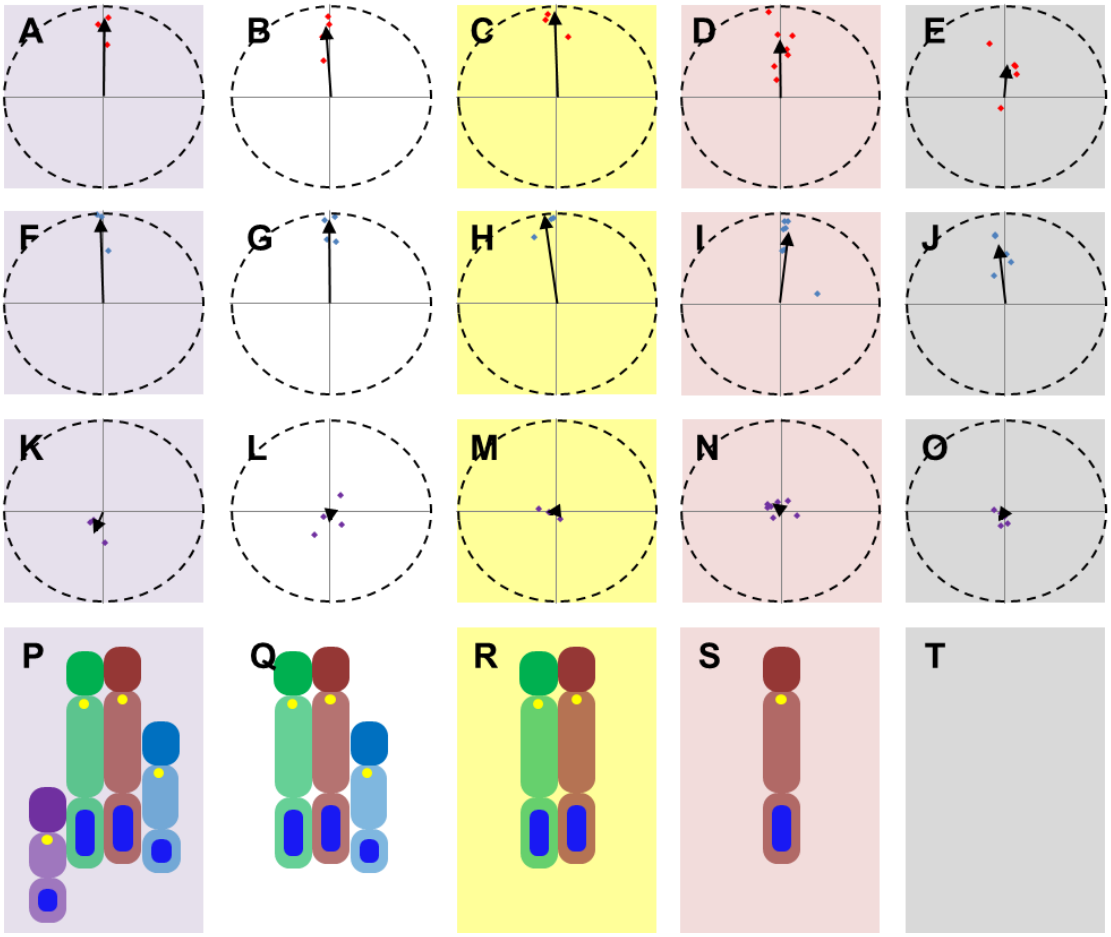

Figure 14. Addition of UV light does not increase basal body patterning in UV-sensitive cones, but reduced light exposure corresponds with decreased patterning in zebrafish cones that are oriented towards the optic nerve under normal light conditions.

A-O: The purple (A,F,K), white (B,G,L), yellow (C,H,M), red (D,I,N), and gray (E,J,O) background colors indicate fish that were exposed to UV+white light, white light, yellow light, red light, and limited light, respectively. Mean vectors of basal body positions from individual fields of red-/green-, blue-, and UV-sensitive cones are plotted with red, blue, and purple diamonds, respectively. The grand mean vectors are plotted with black arrows. **P-T**: These illustrations represent which cones were primarily stimulated in each light condition: all cones in UV+white (P), all cones except UV-sensitive in white (Q), only red-/green-sensitive cones in yellow (R), only red-sensitive cones in red (S), and no cones in limited (T).

Table 3. Numerical Analysis of Basal Body Position (2)

Sample	Rearing environment	Photoreceptor subtype	Mean angular position (0-360°)	95% Confidence interval (°)	Circular s.d.	Avg. No. cells/ field	No. fish
Zebrafish, wild type	UV light	Red/green	89	ND	42	82	3
		Blue	91	ND	35	67	
		UV	251	ND	72	88	
	Normal	Red/green	93	85-147	46	124	4
		Blue	89	68-107	37	76	
		UV	273	ND	78	79	
	Yellow filter	Red/green	91	50-109	36	82	4
		Blue	96	80-130	31	93	
		UV	214	ND	79	133	
	Red filter	Red/green	90	72-105	55	98	7
		Blue	82	46-95	47	102	
		UV	145	ND	79	129	
	Dark	Red/green	82	ND	69	114	5
		Blue	94	66-120	55	89	
		UV	247	ND	77	98	
Zebrafish, wild-caught	Wild	Red/green	87	79-105	32	108	4
		Blue	85	ND	45	98	
		UV	280	ND	74	102	
Red shiner	Wild	Red/green-like	102	ND	58	100	4
		Blue-like	21	ND	73	37	
		UV-like	48	ND	78	58	

When I examined the fields with decreased net organization, rather than observing increased general disorganization, I observed increased bimodality. Basal bodies were positioned both towards and away from the optic nerve, leading to the decreased overall trend (Figure 15). This bimodality was particularly strong in blue-sensitive cones. To visualize and quantify the bimodality, I applied the doubling of angles test that converts a bimodal circular distribution with diametrically opposed modes to a unimodal distribution. If a distribution is bimodal, an increased trend in one direction will be observed, which can be assessed visually and by an increase in the mean resultant length of the mean vector. As expected, no bimodality was observed in the UV-sensitive cones (compare Figure 15G to 15H, 15P to 15Q, 14N to 15I, and 14O to 15R). However, weak bimodality was observed in red-/green-sensitive cones (compare Figure 15A to 15B, 15J to 15K, 14D to 15C, and 14E to 15L), and stronger bimodality was observed in blue-sensitive cones (compare Figure 15D to 15E, 15M to 15N, 14I to 15F, and 14J to 15O). After the bimodality test was applied, although some disorganization was still evident in the red-/green-sensitive cones, almost every field of blue-sensitive cones became strongly oriented towards the optic nerve.

Figure 15. When zebrafish are reared in red light or the dark, bimodal distribution of basal bodies occurs in blue-sensitive cones and, to a lesser extent, in red-/green-sensitive cones.
In the first column (A, D, G, J, M, P), vectors of individual basal body positions within a single sample field for red-/green- (A, J), blue- (D, M), and UV- (G, P) sensitive cones are plotted with red, blue, and purple diamonds, respectively. The mean vector from each field is plotted with a black arrow. In the middle column (B, E, H, K, N, Q), the same is shown after the bimodality test has been applied. In the third column (C, F, I, L, O, R), mean vectors of basal body positions from individual fields of red-/green- (C, L), blue- (F,O), and UV- (I,R) sensitive cones after the bimodality test has been applied are plotted with red, blue, and purple diamonds, respectively. The grand mean vectors are plotted with black arrows, and an increased arrow length corresponds with an increased strength of the trend in that direction. The red (A-I) and gray (J-R) background colors indicate fish that were exposed to red light and limited light, respectively.

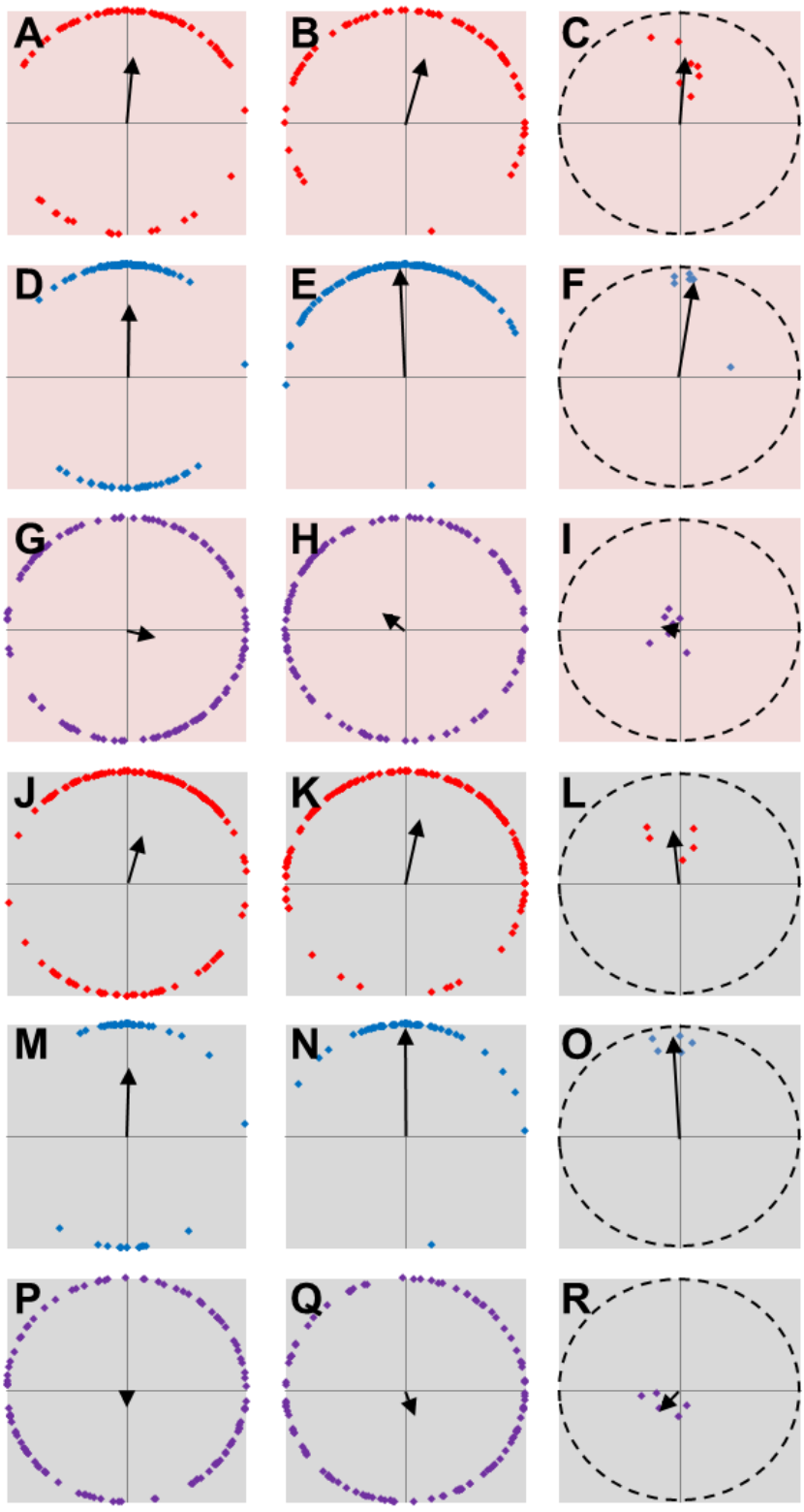
A
B
C
D
E
F
G
H
I
J
K
L
M
N
O
P
Q
R

To determine if the differences in basal body orientation corresponded to differences in visually-mediated behaviors, I used an optomotor response (OMR) assay (Figure 16) and a feeding assay (Figure 17) to test visual behavior. The OMR assay did not reveal any change in behavior based on rearing or testing environment. For the feeding assay, there was no difference according to testing environment, except for those tested in minimal light, which showed minimal feeding behavior during this dark interval (Figure 17A, first 15 seconds). This negative control supports that feeding behavior in zebrafish is a highly visually mediated behavior. While fish raised in various wavelengths of lights showed similar feeding behavior, fish raised in minimal light showed reduced feeding behavioral overall, regardless of if light was present (Figure 17F).

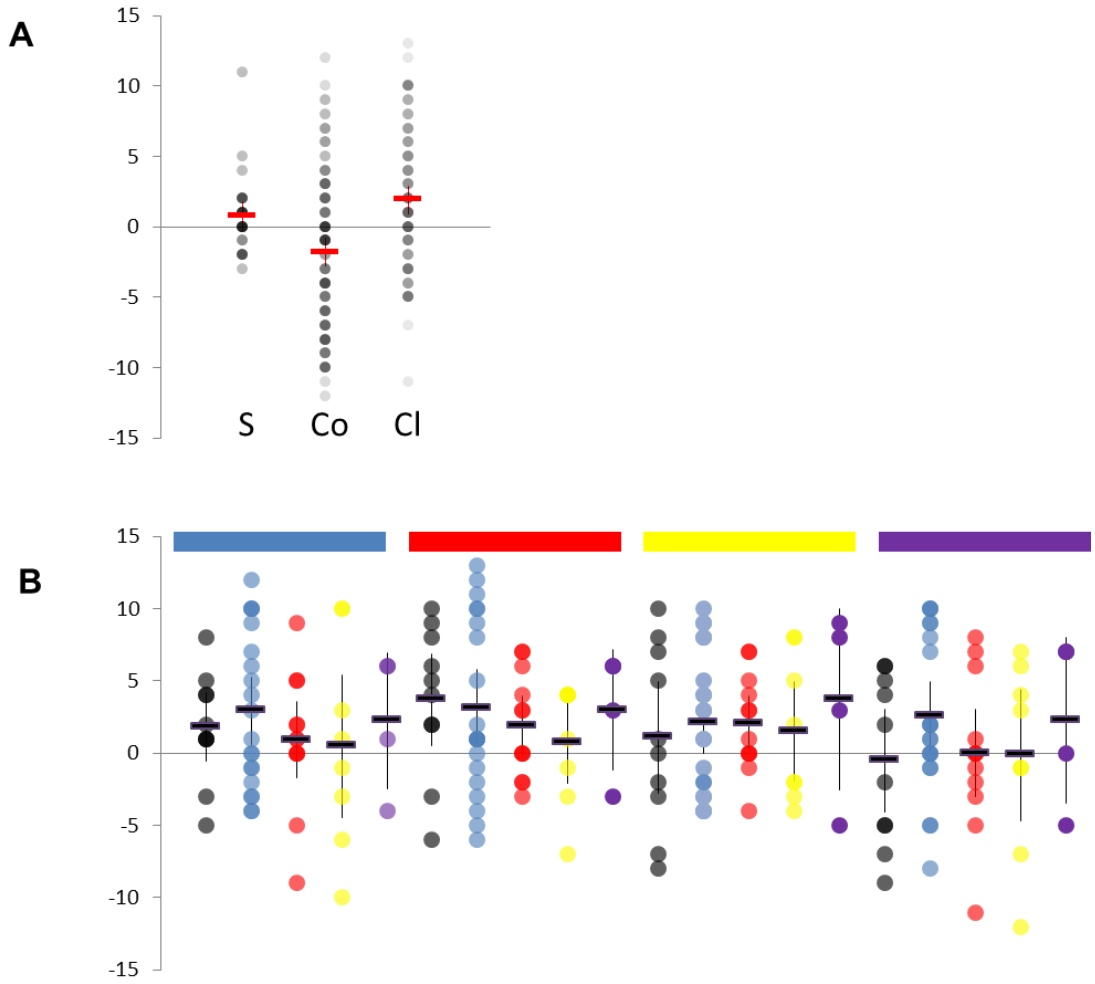

Figure 16. Zebrafish exposed to different light wavelengths during development do not exhibit different optomotor responses.
A: Results from all OMR trials are combined. A positive y-axis value is a net clockwise direction and a negative value is a net counterclockwise direction. S, Co, and Cl indicate trials that were run while the bars were still, moving counterclockwise, and moving clockwise, respectively. Red horizontal bars represent mean values, and vertical error bars show 95% confidence intervals. Darkness of circles increases as the number of trials with results corresponding with that data point increase. **B:** Results from OMR trials are organized as follows: the bar above each group represents the light used during the trial, and the circle colors denote the environmental light wavelengths used during development. Gray, blue, red, yellow, and purple represent dark, white, red, yellow, and UV light environments, respectively. A positive y-axis value indicates net fish rotations/minute in the direction of the moving bars while a negative value indicates net fish movement in the opposite direction of the moving bars. Black horizontal bars represent mean values, and vertical error bars show 95% confidence intervals. Darkness of circles increases as the number of trials with results corresponding with that data point increase.

Figure 17. Zebrafish reared in minimal light show reduced feeding behavior compared to those raised in other light conditions.
Red, light gray, black, yellow, and purple lines indicate fish raised (A-E) or feeding trials conducted (F-J) in red, white, minimal, yellow, or white+UV light, respectively. In all panels, X-axes show time (seconds) and Y-axes show number of pellets remaining. X-axis time points are staggered to allow visualization of error bars. Error bars indicate standard deviation. For each panel, the bar at the top center indicates the rearing conditions for those fish and the bar at the bottom left indicates the conditions that the first fifteen seconds of the test were under. A solid color of the bar indicates all fish in that panel were either reared (if the bar is at the top center) or tested (if the bar is at the bottom left) under that color; a multi-colored bar indicates that the colors of the lines, rather than that bar, indicate the rearing (if the bar is at the top center) or testing (if the bar is at the bottom left) conditions.

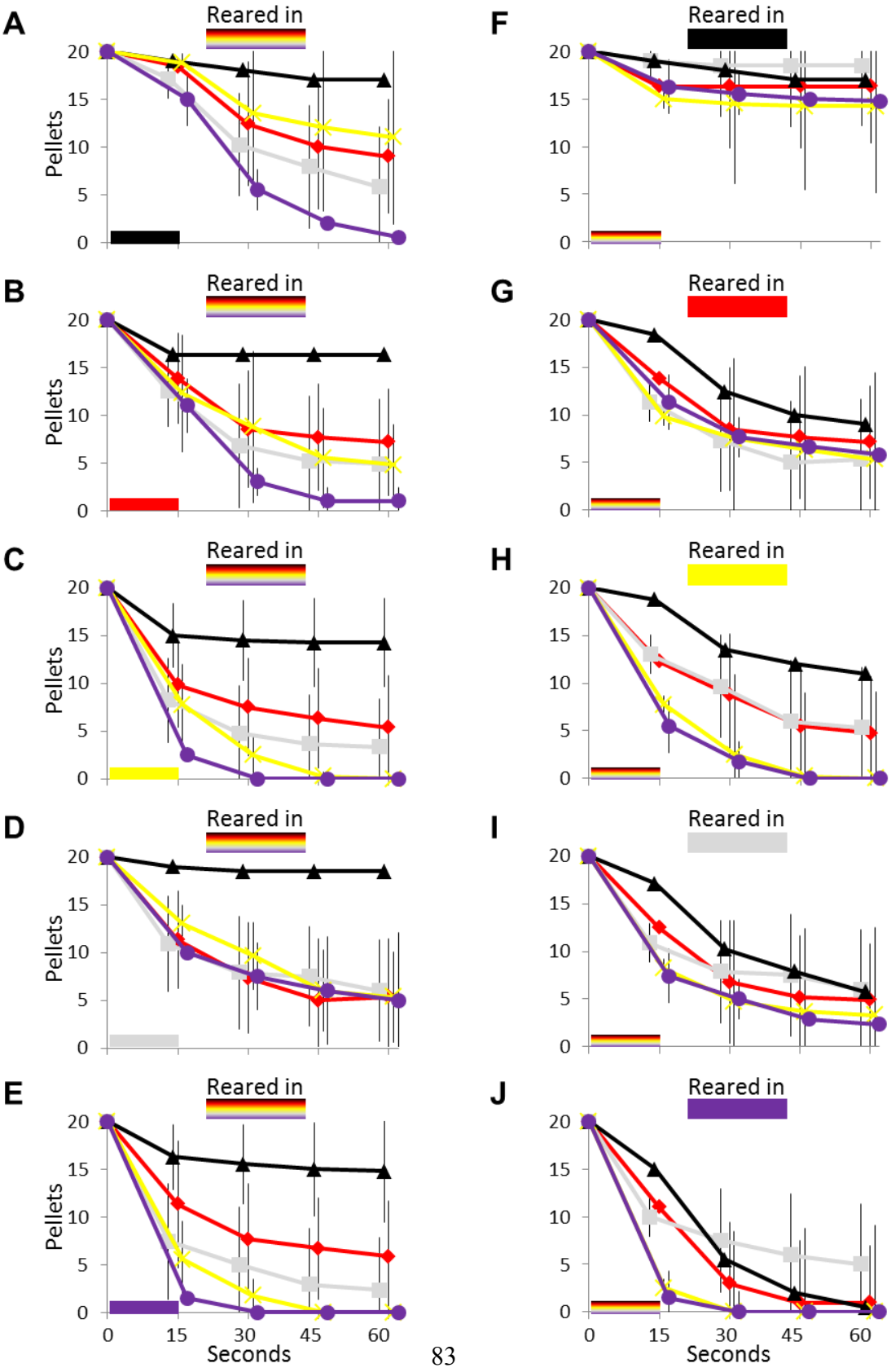
A
Reared in
Pellets
20
15
10
5
0
F
Reared in
B
Reared in
Pellets
G
Reared in
C
Reared in
Pellets
H
Reared in
D
Reared in
Pellets
I
Reared in
E
Reared in
Pellets
0
15
30
45
60
Seconds
J
Reared in
0
15
30
45
60
Seconds

To confirm that the reduced feeding behavior in the dark and the otherwise consistent feeding behavior in the other light environments were not due to a change in motivation on the day of testing, fish were given 45 seconds in white light to eat after the experimental 15 seconds. At the end of this total period, similar numbers of pellets were left each day (Figure 18B). The experimental design required that the fish be tested sequentially each day. However, the order that the fish were tested was randomized each day, and no positional effect was observed (Figure 18C,D).

Laboratory zebrafish lines are not generally raised in the presence of UV light. Therefore, if the basal bodies of UV-sensitive cones are patterned in the wild then this patterning might be lost in laboratory lines due to relaxed selection on UV visual function. To test this possibility, I looked at the basal body patterning in wild-caught zebrafish (Figure 19, Table 3). However, no change in patterning was seen in these fish, suggesting that lab wild type lines do not differ from wild zebrafish in cone basal body positioning. Combined with the lack of patterning in UV-sensitive cones in UV light exposed zebrafish, this suggests that UV light exposure has no influence on the basal body patterning.

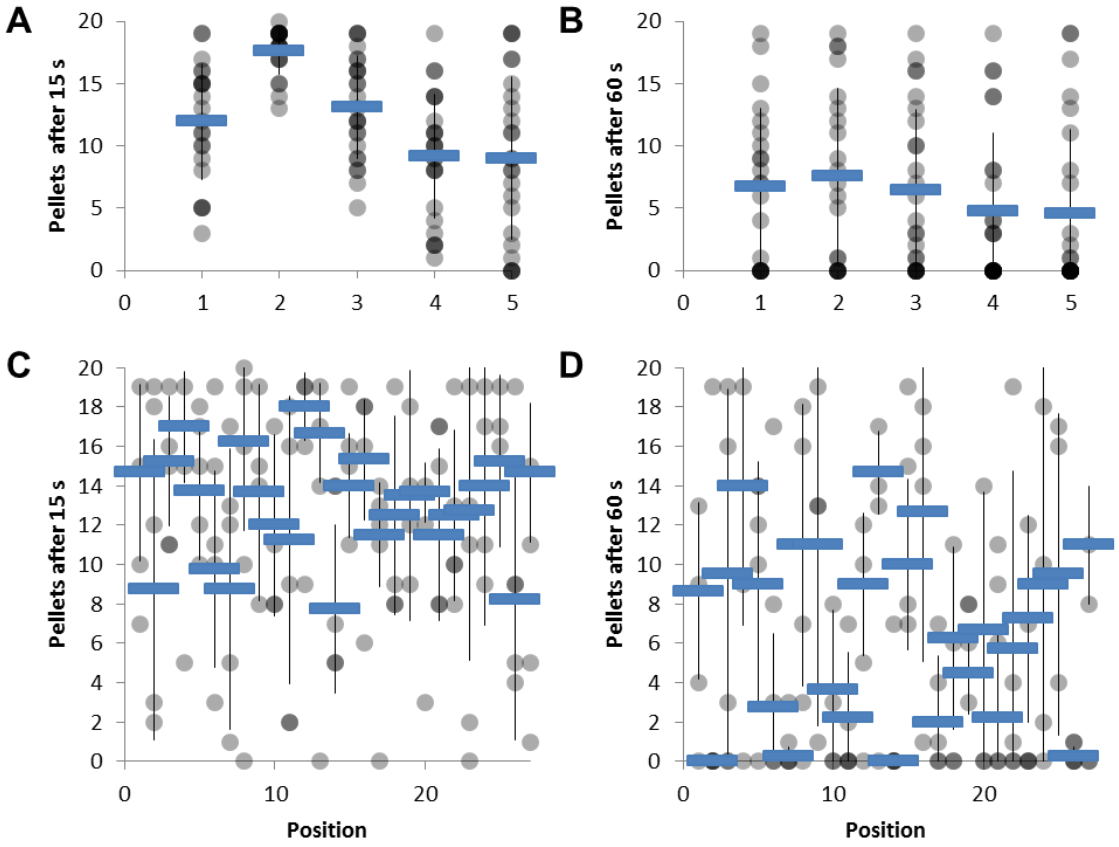

Figure 18. Controls for feeding assay support that fish hunger and motivation did not vary among different days or different trial times.
The feeding assay assesses a visually-mediated behavior. **A:** Different light environments led to a different feeding rate. **B:** Fish overall hunger did not vary from day to day. **C:** The feeding rate was not dependent on the time the trial was conducted. **D:** Fish overall hunger did not vary in relation to the time the trial was conducted. Y-axis indicates the number of pellets remaining after 15 (A,C) or 60 (B,D) seconds. X-axis indicates the day of testing (A,B; with day 1, 2, 3, 4, and 5, corresponding with white, dark, red, yellow, and UV+white light, respectively) or the position that a fish was tested (C,D; that is, 1st, 2nd, 3rd, etc.). Blue horizontal bars represent mean values, and vertical error bars indicate standard deviation.

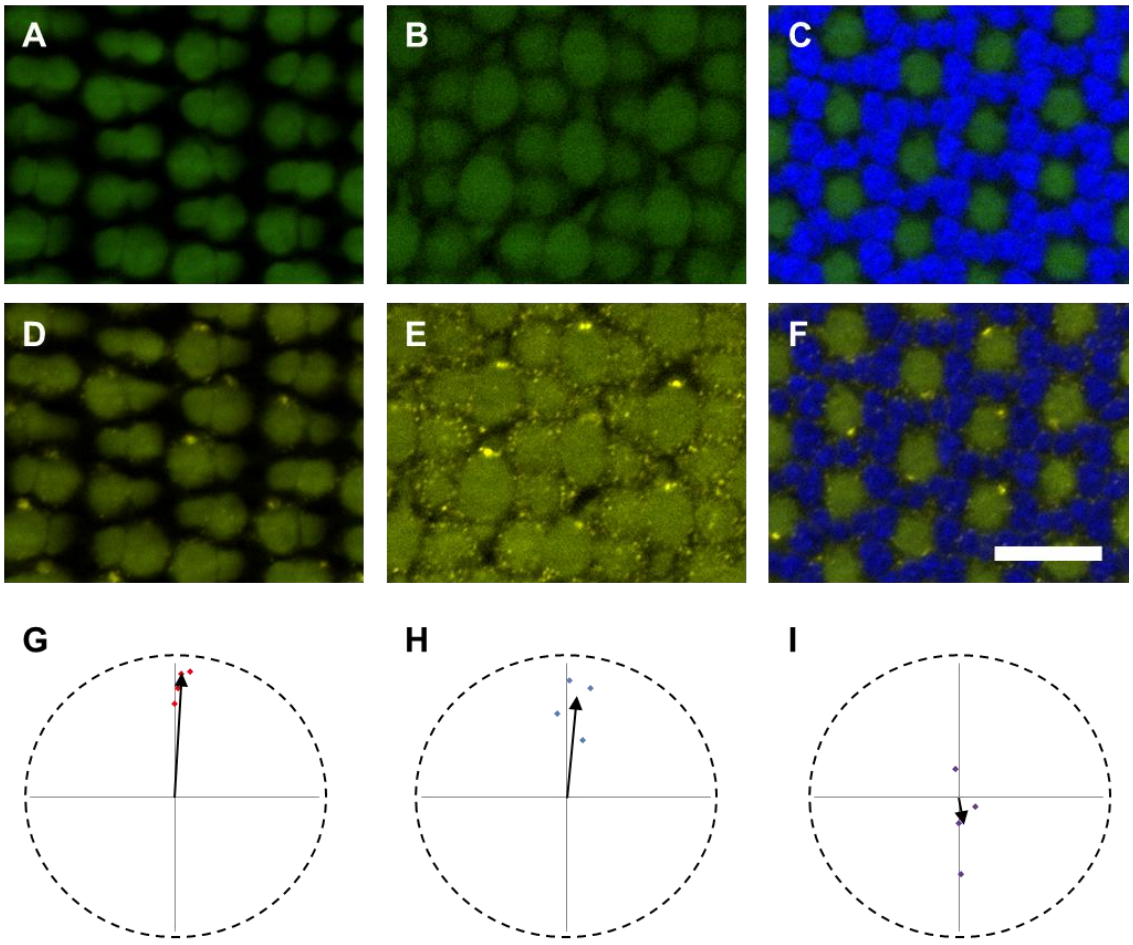

Figure 19. Cone photoreceptor basal body orientation in wild-caught zebrafish is similar to lab-reared zebrafish.
A-F: Photoreceptors from wild-caught zebrafish are shown at the depth of red-/green-sensitive cone basal bodies (A,D), blue-sensitive cone basal bodies (B,E), and UV-sensitive cone basal bodies (C,F). Nuclei were stained with DAPI (blue), and inner and outer segments are visible through autofluorescence under 488-nm excitation (green) (A-F). Basal bodies are localized with anti-γ-tubulin (yellow) (D-F). Scale bar is 10 μM. **G-I:** Mean vectors of basal body positions from individual fields of red-/green-, blue-, and UV-sensitive cones from wild-caught zebrafish are plotted with red, blue, and purple diamonds, respectively. The grand mean vectors are plotted with black arrows. Optic nerve is up in all panels.

An alternate hypothesis for basal body patterning is that the establishment of such a polarization requires cell-cell contact at the level of the cell body and/or inner segment, and the UV-sensitive cones lack sufficient contacts with the red-, green-, and blue-sensitive cones to propagate the pattern. To test this, I analyzed the retinas from several cyprinids to identify a mosaic that was similar to the row mosaic of the zebrafish but which exhibited alternative tiering. I discovered that red shiners (*Cyprinella lutrensis*) exhibit a pattern like this (Figure 20, Table 3). Like zebrafish, they have double cones, long single cones, and short single cones. I refer to these cones as red-/green-sensitive-like, blue-sensitive-like, and UV-sensitive-like, respectively. These cones are arranged in a row pattern similar to what is seen in zebrafish, with the exception that the single cone rows are offset from the double cone rows (Figure 20A-D). The tiering of these cones, however, is different. In the red shiners, the basal bodies of the blue- and UV-sensitive-like cones were both found at a similar depth, lower than the red- and green-sensitive-like cones (Figure 20E-F). Supporting this hypothesis that cell-cell contact is necessary for basal body patterning, I discovered that the basal bodies of both the blue- and UV-sensitive-like cones were disorganized (Figure 20J,K,M,N), whereas the basal bodies of red- and green-sensitive-like cones tended to be positioned towards the optic nerve with a trend similar to, though weaker than, the basal bodies of zebrafish red- and green-sensitive cones (Figure 20I,L).

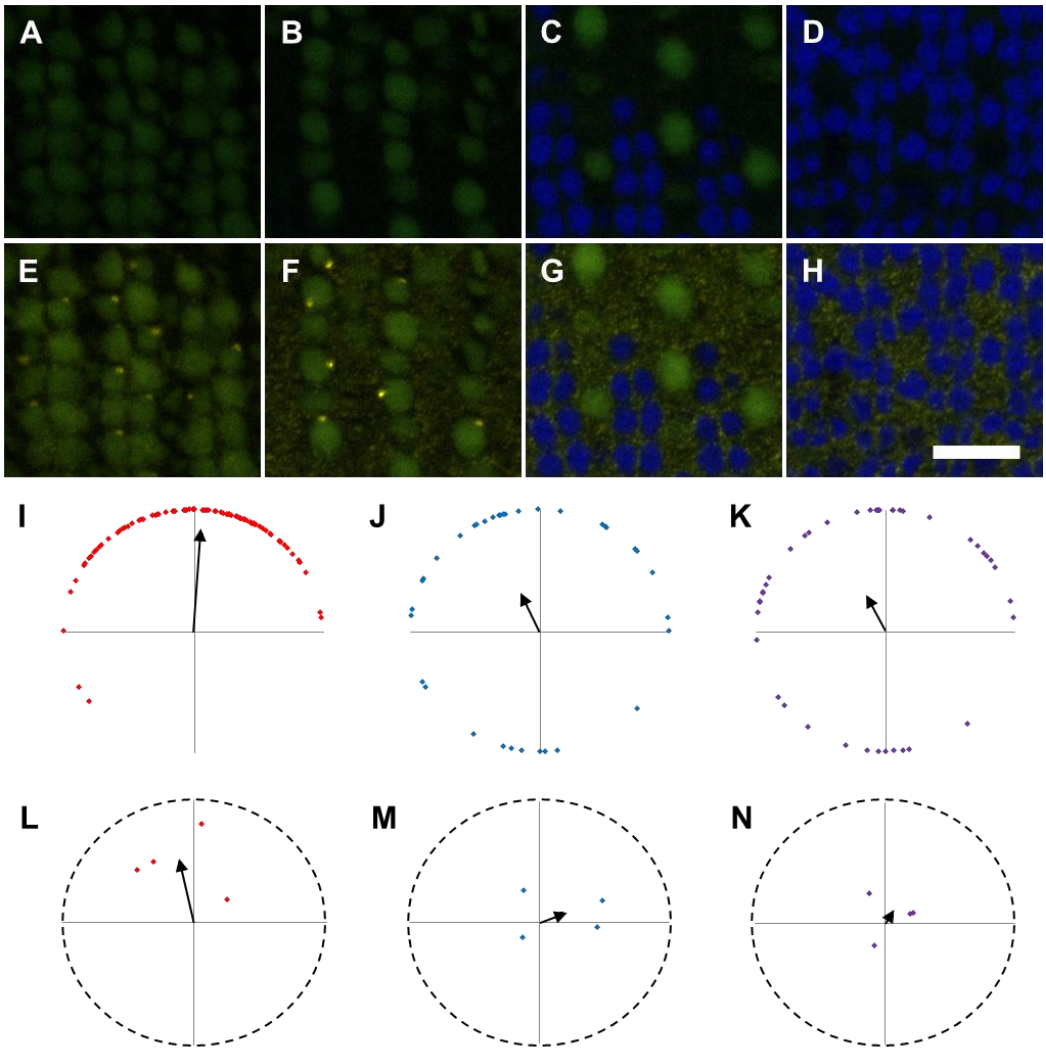

Figure 20. Row mosaic of the red shiner (*Cyprinella lutrensis*) is similar to the mosaic of zebrafish, but tiering of the different cone types is different, and this difference correlates with changes in basal body positioning.
A-H: Photoreceptors are shown at the depth of red-/green-sensitive-like cone basal bodies (A,E), blue-sensitive-like and UV-sensitive-like cone basal bodies (B,F), the UV-sensitive-like cone inner segments (C,G), and the red-/green- and blue-sensitive-like nuclei (D,H). Nuclei were stained with DAPI (blue), and inner and outer segments are visible through autofluorescence under 488-nm excitation (green) (A-H). Basal bodies are localized with anti-γ-tubulin (yellow) (E-H). Scale bar is 10 μM. **I-K:** Vectors of individual basal body positions within a single sample field are shown for red-/green- (I), blue- (J), and UV-sensitive-like (K) cones. The mean vector from each field is plotted with a black arrow. **L-N:** Mean vectors of basal body positions from individual fields of red-/green- (L), blue- (M), and UV-sensitive-like (N) cones are plotted with red, blue, and purple diamonds, respectively. The grand mean vectors are plotted with black arrows. Optic nerve is up in all panels.

Because the PCP pathway involves cell-cell contact, I determined if genes involved in the PCP pathway were expressed in the zebrafish retina (Figure 21). The retinal expression of the core PCP genes dishevelled2, frizzled7a, inversin, van gogh-like2, and prickle1a and of the downstream PCP gene inturned, supports that the PCP pathway may be involved in the basal body patterning I observed.

Discussion

I investigated the possibilities that lack of UV light exposure, inbreeding, and lack of cell-cell contact contribute to the failure of basal bodies to be planar polarized in UV-sensitive cones. Though not mutually exclusive, I find no evidence that lack of UV light exposure or inbreeding have contributed to the disorganization of UV-sensitive cones, as the basal body positioning found in UV-exposed and wild zebrafish is consistent with previous results (Ramsey and Perkins 2013).

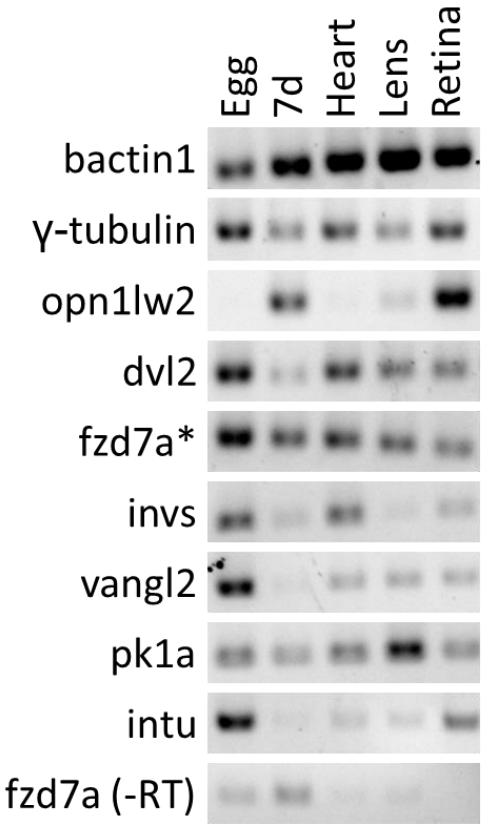

Figure 21. RT-PCR reveals transcripts of PCP genes in the zebrafish retina.
The genes encoding beta-actin (bactin1), gamma-tubulin, red opsin (opn1lw2), dishevelled2 (dvl2), frizzled7a (fzd7a), inversin (invs), van gogh-like 2 (vangl2), prickle (pk1a), and inturned (intu) were amplified from cDNA from unfertilized eggs, 7 day larvae, adult hearts, adult lenses, and adult retinas. Asterisk indicates sequence where the genomic amplification length is the same as the cDNA length.

In contrast, I found evidence that suggests that the lack of cell-cell contact may contribute to UV-sensitive cone basal body disorganization. The first evidence of this is from the red shiners, where the UV- and blue-sensitive-like cones are found at a similar and lower position within the retina than the red- and green-sensitive-like cones. In these retinas, not only the UV-, but also the blue-sensitive-like cones have disorganized basal bodies. In addition to the change in tiering, it is also possible that the offsetting of the rows of the cones of red shiners contributes to the lack of direct cell-cell contact, since rather than the blue-sensitive cones being situated directly between two red-/green-sensitive cone pairs to form a five cell row that has been referred to as a pentameric unit, as occurs in zebrafish (Zou, Wang et al. 2012), the blue-sensitive-like cones of red shiners are situated centrally between four double cone pairs. Both of these distinctions between the zebrafish and red shiner are examples of less direct cell-cell contact between the blue-sensitive-like cones and the red- and green-sensitive-like cones. Furthermore, the organization seen in the basal bodies of the red- and green-sensitive-like red shiner cones suggests that the blue-sensitive-like cones are not necessary for the polarization of the basal bodies of the other cones. However, the weaker organization seen in the double cones of red shiners versus the double cones of zebrafish suggests that, albeit not necessary, the presence of a pentameric unit in zebrafish may contribute positively to the planar polarization of these cells. The future discovery of a fish species or mutant line with a non-offset row mosaic and with all cone subtypes at a higher and uniform depth

in the retina would allow us to test if all cone basal bodies, including the basal bodies in the short single cone, were positioned towards the optic nerve.

Additional evidence supporting the importance of cell-cell contact in basal body patterning is found in the reduced positioning towards the optic nerve that I observed in the basal bodies of zebrafish reared in the lowest light conditions. As a consequence of the retinomotor movements of rods, cones, and the retinal pigment epithelium (RPE), light adapted zebrafish cones are situated beneath the RPE apical processes, whereas dark adapted cones are surrounded by these processes (Cunningham and Gonzalez–Fernandez 2000; Hodel, Neuhauss et al. 2006). When the photoreceptors are given little opportunity to exist in a light-adapted state during development, this may limit the cell-cell contact between the cones and prevent the establishment of polarity in these cells. It is unknown if the different cone subtypes of zebrafish exhibit retinomotor movements in unison or based on the stimulation of individual cone types; evidence exists for both possibilities in other fish retinas (Burnside and Nagle 1983; Kirsch, Wagner et al. 1989; Burnside, Wang et al. 1993). Therefore, the mildly reduced positioning towards the optic nerve seen in the red-, green-, and blue-sensitive cones of fish reared in red light could be a result of the red-sensitive cones alone maintaining a light-adapted state during the day, or it could be a result of the lower light intensity leading to an intermediate state of dark adaptation.

The failure of basal bodies to be positioned nearest to the optic nerve was surprisingly not simply due to random positioning as seen in the UV-sensitive cones.

Especially in the blue-sensitive cones, diametrically opposed bimodal positioning was observed. One possible cause for this could be that two or more separate processes are involved in the planar positioning of basal bodies. While dark adaptation limited the likely cell-cell contact mediated process necessary to signal if the basal bodies should position near or away from the optic nerve, another process was maintained that minimized the positioning of basal bodies along the perpendicular axis. The presence of PCP gene transcripts in the zebrafish retina supports that the PCP pathway is involved in at least one of these processes.

The functional consequence of the changes in basal body positioning is not known. The changes in feeding behavior in the dark-reared zebrafish could indicate decreased retinal function in these fish. However, because no significant decrease in OMR was seen, I think it is more likely to be caused by different learned behavior. Whereas zebrafish under lighted conditions tend to move quickly to consume food immediately after it is available due to the high competition from other fish, it is likely that the fish in the dark exhibited less motivation since they could not all see all the food at a certain time and that they would be more likely to eat more leisurely. Therefore, though they may have been aware of the food during the feeding assay, the presence of food for these fish may not have triggered an immediate response to consume as much as possible in as little time as possible.

In summary, these data suggest that cell-cell contact is important for establishing translational polarity in zebrafish red-, green-, and blue-sensitive cone photoreceptors.

One informative future study would be to determine if the rods of fish raised in the dark exhibited organized basal bodies. If they are organized, this would indicate that rods retain the ability to respond to the signal that polarizes basal bodies, and it would highlight the importance of cell-cell contact for this signal to be propagated. This would also suggest that direct contact with the cone photoreceptors is not necessary to propagate the signal. If the basal bodies of rods were not polarized, then the signal might be relayed through the cones. Alternatively, or in addition, the rods, like potentially the UV-sensitive cones, might not be receptive to the signal, which would be supported by the finding that rods and UV-sensitive cones have a common progenitor (Alvarez-Delfin, Morris et al. 2009). Furthermore, the growing number of new zebrafish knockout mutants available (Kettleborough, Busch-Nentwich et al. 2013), particularly of PCP pathway genes, presents an opportunity to directly assess the role of candidate genes in the establishment of photoreceptor basal body polarity.

CHAPTER IV

CHARACTERIZATION OF THE SWORDTAIL (*XIPHOPHORUS MALINCHE*, *XIPHOPHORUS BIRCHMANNI*, AND HYBRID) CONE PHOTORECEPTOR MOSAIC

Overview

Swordtail fish are commonly used to study visually-mediated social behavior, yet little is known about the physiology of their photoreceptor mosaic and how this mosaic influences behavior. The interbreeding of swordtail species leads to hybrids that vary morphologically and behaviorally, and incompatibilities among the parental species could lead to hybrid breakdown in the form of sensory dysfunction among the hybrids. Different patterns and organization states of the photoreceptor mosaic have been associated with many functional consequences, including differences in behavior, visual acuity, and polarization vision. Therefore, I characterized the cone photoreceptor mosaic in *Xiphophorus malinche*, *Xiphophorus birchmanni*, and their hybrids according to the general pattern of cell arrangement and according to changes in the density and angular structure of the photoreceptor mosaic. I found that these swordtails in general exhibited an organized square mosaic, although I identified some variations in this pattern within wild populations of these fish. The variation seen is similar among *X. malinche*, *X. birchmanni*, and their hybrids. Within hybrids, whereas different visually-based behavioral mating preferences were found, there was no relationship between

photoreceptor mosaic structure and these preferences. The angular arrangement of photoreceptors differed between male and female parentals. The characterization of the swordtail photoreceptor mosaic lays a foundation for future studies to identify functionally significant changes in this mosaic.

Introduction

Swordtails are freshwater fish used extensively to study mate choice and other visually-mediated behaviors (for review, see Rosenthal and Garcia de Leon 2006). In mate choice, swordtails have been shown to attend to a variety of visual cues. In general, female swordtails prefer larger males (Fisher, Mascuch et al. 2009). Some swordtails prefer symmetry between vertical bars that pattern both sides of the males (Morris and Casey 1998). However, other female preferences vary among swordtail species: some prefer swords (Rosenthal and Evans 1998) whereas others prefer no swords (Wong and Rosenthal 2006) or have no preference (Rosenthal, Wagner Jr et al. 2002); some prefer UV coloration whereas others show no preference (Cummings, Rosenthal et al. 2003). Other female preferences even vary within species; for one swordtail species, *Xiphophorus pygmaeus*, coloration preferences only occur in fish from areas with low predation (Kingston, Rosenthal et al. 2003). Differences in preference can be caused by differences in sensory perception or by differences in sensory processing (for review, see Ryan and Cummings 2013). Visual preferences, for example, are dependent on the specific light wavelengths photoreceptors can absorb and by how this information is organized and interpreted by other neurons in the retina and

brain. Though it is known that some differences in visual preferences are due to processes downstream of sensory perception (for example, having a learned preference for the species an individual is reared with (Verzijden and Rosenthal 2011)), less is known about the potential physiological changes that may be directly influencing sensory perception (for review, see Coleman 2011).

Xiphophorus malinche and *Xiphophorus birchmanni* are two species of swordtails native to Mexico. At the disturbance of olfactory cues, *X. malinche* and *X. birchmanni* will interbreed (Fisher, Wong et al. 2006). Though first generation hybrids are rare, hybrids will breed with each other and with parental species, leading to populations with both hybrids and parentals (Culumber, Fisher et al. 2011). Interestingly, work in the Rosenthal lab suggests that hybrids, when associating with other swordtails, are individually indifferent to the same visual cues that the parental species attend to (Coleman, SW, BD Perkins, GG Rosenthal. Unpublished data). Furthermore, since hybrids are morphologically more variable than parentals (Rosenthal, de la Rosa Reyna et al. 2003), I hypothesized that different hybrids would show different behavioral responses to parental stimuli that could be the product of variation in their photoreceptors.

Because of the visually-mediated behavioral differences in swordtail males versus females, in *X. malinche* versus *X. birchmanni*, in these parentals versus their hybrids, and potentially among different individual hybrids, I chose this system to investigate the potential association between retinal morphology and visual behavior. To accomplish this, I first characterized the morphology of the retina in the parental

species and in the hybrids. I focus on two retinal attributes: cone patterning and cone density.

Although not all teleosts have well organized photoreceptor mosaics, many do, with the two most common basic patterns being the row mosaic, as exemplified by the zebrafish (*Danio rerio*) (Figure 22A)(Engström 1960; Larison and Bremiller 1990; Raymond, Barthel et al. 1993), and the square mosaic, as exemplified by the medaka (*Oryzias latipes*) (Figure 22B)(Tohya, Mochizuki et al. 2003). Several authors have hypothesized that an organized mosaic, either in the form of a row or square mosaic, is selected for when vision is important (Lyall 1957; Engström 1963; Zaunreiter, Junger et al. 1991). For example, in a comparative study between many fish species, Engström observed that the most organized mosaics were found in fish that hunted fast prey, and the most disorganized mosaics were found in bottom-dwelling and nocturnal fish whose behavior was not highly visually-oriented (Engström 1963). Because of the important role that vision plays in swordtail behavior, I test the hypotheses that 1) swordtails will exhibit an organized photoreceptor mosaic, and 2) that organization of the mosaic will decrease in swordtails with decreased visual preferences.

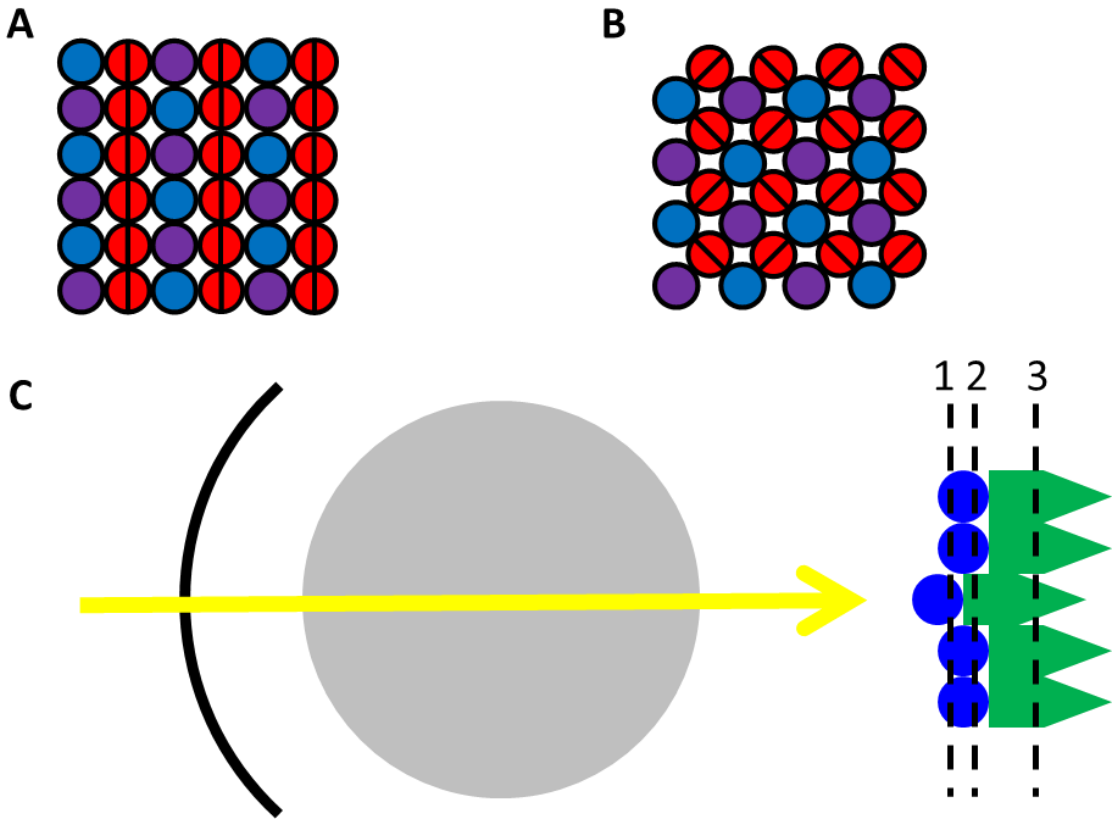

Figure 22. Illustrations depict the two common cone photoreceptor mosaics in teleosts and photoreceptor tiering.
A-B: Illustrations of a row mosaic (A), exemplified by the zebrafish, and a square mosaic (B), exemplified by the medaka, are shown. Red, blue, and purple represent double, long single, and short single cones, respectively. In both the zebrafish and medaka, these cone types correspond with red-/green-sensitive cones, blue-sensitive cones, and UV-sensitive cones, respectively. **C:** Illustration depicts the location and orientation of the retinal slices (black dashed lines) in Figure 23 in relation to photoreceptor nuclei (blue small circles) and inner/outer segments (green). The dissection planes represented by dashed lines 1, 2, and 3 correspond with Figures 2A-C, D-F, and G-I, respectively and extend perpendicular to the page. Direction of light (arrow) and location of lens (large gray circle) are shown for reference. Illustrations not drawn to scale.

Besides observing the general mosaic patterns, I also wanted to more precisely quantify differences between the different groups. In a study comparing cyprinid retinas, cone densities and behavior were correlated; for example, a greater cone density was found in the retinal region used for looking upward in asps (*Aspius aspius*), a fish that locates its prey from below (Zaunreiter, Junger et al. 1991). In humans, decrease in photoreceptor density and in the organization of the photoreceptor mosaic has been observed in various degenerative diseases in the retina (Talcott, Ratnam et al. 2011; Makiyama, Ooto et al. 2013; Makiyama, Ooto et al. 2013; Mrejen, Sato et al. 2013). Therefore, I quantified photoreceptor density in addition to looking for general differences in the photoreceptor mosaics.

In this study, I find that the photoreceptor cones of *X. malinche*, *X. birchmanni*, and their hybrids form a well-organized square photoreceptor mosaic. There is modest variation among individuals, but there is no detectable difference between species or between parentals and hybrids. Although I do find variation in the mating preferences of hybrids, these differences do not correspond to differences in the photoreceptor mosaic. I do find a sexual dimorphism in the mosaic patterns of the parentals.

Materials and Methods

Animals

Xiphophorus malinche (2 males and 8 females), *Xiphophorus birchmanni* (5 males and 5 females), and their hybrids (81 females) were collected near the CICHAZ

research station in Hidalgo, Mexico. *X. malinche* were collected from the Chicayotla collection site; *X. birchmanni* were from the Garces and Coacuilco collection sites (Culumber, Shepard et al. 2012).

Behavioral assay

81 hybrid swordtails were screened for parental preference as described (Verzijden and Rosenthal 2011). Individual hybrid females were given the choice between (A) a computer representation of a *X. malinche* male combined with *X. malinche* olfactory cues or (B) a computer representation of a *X. birchmanni* male combined with *X. birchmanni* olfactory cues. Three trials were conducted with each individual. Each trial consisted of two subtrials. The stimuli for each parental type were presented on opposite sides in the subtrials to control for side bias. The time a fish spent near the *X. malinche* stimuli, near the *X. birchmanni* stimuli, and in the middle of the tank was measured for five minutes for each subtrial. The time for each subtrial was averaged to determine that trial's time. If a fish failed to move to a different area of the tank during one subtrial, the data from the responsive subtrial was used for that trial. If a fish failed in both subtrials within the same trial to move to a different area of the tank, the fish was classified as non-responsive. The majority of fish that were responsive in the first trial (31/37) continued to be responsive in the following trials. Fish that were not responsive to the test or died before the trials could be completed (50/81) were excluded from further analysis. All remaining 31 responsive fish were characterized based on their behavior and retina morphology. For each fish, the time spent near each

parental in each trial was assessed. If a fish spent more time with the same parental for all three trials, it was classified as a preferrer for that parental species; otherwise, it was classified as a non-preferrer.

Histology

Retina dissections were performed as described in Ramsey and Perkins (2013). Sections were washed in 0.1% Tween 20 and 0.1% dimethyl sulfoxide in phosphate buffered solution (PBS: 137 mM NaCl, 2.7 mM KCl, 10 mM Na2HPO4, 1.76 mM KH2PO4, pH 7.4) (PBSTD). Nuclei were stained with the fluorescent 4,6-diamidino-2-phenlindole dihydrochloride (DAPI) diluted 1:10,000 in 5% normal goat serum in PBSTD, which optimized autofluorescence of inner and outer segments.

Microscopy and image analysis

Microscopy was performed as described in Ramsey and Perkins (2013). All images were taken in the middle or peripheral retina.

Because of the consistent ratio of short single cones to long single and double cones that is a consequence of the organization of the square mosaic (Figure 22B), the number of short single cones was used to assess photoreceptor density. For each image, the number of short single cones that had any part visible within a 6014 μM^2 square was counted. Because photoreceptor density varies throughout the retina (Zaunreiter, Junger et al. 1991), the number of cones in two images (fields) taken at different locations was averaged to obtain a mean cone density. Standard deviations were calculated from the

mean cone densities. Type III sum of squares analyses of variance (ANOVAs) were performed from the mean cone densities.

Mosaic angles are measured as follows. Five short single cones in a row are used to create each side of a triangle. The first side is made of short single cones alternating with long single cones. For hexagonal mosaics (Figure 26H), where there are two choices of directions for the first side of different lengths, the shortest side is chosen. The second side is made of short single cones alternating with long double cones. For row mosaics (Figure 26G), where there are three choices of directions for the second side, the middle direction is selected. For other mosaics (Figure 26H, I) where there are two choices for the second side, the acute angle is selected. When the correct first and second sides have been selected, then the third side will be composed of five short single cones alternating with long double cones. The angle between the first and second sides is then calculated. For each fish, the angles from two different fields were averaged to obtain a mean mosaic angle. For a single hybrid with no preference (#26), one of the two fields was too disorganized to measure the mean mosaic angle. For this individual, the angle from the single field was used for further analysis. Standard deviations were calculated from the mean cone angles. Type III sum of squares analyses of variance (ANOVAs) were performed from the mean cone angles.

Results

Within the retinas of *X. malinche*, *X. birchmanni*, and their hybrids, I found similar cone photoreceptor mosaics (Figure 23). Within all of these mosaics, I identified

short single cones, long single cones, and double cones. These cones were tiered, with short single cones being located farther from the retina pigment epithelium at the back of the retina, and closer to the lens, than the other cone subtypes (Figure 22C). Both the patterning of the cone mosaic and the tiering of the cone subtypes was most evident at the depth in the retina corresponding with the inner segment of the short single cone and the nuclei of the other cone subtypes (Figure 22C, Figure 23D,E,F). The pattern consisted of alternating rows of single cones and double cones. Single cone rows consisted of alternating long single and short single cones. Double cone rows consisted of pairs of double cones. The angle of each pair of double cones was approximately 45° offset from the angle of the rows, and alternating pairs of double cones alternated whether this offset was in a clockwise or counterclockwise direction. Most commonly, the rows of double cones were offset from the single cones. This offset resulted in the angles of double cones pointing toward long single cones and, conversely, away from the short single cones, to form a square mosaic pattern, similar to the pattern seen in the medaka (Figure 22B).

Figure 23. The photoreceptors of *X. malinche* (left-A,D,G), *X. birchmanni* (right-C,F,I), and their hybrids (middle-B,E,H) are all arranged in similar mosaics. **A-I:** The mosaics are shown at different depths in the retina, with A-C being closest to the lens, D-F being in the middle, and G-I being closest to the RPE. **J-R:** Images from A-I are overlaid to indicate the locations of some long double cones (red circles), long single cones (blue circles), and short single cones (purple circles). Nuclei are stained with DAPI (blue). Autofluorescence at 488 nm (green) shows inner segments and outer segments. Scale bar is 10 μm (all panels). Optic nerve is up in all panels. All images are from the middle or peripheral retina.

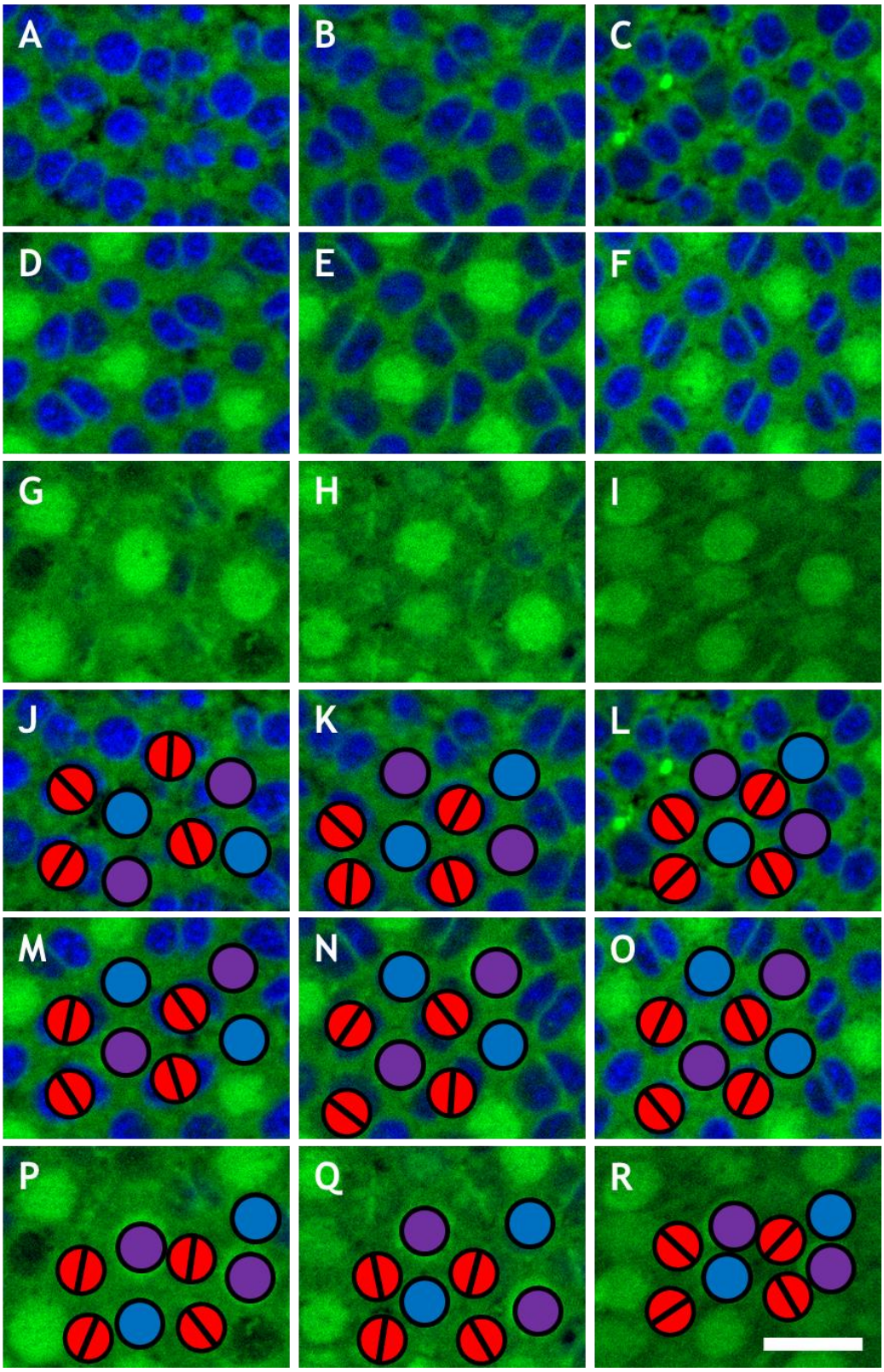
A
B
C
D
E
F
G
H
I
J
K
L
M
N
O
P
Q
R

The hybrids whose retinas I examined had previously undergone behavioral tests that involved providing each hybrid with the choice to spend time in proximity with visual and olfactory cues of either of the parental species, *X. malinche* or *X. birchmanni*. These preference tests revealed that different hybrids exhibited different preferences. Some hybrids consistently spent more time near one of the parentals than the other and were called *X. malinche* preferrers or *X. birchmanni* preferrers (Figure 24A), whereas others showed no tendency to spend time near one of the parentals and were called non-preferrers (Figure 24B).

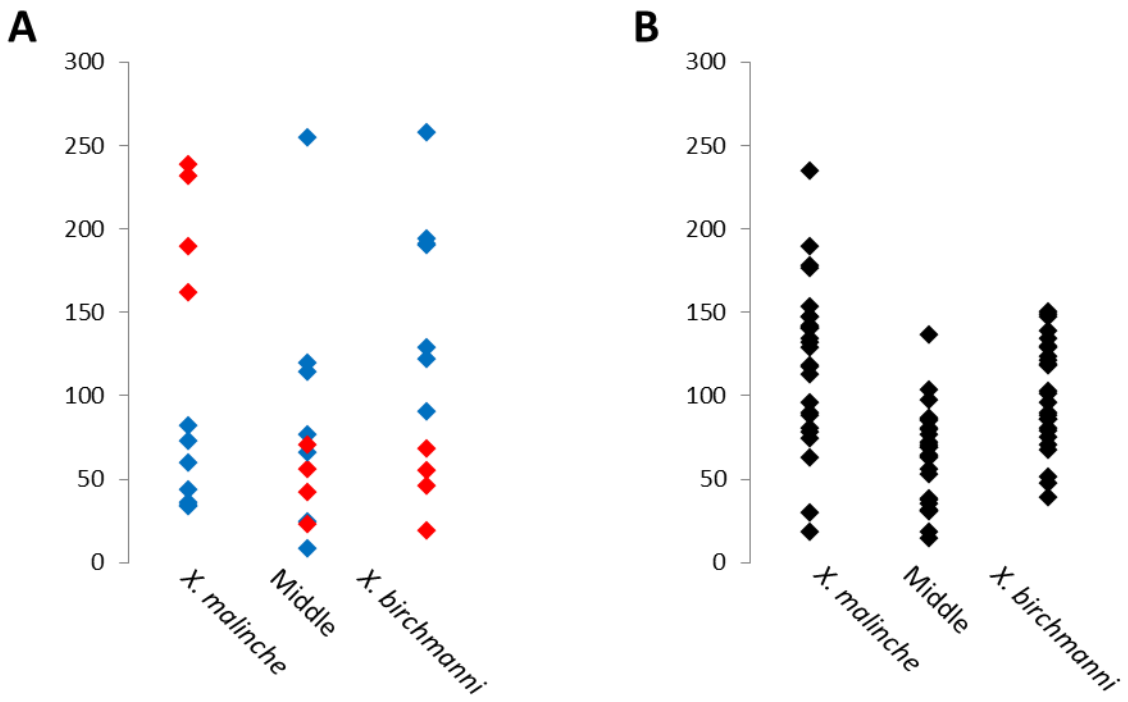

Figure 24. Different hybrids exhibit different preferences for parental species. Mean time (Y-axis, seconds) spent near the *X. malinche* stimuli, middle of the tank, and *X. birchmanni* stimuli, among the three trials by hybrids that had a preference (A) and had no preference (B) is shown. Hybrids with a preference for *X. malinche* are represented with red diamonds, a preference for *X. birchmanni* with blue diamonds, and no preference with black diamonds. Each fish is represented by 3 diamonds—one representing the time spent in each possible tank location.

Based on this information, I wanted to determine if there were any photoreceptor mosaic differences that corresponded with either the species of origin (*X. malinche*, *X. birchmanni*, or hybrids), or, among the hybrids, their preference, or, among the parentals, their sex. I first looked at photoreceptor density. Within individual retinas, regardless of swordtail species, I observed that although there was some variation based on location within the same retina, as expected, there was a greater difference between individuals (Figure 25A-C). However, the difference seen between individuals did not correspond with differences in their species, preference, or sex (Figure 25D-F, Table 4). Therefore, although I cannot eliminate the possibility that photoreceptor density corresponds with some other trait associated with sexual selection, I have not observed any correlation.

Figure 25. Photoreceptor density does not change according to swordtail species, hybrid preference, or swordtail sex.
A-C: Photoreceptor density varies mildly within individual retinas and more among individuals in *X. malinche*, *X. birchmanni* , and their hybrids. **D:** Photoreceptor density is similar when comparing *X. malinche*, *X. birchmanni*, and their hybrids. **E:** Photoreceptor density is similar among hybrids that exhibit a preference for *X. malinche*, *X. birchmanni*, or no preference. **F:** Photoreceptor density is similar between male and female swordtails. Black squares indicate the short single cone density (y-axis, cones per field) according to each fish (x-axis) (A-C). Each fish has two data points that correspond to the two fields analyzed for that fish. Red diamonds indicate the mean density (y-axis) for each fish (A-F). Blue triangles indicate the mean density according to species (D), according to sex (F), or, among hybrids, according to preference (E). Measurements from all 10 *X. malinche*, 10 *X. birchmanni*, and 31 hybrids are shown.

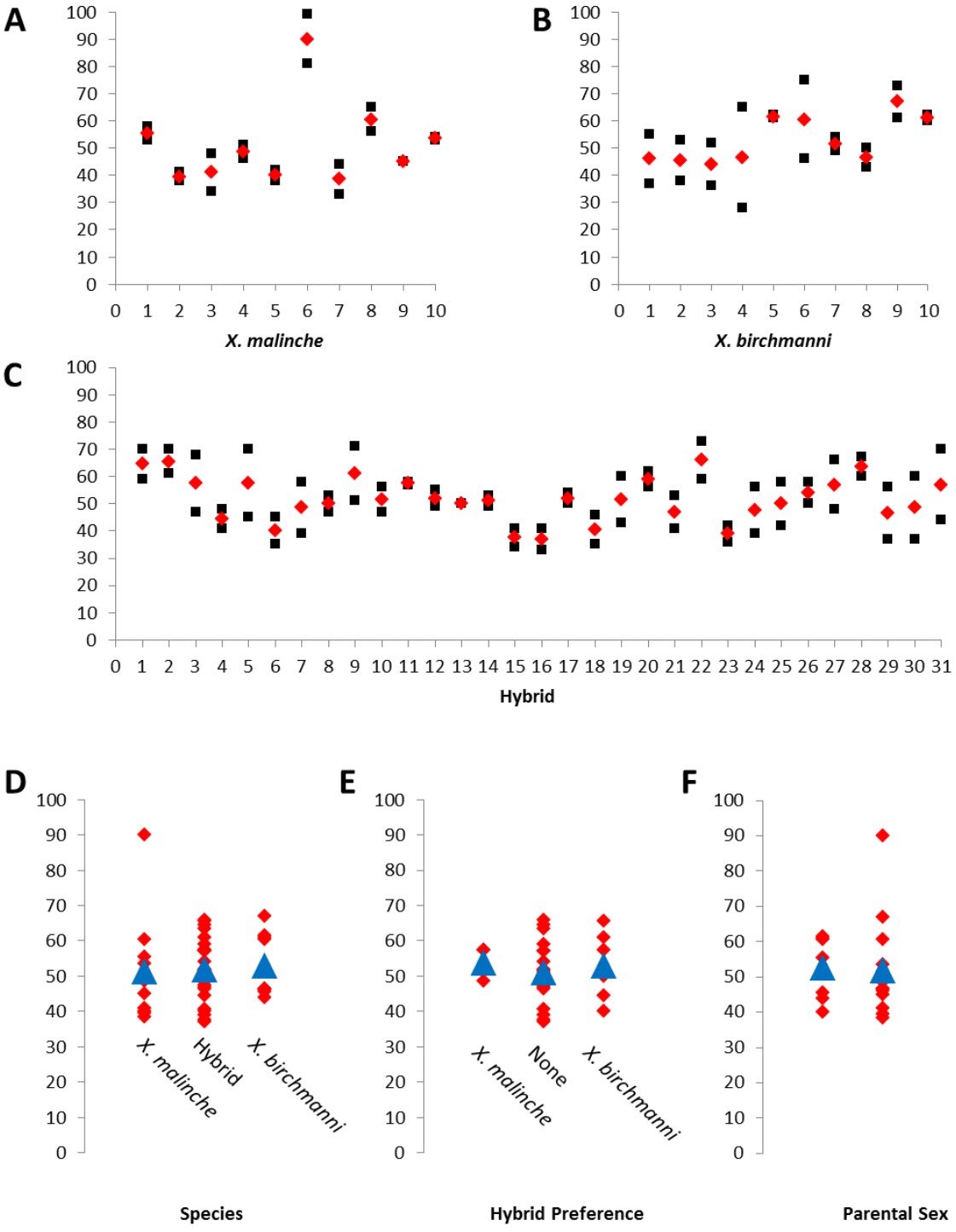
A
B
C
D
E
F
X. malinche
X. birchmanni
Hybrid
X. malinche
Hybrid
X. birchmanni
Species
X. malinche
None
X. birchmanni
Hybrid Preference
Parental Sex

Table 4. Swordtail Photoreceptor Mosaic Characterization.

	X. malinche			*X. birchmanni*			Hybrid females			
	Sex			Sex			Preference			
	Male	Female	TOTAL	Male	Female	TOTAL	*X. mal.*	*X. bir.*	None	TOTAL
No. fish	2	8	10	5	5	10	4	7	20	31
No. fields	4	16	20	10	10	20	8	14	40	62
Mean density (s.d.)	48 (11)	52 (17)	51 (16)	55 (9)	52 (9)	53 (9)	54 (5)	53 (9)	51 (9)	52 (8)
Mean angle (s.d.)	60 (14)	61 (9)	61 (9)	53 (6)	65 (9)	59 (9)	56 (10)	61 (5)	61 (8)	60 (8)

Analysis of variance (ANOVA)			**Density**		**Angle**	
			F	p	F	p
	All species	***X. malinche*, *X. birchmanni*, hybrid**	0.09	0.92	0.10	0.91
	Hybrid preference	***X. malinche, X. birchmanni*, none**	0.28	0.76	0.52	0.60
	Parental species	***X. malinche*, *X. birchmanni***	0.01	0.94	0.67	0.42
	Sex of parentals	**Male, female**	0.13	0.72	4.74	0.04*
	Interact-ion between parental species and sex		0.30	0.59	1.41	0.25

Regarding the photoreceptor mosaic pattern itself, the general appearance was of a square mosaic. Although some fields of view revealed photoreceptors that were more perfectly organized than others, I did not observe any general trend toward disorganization in any of the subgroups of swordtails, including in the hybrids with no preference. However, despite the generally similar pattern of cone photoreceptors among the different retinal fields, I observed variations in the angle of this pattern in different fields (Figure 26A-F). These variations corresponded with alterations in the offset of the single cone rows from the double cone rows. Interestingly, when illustrated, the differences observed correspond with what might be expected if a field of cells experienced pressure from the sides (Figure 26G-I). I called these different variations row mosaics, hexagonal mosaics, and square mosaics. However, I note that the appearance of the hexagonal mosaic is very similar to the square mosaic and could be characterized as a variation of the square mosaic if placed under the traditional square or row mosaic designation.

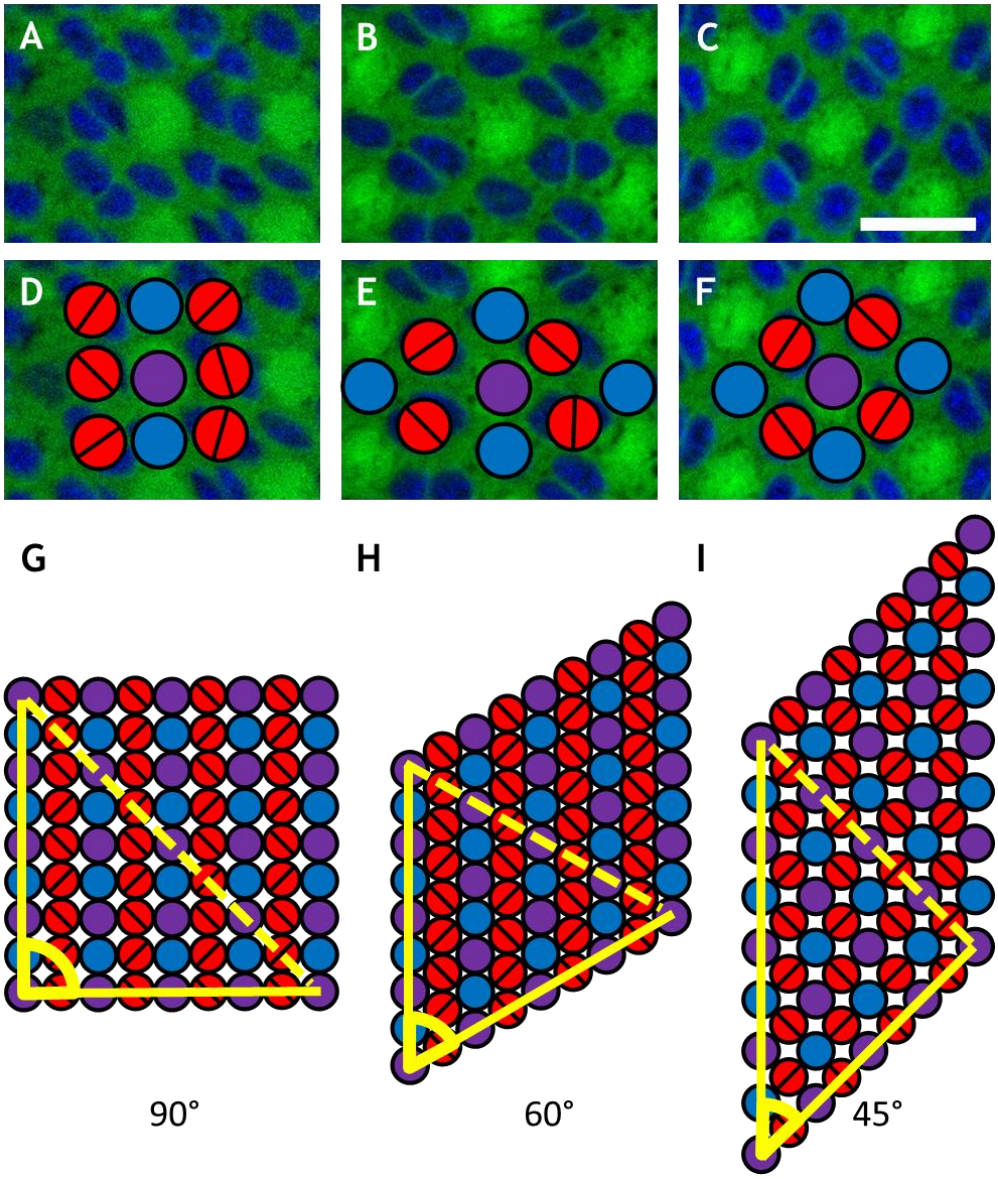

Figure 26. Within swordtail retinas, the angles of the cone photoreceptor mosaics vary.
A-C: Row mosaics (A), hexagonal mosaics (B), and square mosaics (C) are all observed. **D-F:** Images from A-C are overlaid to indicate the locations of some long double cones (red circles), long single cones (blue circles), and short single cones (purple circles). **G-I:** Row mosaics (G), hexagonal mosaics (H), and square mosaics (I) are illustrated to demonstrate how these mosaics may be related to one another. The angles indicated (G-I) correspond with Figure 26. Nuclei are stained with DAPI (blue) (A-F). Autofluorescence at 488 nm (green) shows short single cone inner segments (A-F). Scale bar is 10 μm (A-F). Optic nerve is up in all panels. All images are from the middle or peripheral retina.

The row mosaic seen here, on the other hand, bears distinct features from both the traditional row and square mosaics: whereas the photoreceptors are arranged in rows like in the row mosaic (Figure 22A), the double cones are angled like in the square mosaic (Figure 22B).

These differences were quantified by measuring the angles between different cells within the mosaic. Within all species and as seen in the cell density variations, changes of the mosaic angle were seen within the same retinas, but the variation was greater among different individuals (Figure 26A-C). Also as seen in the cell density variations, changes in the mosaic angles did not correspond with the species or preference (Figure 27D-E, Table 4). However, when comparing males and females among parentals, there was a significant difference between the mosaic angles of the two sexes (ANOVA, $F=4.74$, $p=0.04$), with males having a smaller mosaic angle, in general, than females (Figure 27G).

Figure 27. Mosaic angles do not change according to swordtail species or preference, but, in the parentals, males have a smaller mosaic angle than females. **A-C:** Mosaic angles vary mildly within individual retinas and more among individuals in *X. malinche*, *X. birchmanni* , and their hybrids. **D-E:** Mosaic angles do not vary between species or preferences. **F:** Mosaic angles significantly vary according to gender among parentals (ANOVA, F=4.74, p=0.04). Black squares indicate the mosaic angle (y-axis, degrees) according to each fish (x-axis) (A-C). With the exception of hybrid 26, each fish has two data points that correspond with the two fields analyzed from that fish. Red diamonds indicate the mean mosaic angle (y-axis) for each fish (A-F). Blue triangles indicate the mean density according to species (D), or, among hybrids, according to preference (E), or, among parentals, according to sex (F). Measurements from all 10 *X. malinche*, 10 *X. birchmanni*, and 31 hybrids are shown.

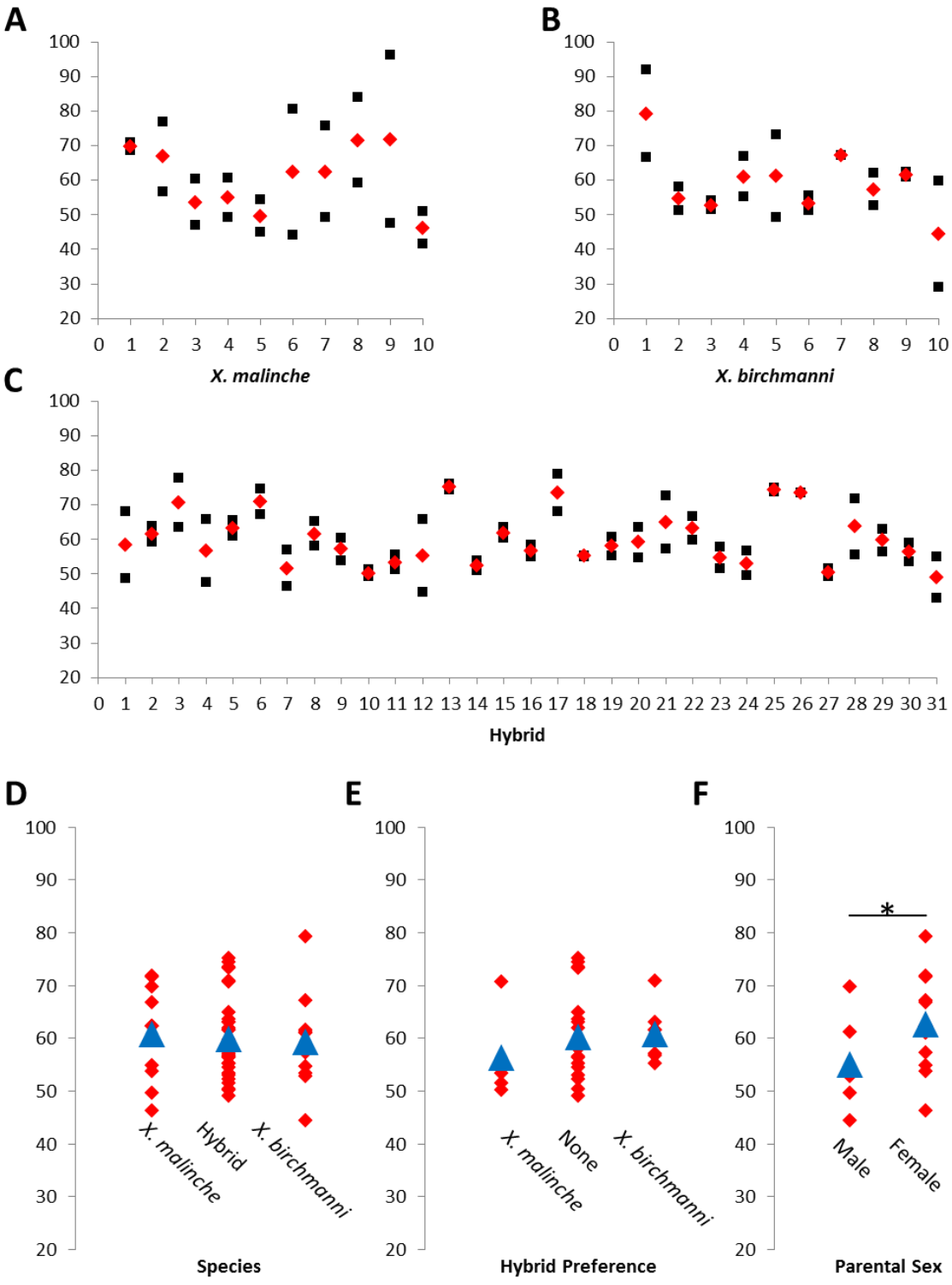
A
B
C
D
E
F
X. malinche
X. birchmanni
Hybrid
Species
Hybrid Preference
Parental Sex
X. malinche
Hybrid
X. birchmanni
None
Male
Female
*

Discussion

Here, I present a characterization the swordtail photoreceptor mosaic in the parental species *X. birchmanni* and *X. malinche* and in their hybrids. The well-organized generally square cone photoreceptor mosaic I found is in line with the brief previous written descriptions of single specimens of two poeciliid mosaics, including the swordtail *Xiphophorus hellerii* (Engström 1963). As swordtails exhibit highly visually-mediated behaviors such as mating and predator avoidance, this supports the hypothesis that more organized photoreceptor mosaics are selected for in fish that strongly depend on vision; for example, very organized mosaics as are present in many teleosts including zebrafish (*Danio rerio*), wrasses (Family Labridae), and perch (*Perca fluviatilis*), but they are absent in teleosts that rely more on other senses, such as snail fish (*Liparisliparis*), zander (*Lucioperca lucioperca*), and carp (*Cyprinus carpio*) (Lyall 1957; Engström 1960; Engström 1963).

If swordtail photoreceptor attributes correspond with the well characterized photoreceptors in the zebrafish, then the double-cones would be classified as red-/green-sensitive, the long single cones would be blue-sensitive, and the short single cones would be ultraviolet (UV)-sensitive (Branchek and Bremiller 1984; Raymond, Barthel et al. 1993). Though less well characterized, the more closely related medaka has a square mosaic with multiple pigment classes that have been likewise categorized as red-, green-, blue-, and UV-sensitive and that are suggested to be specific to the same double and single cones as in the zebrafish (Ohki and Aoki 1985; Nishiwaki, Oishi et al. 1997; Matsumoto, Fukamachi et al. 2006; Kitambi and Malicki 2008). Recently, five cone

pigment classes (called UV (365 nm), violet (405 nm), blue (459 nm), green (534 nm), and yellow (568 nm) based on the colors of their absorbance maxima) were found via microspectrophotometry (MSP) in *X. hellerii* (Watson, Lubieniecki et al. 2010). With the exception of the 534 nm peak, these spectral peaks are very similar to the spectral peaks of zebrafish cones (called UV (362), blue (407), green (473), and red (564) based on traditional designations for short, middle, and long wavelength sensitive cones) (Robinson, Schmitt et al. 1993; Cameron 2002). In an earlier study, similar spectral peaks to the more recent study in *X. helleri* were identified in a variety of swordtail species, with the exception of the 568 nm peak, which was not identified (Rush 1996). One possible explanation for this is that the peaks identified at 534 nm and 568 nm have total absorbance spectra that overlap significantly and may have been difficult to resolve. These two peaks might not represent two morphologically different cones, but rather they might both represent long wavelength sensitive cones that have different opsins expressed in them. Supporting this is the observation of a square mosaic in two swordtail species that is composed of four, not five, morphological cone types. Furthermore, in *X. hellerii*, contributions from 10 opsins were identified, including 4 long wavelength opsins potentially controlled by at least two regulatory regions (Watson, Lubieniecki et al. 2010). In zebrafish, genomic duplication has led to several red and green opsins for each of these morphological cone types (Chinen, Hamaoka et al. 2003), and these opsins are expressed at different times and in different regions within the retina (Takechi and Kawamura 2005). It is an intriguing possibility that the differential opsin expression is also occurring in swordtails. Accordingly, differential

opsin expression between the two studies could have allowed two peaks to be more evident in the latter. Now that the morphology of the photoreceptor mosaics of *X. birchmanni* and *X. malinche* has been described, an important next step is the localization of RNA expression of the different swordtail opsins. Not only would this confirm the general sensitivities of the different cone types, but it would also allow us to begin to examine a potential genetic contribution to already well-established swordtail behavioral variation.

Interestingly, although the mosaics I observed were generally square, I often observed square-like hexagonal mosaics, and I occasionally observed row mosaics (Figure 27A-C). Observations of mosaics similar to what I have called a hexagonal mosaic have previously been described in other Atherinomorphs that also have square mosaics, including in *Ameca splendens*, another member of the order Cyprinodontiformes (Reckel and Melzer 2003). There are also several other examples where the row and square mosaic have been found together within the same retinas, such as in herrings (Engström 1963), trout (Lyall 1957), and goldfish (Wan and Stenkamp 2000). However, to my knowledge, the measurements of the angles that differentiate the row, hexagonal, and square mosaics that I observe in swordtails is the first quantification of this progression. The variation found within these different retinas supports the model that both row and square mosaics are formed by similar processes that vary only in the affinities between different cell types (Tohya, Mochizuki et al. 2003). Interestingly, this model leads to a disorganized mosaic when the parameters are set in-between the parameters necessary to make either the square or the row mosaic.

However, the fields I observed were too small to see, in retinas that contained both square and row mosaics, if disorganization was present between them. The authors of the previously described model hypothesize that there is no benefit to an organized square over an organized row mosaic, but that an evenly distributed mosaic that would allow higher and consistent resolution for all light wavelengths would be selected for over a random distribution; therefore, they hypothesize that this could lead to stabilizing selection for either the row or square mosaic (Tohya, Mochizuki et al. 2003). Whereas the square mosaic was most common overall with *X. birchmanni* and *X. malinche*, if another *Xiphophorus* species could be found with an overall row mosaic, I could test this hypothesis to see if the hybrids showed a disorganized mosaic and if this disorganization corresponded with decreased visual ability. However, if selection is strong enough for an organized mosaic, a common ancestor with a square mosaic for all swordtails might mean that primarily row mosaics are absent among swordtails. This is similar to what Engström predicts: that phylogeny determines the type of mosaic whereas function determines the degree of organization of the mosaic (Engström 1963). On the other hand, even a short period of relaxation on the importance of the visual abilities of a past *Xiphophorus* population may have sufficiently allowed mutation to introduce the alternative mosaic and genetic drift to fix it within the population.

In one intriguing alternative (though not mutually exclusive) hypothesis is that double cones, where arranged in a square mosaic, contribute to an organism's ability to detect changes in light polarization. If combined with the previous hypotheses, this would suggest that while there is an advantage to the square over the row mosaic, the

difficulty of switching from a row to a square mosaic would lead to the canalization of whichever organized mosaic was first present. Polarization vision has been well documented in many animals, including arthropods, cephalopods, and fish, and it is thought to play a role in migration, orientation in murky water, sexual selection, communication, and enhancing visual contrast; however, the mechanism behind polarization vision in vertebrates is not well understood (for review, see Cronin 2011; Marshall and Cronin 2011; Shashar, Johnsen et al. 2011). In one study of goldfish (*Carassius auratus*), polarization sensitivity was detected in green-sensitive cones; combined with an organized photoreceptor mosaic, the authors proposed that this could allow polarization information to be used in downstream processing (Roberts and Needham 2007). In another study, based on reflection patterns of polarized light that were observed within retinas from the pumpkinseed sunfish (*Lepomis gibbosus*), green sunfish (*Lepomis cyanellus*), and rainbow trout (*Oncorhynchus mykiss*), it was hypothesized that double cones arranged in alternating directions, as is seen in a square mosaic, would provide a means for vertebrate cones to detect different polarization states of light (Flamarique, Hawryshyn et al. 1998). UV light vision has already been shown to be part of a discrete messaging system for some swordtails, allowing males to be arrayed in UV-coloration that is attractive to females but invisible to predators (Cummings, Rosenthal et al. 2003); it is an interesting possibility that the ability to detect changes in light polarization could be similarly used. As the lack of organized photoreceptor mosaics in fish has been correlated with lack of polarization sensitivity (Novales Flamarique and Hawryshyn 1998), if swordtails were shown to be sensitive to

polarization changes, and if any swordtails were found with a disorganized mosaic, it would be important to test for changes in their polarization vision in addition to other changes.

I did find a small difference between the mosaic angle of males and females in the parental species. It is possible that there is a functional significance for the different types of mosaics. However, the lack of difference in photoreceptor density does not suggest a difference in resolution. It is also possible that the pattern is correlated with another trait that varies between the males and females, but that the pattern itself is not functionally significant.

Decreased retinal function sometimes corresponds with changes in photoreceptor density and in the photoreceptor mosaic, and I find no evidence for these types of retinal degeneration within the parental species *X. birchmanni* and *X. malinche*. How species are maintained is an important question in evolutionary biology, in part because it contributes to our understanding of what must be overcome for the hybridization of similar species to contribute to the evolution of those species. One mechanism for maintaining independent lines is hybrid breakdown, where the hybrid between two species has a lower fitness due to incompatibility between the two lines. One hypothetical mechanism for hybrid breakdown is sensory dysfunction, where one of the senses, for example vision or olfaction, is impaired, resulting in decreased foraging, predator avoidance, mating, or other activities that are crucial for survival and reproduction. Although I did not find evidence of sensory dysfunction in the photoreceptor mosaics of *X. malinche* and *X. birchmanni* hybrids, other changes to these

photoreceptors, such as regulation of opsin expression as described above, could lead to sensory dysfunction. It is also possible that hybrids have no sensory dysfunction but could still have hybrid breakdown, for example, in the form of disrupted downstream neural processes.

It will be interesting to see if other *Xiphophorus* species and other hybrids exhibit evidence of changes in their photoreceptor mosaics, or if the photoreceptor mosaic observed is something most *Xiphophorus* species have in common. Furthermore, the highly organized swordtail mosaic offers promise for future studies, as any future individuals with changes in visual behavior could be screened for changes in the photoreceptor mosaic.

CHAPTER V

CONCLUSIONS

The possibility that the PCP pathway is involved in organizing vertebrate photoreceptors invites more direct studies of this phenomenon. One technique is to observe zebrafish with mutations in the PCP pathway to determine if the planar positioning of photoreceptor basal bodies is disrupted in them. One such characterized mutant exists: PCP signaling is disrupted in the zebrafish *trilobite* line, which is mutated in *vangl2* (Borovina, Superina et al. 2010). Unfortunately, because patterning is established later in development, as in the inner ear (Jones, Chen et al. 2008), direct observation cannot be done; the PCP pathway is crucial throughout the body in development, and these mutants do not survive past early larval stages. To get around this, a cross between the mutant line and the *Tg(TαCP:eGFP)* line, which expresses GFP in cones (Kennedy, Alvarez et al. 2007), will allow mutant cones to be GFP-tagged. Blastula transplants of these mutant cells into wild type embryos will allow smaller subsets of mutant cells to develop into retinal tissue, and the mutant clones of photoreceptors can then be analyzed for PCP defects. New zebrafish knockout mutants are also available via the Zebrafish Mutation Project (Kettleborough, Busch-Nentwich et al. 2013). Knockout mutants of the following PCP pathway genes are currently available: prickle1a, prickle2, vangl1, vangl2, dvl1b, dvl3, fzd7a, fzd7b, fat1, fat2, and dchs1. In 2014, the following will also be available: dvl1a, dvl2, fzd3, fzd3l, fzd6, and

fat3. Alternatively, the Tol2Kit (Kwan, Fujimoto et al. 2007) and Gateway cloning can be used to create transgenic zebrafish lines that express a dominant negative PCP protein exclusively in the cones, using the same promoter used to express GFP in exclusively cones. For example, the dominant negative Dsh, Xdd1, was previously characterized in *Xenopus* (Sokol 1996) and has been successfully used to block PCP signaling in zebrafish (Gong, Mo et al. 2004). Another approach to more directly investigate if the PCP pathway is involved in the planar cell polarity observed in zebrafish photoreceptors is to complete immunohistochemical analysis of the localization of PCP proteins in the photoreceptors to look for planar positioning of these proteins in addition to the already established planar polarization of the basal bodies and the Crumbs complex.

Despite clues regarding the pathway(s) organizing basal bodies in zebrafish photoreceptors, many questions still remain. Why are the basal bodies of UV-sensitive cones, rods, and larval photoreceptors randomly localized, whereas the basal bodies of red-, green-, and blue-sensitive cones from dark reared zebrafish exhibit bimodality? Do retinomotor movements change cell-cell contacts in dark reared zebrafish in a way that disrupts only part of the pathway? Could two pathways be involved along the two axes, one that controls *not the sides* and one that designates *this end, not that end*, with only the latter being disrupted under dark conditions? There is evidence that PCP itself is controlled by two, not one, PCP pathways, sometimes called the Stan system (involving the core PCP proteins) and the Ds system (involving Ft/Ds) (for reviews, see Casal, Lawrence et al. 2006; Lawrence, Struhl et al. 2007). In *Drosophila*, if the Stan system is

disrupted, overexpression of the Ds system can sometimes compensate. Also, sometimes blocking either the Stan or Ds system leads to a slight weakening effect on polarization, but blocking both leads to a dramatic effect. In vertebrates, evidence of the Ds system has also been found. In the mouse inner ear, an important location for mouse PCP, fat-j, fat1, fat3, dchs1, and fjx1 are expressed (Rock, Schrauth et al. 2005). The *in situ* images published in the same study suggest fat-j, fat1, and dchs1 are also strongly expressed in the eye. Also, *Fat4* mouse mutants exhibit PCP defects (Saburi, Hester et al. 2008). In the *Drosophila* eye, like in the mouse inner ear, there a symmetry so that dorsal ommatidia orient dorsally while ventral ommatidia orient ventrally (for review, see Fanto and McNeill 2004). Interestingly, the loss of Ft and Ds leads to random dorsal-ventral polarity. One possibility to explore is that disruption of the Ds system in dark-reared zebrafish could be a factor leading to the bimodality observed.

The characterization of the swordtail photoreceptor mosaic is an important step in understanding the physiological mechanisms behind visually-based variations in mate preferences and hybrid dysfunction in swordtails. The photoreceptor mosaics in swordtails exhibiting different visual behaviors can be compared by various criteria, including changes in the pattern or organization of the photoreceptor mosaic, changes in cone density, and changes in opsin expression.

An intriguing possible functional advantage of the square mosaic itself in swordtails is that it might allow sensitivity to changes in light polarization. The polarization of light, though not directly detectable by human eyes, is an additional attribute of light beyond its wavelength that some animals can detect and make use of

(for review, see Blaxter 1970; Cronin 2011; Roberts, Porter et al. 2011; Shashar, Johnsen et al. 2011). Polarized light is believed to play a role in insect navigation in relation to bodies of water and the sky. It may play a role in bird migration. Some animals, such as cephalopods, can see differences in polarized light similar to how I see differences in light wavelengths—that is, two objects that appear the same to us, because they reflect the same wavelength, can be discriminated between by a cephalopod, because they polarize light differently. Cephalopods can even change how light is polarized from their body, as a form of communication that many other animals cannot detect. For aquatic organisms, polarized light vision may help with navigation, contrast in vision, and communication. Several fish, including the damselfish and rainbow trout, have been shown to be able to discriminate between different polarization states. Though natural light sources do not produce polarized light, processes within nature can polarize light. For example, particles in the air or in water can partially polarize light by scattering it, and some surfaces such as vegetation or fish scales can polarize light by reflecting it. The mechanisms behind vertebrate polarized vision are currently not well known. In vertebrates, although opsins are intrinsically sensitive to specific polarizations, many of these molecules are arranged within a single photoreceptor. Therefore, in order for that photoreceptor to be sensitive to a specific polarity, all opsins within it must be oriented in the same way. Because the disks containing opsins in vertebrate photoreceptors are perpendicular to the plane of incoming light, vertebrate photoreceptors are rarely sensitive to polarization. In arthropod and cephalopod photoreceptors, on the other hand, opsins are arranged so that they align, meaning that these cells are frequently sensitive to

polarization. Some vertebrates are known to orient their outer segments sideways, which could be one mechanism to allow polarization sensitivity. Birefringent eyelids may also help fish orient using polarized light. There is some evidence that interactions between opsin molecules may lead to organized crystal-like planes of opsin, which is one proposed mechanism for vertebrate polarized light detection.

In goldfish, UV-, green-, and red-sensitive cones have been shown to be sensitive to polarized light, while blue-sensitive cones were not (Hawryshyn and McFarland 1987). In a similar goldfish study, the sensitivity to a polarized light wavelength specific to the green-sensitive cones and rods was constant for rods, but varied based on the polarization angle in green-sensitive cones (Roberts and Needham 2007). The authors of this study propose that the sensitivity of these cones to changes in polarization, combined with an organized photoreceptor mosaic, could allow polarization information to be used in downstream processing. Based on reflection patterns of polarized light that they observed within retinas from the pumpkinseed sunfish (*Lepomis gibbosus*), green sunfish (*Lepomis cyanellus*), and rainbow trout (*Oncorhynchus mykiss*), other authors proposed that double cones arranged in alternating directions, as is seen in a square mosaic, would provide a means for vertebrate cones to detect different polarization states of light (Flamarique, Hawryshyn et al. 1998). Furthermore, in cyprinids and salmonids, UV cones and square photoreceptor mosaics have together been suggested to be important contributors to polarization vision; in contrast, the white sucker (*Catostomus commersoni*), a closely related fish to cyprinids with UV sensitivity but a more disorganized mosaic, is not sensitive to light polarization (Novales Flamarique and

Hawryshyn 1998). Together, these data suggest that UV-cones, double cones, and a square mosaic are all important to polarization vision, supporting the possibility of swordtail polarized vision.

Results from a recent study in swordtails suggest that swordtails are sensitive to changes in polarization and that this sensitivity may play a role in mate choice (Calabrese, Brady et al. 2014). In this study, male and female *X. nigrensis* were dimorphic regarding the polarized light they reflected. Furthermore, males changed how their polarization appeared when courting, and mate choice behavior depended on polarization. Polarized light reflection also differs between sexes in other organisms, such as butterflies and shrimp (for review, see Marshall and Cronin 2011). These results support the possibility that the square swordtail photoreceptor mosaic functions in polarization vision and mate choice. It would be intriguing to determine if swordtail predators have polarization vision, and if there are mosaic differences in swordtails based on their predators. Like has been previously shown with UV sensitivity, polarization sensitivity may function as another cryptic form of communication among swordtails. Additionally, if swordtails do have polarization vision, the importance of the organized square mosaic on this vision might be directly investigated by determining if polarization vision ability decreases after inducing photoreceptor death and regeneration through light damage. In zebrafish, photoreceptor regeneration after light damage fails to include re-establishment of the organized photoreceptor mosaic and even leads to red- and green-sensitive cones sometimes failing to exist as double cones (Vihtelic and Hyde

2000). If this is also the case in swordtails, this could be an ideal system to test the importance of the square mosaic for polarization vision.

Summary

The discovery of planar cell polarity in the localization of basal bodies within zebrafish photoreceptors is the first characterization of this organization in vertebrate photoreceptors. This may enable new insights into the pathways involved in photoreceptor development and maintenance, leading to a better understanding of retinopathies. Also, as the first zebrafish model of a large field of cells with translationally polarized nonmotile cilia, this may lead to the establishment of a new model to study the PCP pathway. Therefore, future studies are needed to directly confirm that the PCP pathway is involved in photoreceptor basal body positioning.

The characterization of the swordtail photoreceptor mosaic enables future behavioral studies to better consider possible mechanisms behind preferences that are observed. Multivariate traits are important to consider when trying to understand mate choice. Cone mosaic organization, particularly in females, and physical appearance under polarized light, particularly in males, are attributes that may influence behavior that are worth considering in future studies.

REFERENCES

Adams, N. A., A. Awadein, et al. (2007). "The retinal ciliopathies." Ophthalmic. Genet. **28**(3): 113-125.

Ahnelt, P. K. and H. Kolb (2000). "The mammalian photoreceptor mosaic-adaptive design." Prog Retin Eye Res **19**(6): 711-777.

Allison, W. T., L. K. Barthel, et al. (2010). "Ontogeny of cone photoreceptor mosaics in zebrafish." J Comp Neurol **518**(20): 4182-4195.

Alvarez-Delfin, K., A. C. Morris, et al. (2009). "Tbx2b is required for ultraviolet photoreceptor cell specification during zebrafish retinal development." Proceedings of the National Academy of Sciences **106**(6): 2023-2028.

Antic, D., J. L. Stubbs, et al. (2010). "Planar cell polarity enables posterior localization of nodal cilia and left-right axis determination during mouse and Xenopus embryogenesis." PLoS One **5**(2): e8999.

Batschelet, E. (1981). Circular statistics in biology. London ; New York, Academic Press.

Beales, P. L., A. M. Warner, et al. (1997). "Bardet-Biedl syndrome: a molecular and phenotypic study of 18 families." Journal of Medical Genetics **34**(2): 92-98.

Bergmann, C. (2012). "Educational paper : ciliopathies." European Journal of Pediatrics **171**(9): 1285-1300.

Besharse, J. C., D. M. Forestner, et al. (1985). "Membrane assembly in retinal photoreceptors. III. Distinct membrane domains of the connecting cilium of developing rods." J. Neurosci. **5**(4): 1035-1048.

Besharse, J. C. and P. Witkovsky (1992). "Light-evoked contraction of red absorbing cones in the Xenopus retina is maximally sensitive to green light." Visual Neuroscience **8**(3): 243-249.

Blaxter, J. H. S. (1970). Light: fishes. Marine Ecology. O. Kinne. London, Wiley-lnterscience. **1.1:** 213- 320.

Boisvieux-Ulrich, E., M. C. Laine, et al. (1990). "Cytochalasin D inhibits basal body migration and ciliary elongation in quail oviduct epithelium." Cell Tissue Res. **259**(3): 443-454.

Borovina, A., S. Superina, et al. (2010). "Vangl2 directs the posterior tilting and asymmetric localization of motile primary cilia." Nat Cell Biol **12**(4): 407-412.

Branchek, T. (1984). "The development of photoreceptors in the zebrafish, Brachydanio rerio. II. Function." J Comp Neurol **224**: 116 - 122.

Branchek, T. and R. Bremiller (1984). "The development of photoreceptors in the zebrafish, Brachydanio rerio. I. Structure." J Comp Neurol **224**(1): 107-115.

Brockerhoff, S. E., J. B. Hurley, et al. (1995). "A behavioral screen for isolating zebrafish mutants with visual system defects." Proc. Natl. Acad. Sci. U. S. A. **92**(23): 10545-10549.

Brody, S. L., X. H. Yan, et al. (2000). "Ciliogenesis and left-right axis defects in forkhead factor HFH-4-null mice." Am. J. Respir. Cell Mol. Biol. **23**(1): 45-51.

Brown, D. D. (1997). "The role of thyroid hormone in zebrafish and axolotl development." Proc. Natl. Acad. Sci. U. S. A. **94**(24): 13011-13016.

Burnside, B. and B. Nagle (1983). "Chapter 3. Retinomotor movements of photoreceptors and retinal pigment epithelium: mechanisms and regulation." Progress in Retinal Research **2**(0): 67-109.

Burnside, B., E. Wang, et al. (1993). "Retinomotor movements in isolated teleost retinal cone inner-outer segment preparations (CIS-COS): effects of light, dark and dopamine." Experimental Eye Research **57**(6): 709-722.

Burton, R. S. and F. S. Barreto (2012). "A disproportionate role for mtDNA in Dobzhansky-Muller incompatibilities?" Molecular Ecology **21**(20): 4942-4957.

Calabrese, G. M., P. Brady, et al. (2014). Dynamic Polarization Signaling in Swordtails Alters Female Mate Preference (Presentation Abstract). Society for Integrative and Comparative Biology Annual Meeting, Austin, Texas.

Cameron, D. A. (2002). "Mapping absorbance spectra, cone fractions, and neuronal mechanisms to photopic spectral sensitivity in the zebrafish." Visual Neuroscience **19**(3): 365-372.

Casal, J., P. A. Lawrence, et al. (2006). "Two separate molecular systems, Dachsous/Fat and Starry night/Frizzled, act independently to confer planar cell polarity." Development **133**(22): 4561-4572.

Case, C. P. and C. J. Plummer (1993). "Changing the light intensity of the visual environment results in large differences in numbers of synapses and in photoreceptor size in the retina of the young adult rat." Neuroscience **55**(3): 653-666.

Chen, W. S., D. Antic, et al. (2008). "Asymmetric homotypic interactions of the atypical cadherin flamingo mediate intercellular polarity signaling." Cell **133**(6): 1093-1105.

Chinen, A., T. Hamaoka, et al. (2003). "Gene duplication and spectral diversification of cone visual pigments of zebrafish." Genetics **163**(2): 663-675.

Choi, S. S., N. Doble, et al. (2006). "In vivo imaging of the photoreceptor mosaic in retinal dystrophies and correlations with visual function." Investigative Ophthalmology & Visual Science **47**(5): 2080-2092.

Coleman, S. W. (2011). Sensory ecology. Ecology and Evolution of Poeciliid Fishes. J. P. A. P. I. S. Evans. Chicago, The University of Chicago Press.

Coleman, S. W. and G. G. Rosenthal (2006). "Swordtail fry attend to chemical and visual cues in detecting predators and conspecifics." PLoS One **1**: e118.

Cronin, T. W. (2011). Polarized-light vision in land and aquatic animals. The Retina and Its Disorders. J. C. B. D. Besharse. San Diego, CA, Academic Press.

Culumber, Z. W., H. S. Fisher, et al. (2011). "Replicated hybrid zones of Xiphophorus swordtails along an elevational gradient." Molecular Ecology **20**(2): 342-356.

Culumber, Z. W., D. B. Shepard, et al. (2012). "Physiological adaptation along environmental gradients and replicated hybrid zone structure in swordtails (Teleostei: Xiphophorus)." Journal of Evolutionary Biology **25**(9): 1800-1814.

Cummings, M. E., G. G. Rosenthal, et al. (2003). "A private ultraviolet channel in visual communication." Proceedings. Biological Sciences / The Royal Society **270**(1518): 897-904.

Cunningham, L. L. and F. Gonzalez–Fernandez (2000). "Coordination between production and turnover of interphotoreceptor retinoid-binding protein in zebrafish." Investigative Ophthalmology & Visual Science **41**(11): 3590-3599.

Dawe, H. R., H. Farr, et al. (2007). "Centriole/basal body morphogenesis and migration during ciliogenesis in animal cells." J. Cell Sci. **120**(Pt 1): 7-15.

De Robertis, E. (1956). "Morphogenesis of the retinal rods." J. Biophysic. and Biochem. Cytol. **2**(4, Suppl.): 209-218.

De Robertis, E. (1960). "Some observations on the ultrastructure and morphogenesis of photoreceptors." J. Gen. Physiol. **43**(6, Suppl): 1-13.

Dixon, L. J., A. L. McDowell, et al. (2004). "Effects of restricted spectral rearing on the development of zebrafish retinal physiology." Documenta Ophthalmologica. Advances in Ophthalmology **109**(1): 17-33.

Dobzhansky, T. (1936). "Studies on hybrid sterility. II. Localization of sterility factors in *Drosophila pseudoobscura* hybrids." Genetics **21**(2): 113-135.

Dudinsky, L. and B. D. Perkins (2011). [Interaction between Vangl2 and Arl13b]. College Station, Texas A&M University**:** Unpublished data.

Easter, S. S., Jr. and A. Macy (1978). "Local control of retinomotor activity in the fish retina." Vision Research **18**(8): 937-942.

Eberhard, W. G. (2009). "Postcopulatory sexual selection: Darwin's omission and its consequences." Proceedings of the National Academy of Sciences **106**(Supplement 1): 10025-10032.

Engström, K. (1960). "Cone types and cone arrangements in retina of some cyprinids." Acta Zool (Stockholm) **41**: 277 - 295.

Engström, K. (1963). "Cone types and cone arrangements in teleost retinae." Acta Zoologica **44**: 179-243.

Engström, K. and E. Rosstorp (1963). "Photomechanical responses in different cone types of Leucisus rutilus." Acta Zoologica **44**(1-2): 145-160.

Fadool, J. M. (2003). "Development of a rod photoreceptor mosaic revealed in transgenic zebrafish." Dev. Biol. **258**(2): 277-290.

Fadool, J. M., D. A. Fadool, et al. (1999). "Characterization of monoclonal antibodies against zebrafish retina." Invest. Opth. Vis. Sci. Suppl. **40**: 1251.

Fanto, M. and H. McNeill (2004). "Planar polarity from flies to vertebrates." Journal of Cell Science **117**(Pt 4): 527-533.

Fisher, H. S., S. J. Mascuch, et al. (2009). "Multivariate male traits misalign with multivariate female preferences in the swordtail fish, Xiphophorus birchmanni." Animal Behaviour **78**(2): 265-269.

Fisher, H. S., B. B. Wong, et al. (2006). "Alteration of the chemical environment disrupts communication in a freshwater fish." Proceedings. Biological Sciences / The Royal Society **273**(1591): 1187-1193.

Fisher, N. I. (1993). Statistical analysis of circular data. Cambridge [England] ; New York, NY, USA, Cambridge University Press.

Flamarique, I. N., C. W. Hawryshyn, et al. (1998). "Double-cone internal reflection as a basis for polarization detection in fish." Journal of the Optical Society of America A **15**(2): 349-358.

Gomperts, B. N., X. Gong-Cooper, et al. (2004). "Foxj1 regulates basal body anchoring to the cytoskeleton of ciliated pulmonary epithelial cells." J. Cell Sci. **117**(Pt 8): 1329-1337.

Gong, Y., C. Mo, et al. (2004). "Planar cell polarity signalling controls cell division orientation during zebrafish gastrulation." Nature **430**(7000): 689-693.

Goodrich, L. V. and D. Strutt (2011). "Principles of planar polarity in animal development." Development **138**(10): 1877-1892.

Gray, R. S., P. B. Abitua, et al. (2009). "The planar cell polarity effector Fuz is essential for targeted membrane trafficking, ciliogenesis and mouse embryonic development." Nat. Cell Biol. **11**(10): 1225-1232.

Gray, R. S., I. Roszko, et al. (2011). "Planar cell polarity: coordinating morphogenetic cell behaviors with embryonic polarity." Developmental Cell **21**(1): 120-133.

Hashimoto, M., K. Shinohara, et al. (2010). "Planar polarization of node cells determines the rotational axis of node cilia." Nature Cell Biology **12**(2): 170-176.

Hawryshyn, C. and W. McFarland (1987). "Cone photoreceptor mechanisms and the detection of polarized light in fish." Journal of Comparative Physiology A **160**(4): 459-465.

Heisenberg, C. P., M. Tada, et al. (2000). "Silberblick/Wnt11 mediates convergent extension movements during zebrafish gastrulation." Nature **405**(6782): 76-81.

Hodel, C., S. C. Neuhauss, et al. (2006). "Time course and development of light adaptation processes in the outer zebrafish retina." The Anatomical Record. Part A, Discoveries in Molecular, Cellular, and Evolutionary Biology **288**(6): 653-662.

Ile, K. E., S. Kassen, et al. (2010). "Zebrafish class 1 phosphatidylinositol transfer proteins: PITPbeta and double cone cell outer segment integrity in retina." Traffic **11**(9): 1151-1167.

Jagger, D., G. Collin, et al. (2011). "Alstrom Syndrome protein ALMS1 localizes to basal bodies of cochlear hair cells and regulates cilium-dependent planar cell polarity." Human Molecular Genetics **20**(3): 466-481.

Jenny, A. (2010). Chapter seven - planar cell polarity signaling in the Drosophila eye. Current Topics in Developmental Biology. L. C. Ross and A. R. Thomas, Academic Press. **Volume 93:** 189-227.

Jessen, J. R., J. Topczewski, et al. (2002). "Zebrafish trilobite identifies new roles for Strabismus in gastrulation and neuronal movements." Nat Cell Biol **4**(8): 610-615.

Jiao, Y., Z. Sun, et al. (1999). "A simple and sensitive antigen retrieval method for free-floating and slide-mounted tissue sections." J. Neurosci. Methods **93**(2): 149-162.

Jones, A. G. and N. L. Ratterman (2009). "Mate choice and sexual selection: what have we learned since Darwin?" Proceedings of the National Academy of Sciences **106**(Supplement 1): 10001-10008.

Jones, C., P. Chen, et al. (2008). Primary cilia in planar cell polarity regulation of the inner ear. Current Topics in Developmental Biology, Academic Press. **85:** 197-224.

Jones, C., V. C. Roper, et al. (2008). "Ciliary proteins link basal body polarization to planar cell polarity regulation." Nature Genetics **40**(1): 69-77.

Kawamura, G., M. Miyagi, et al. (1997). "Retinomotor movement of all spectral cone types of red sea bream Pagrus major in response to monochromatic stimuli and UV sensitivity." Fisheries Science **63**(2): 233-235.

Kennedy, B. N., Y. Alvarez, et al. (2007). "Identification of a zebrafish cone photoreceptor-specific promoter and genetic rescue of achromatopsia in the nof mutant." Invest Ophthalmol Vis Sci **48**(2): 522-529.

Kettleborough, R. N., E. M. Busch-Nentwich, et al. (2013). "A systematic genome-wide analysis of zebrafish protein-coding gene function." Nature **496**(7446): 494-497.

Kingston, J. J., G. G. Rosenthal, et al. (2003). "The role of sexual selection in maintaining a colour polymorphism in the pygmy swordtail, Xiphophorus pygmaeus." Animal Behaviour **65**(4): 735-743.

Kirsch, M., H. J. Wagner, et al. (1989). "Rods trigger light adaptive retinomotor movements in all spectral cone types of a teleost fish." Vision Research **29**(4): 389-396.

Kitambi, S. S. and J. J. Malicki (2008). "Spatiotemporal features of neurogenesis in the retina of medaka, Oryzias latipes." Developmental Dynamics **237**(12): 3870-3881.

Knabe, W. and H. Kuhn (1998). "Disk formation in retinal cones of Tupaia belangeri (Scandentia)." Cell Tissue Res **292**(1): 67-76.

Knabe, W. and H. J. Kuhn (1997). "Ciliogenesis in photoreceptor cells of the tree shrew retina." Anat. Embryol. (Berl) **196**(2): 123-131.

Krauss, A. and C. Neumeyer (2003). "Wavelength dependence of the optomotor response in zebrafish (Danio rerio)." Vision Res **43**: 1273 - 1282.

Kroes, H. Y., P. H. van Zon, et al. (2008). "DNA analysis of AHI1, NPHP1 and CYCLIN D1 in Joubert syndrome patients from the Netherlands." European Journal of Medical Genetics **51**(1): 24-34.

Kwan, K. M., E. Fujimoto, et al. (2007). "The Tol2kit: a multisite gateway-based construction kit for Tol2 transposon transgenesis constructs." Developmental dynamics : An Official Publication of the American Association of Anatomists **236**(11): 3088-3099.

Larison, K. D. and R. Bremiller (1990). "Early onset of phenotype and cell patterning in the embryonic zebrafish retina." Development **109**(3): 567-576.

Lawrence, P. A., G. Struhl, et al. (2007). "Planar cell polarity: one or two pathways?" Nature Reviews. Genetics **8**(7): 555-563.

Levinson, G. and B. Burnside (1981). "Circadian rhythms in teleost retinomotor movement. A comparison of the effects of circadian rhythm and light condition on cone length." Investigative Ophthalmology & Visual Science **20**(3): 294-303.

Li, S., S. Q. Zhang, et al. (2008). "Assessment criteria for rotated stereociliary bundles in the guinea pig cochlea." Otology & Neurotology : Official Publication of the American Otological Society, American Neurotology Society [and] European Academy of Otology and Neurotology **29**(1): 86-92.

Lyall, A. (1957). "Cone arrangements in teleost retinae." Q J Mic Sci **98**: 189 - 201.

Makiyama, Y., S. Ooto, et al. (2013). "Cone abnormalities in fundus albipunctatus associated with RDH5 mutations assessed using adaptive optics scanning laser ophthalmoscopy." American Journal of Ophthalmology.

Makiyama, Y., S. Ooto, et al. (2013). "Macular cone abnormalities in retinitis pigmentosa with preserved central vision using adaptive optics scanning laser ophthalmoscopy." PLoS One **8**(11): e79447.

Marshall, J. and T. W. Cronin (2011). "Polarisation vision." Current Biology : CB **21**(3): R101-105.

Matsumoto, Y., S. Fukamachi, et al. (2006). "Functional characterization of visual opsin repertoire in medaka (Oryzias latipes)." Gene **371**(2): 268-278.

Mirzadeh, Z., Y. G. Han, et al. (2010). "Cilia organize ependymal planar polarity." J Neurosci **30**(7): 2600-2610.

Mitchell, B., J. L. Stubbs, et al. (2009). "The PCP pathway instructs the planar orientation of ciliated cells in the Xenopus larval skin." Curr. Biol. **19**(11): 924-929.

Moens, C. B. and A. Fritz (1999). "Techniques in neural development." Methods Cell Biol **59**: 253-272.

Monson, C. A. and K. C. Sadler (2010). "Inbreeding depression and outbreeding depression are evident in wild-type zebrafish lines." Zebrafish **7**(2): 189-197.

Montcouquiol, M., R. A. Rachel, et al. (2003). "Identification of Vangl2 and Scrb1 as planar polarity genes in mammals." Nature **423**(6936): 173-177.

Morris, A. C., E. H. Schroeter, et al. (2005). "Cone survival despite rod degeneration in XOPS-mCFP transgenic zebrafish." Invest. Ophthalmol. Vis. Sci. **46**(12): 4762-4771.

Morris, M. R. and K. Casey (1998). "Female swordtail fish prefer symmetrical sexual signal." Animal Behaviour **55**(1): 33-39.

Mrejen, S., T. Sato, et al. (2013). "Assessing the cone photoreceptor mosaic in eyes with pseudodrusen and soft drusen in vivo using adaptive optics imaging." Ophthalmology.

Nava, S. S., S. An, et al. (2011). "Visual detection of UV cues by adult zebrafish (Danio rerio)." Journal of Vision **11**(6): 2.

Newton, I. (1676). Adapted from "Newton to Hooke." The correspondence of Isaac Newton. H. W. Turnbull, J.F. Scott, A.R. Hall. (1959). Cambridge, Cambridge University Press. **I:** 416.

Nishiwaki, Y., T. Oishi, et al. (1997). "Three-dimensional reconstitution of cone arrangement on the spherical surface of the retina in the medaka eyes." Zoological Science **14**(5): 795-801.

Novales Flamarique, I. and C. W. Hawryshyn (1998). "The common white sucker (Catostomus commersoni): a fish with ultraviolet sensitivity that lacks polarization sensitivity." Journal of Comparative Physiology A **182**(3): 331-341.

O'Toole, J. F., E. A. Otto, et al. (2006). "Retinitis pigmentosa and renal failure in a patient with mutations in INVS." Nephrology, Dialysis, Transplantation : Official Publication of the European Dialysis and Transplant Association - European Renal Association **21**(7): 1989-1991.

Ohki, H. and K. Aoki (1985). "Development of visual-acuity in the larval medaka, oryzias-latipes." Zoological Science **2**(1): 123-126.

Otto, E. A., B. Schermer, et al. (2003). "Mutations in INVS encoding inversin cause nephronophthisis type 2, linking renal cystic disease to the function of primary cilia and left-right axis determination." Nature Genetics **34**(4): 413-420.

Pan, J., Y. You, et al. (2007). "RhoA-mediated apical actin enrichment is required for ciliogenesis and promoted by Foxj1." J. Cell Sci. **120**(Pt 11): 1868-1876.

Parichy, D. M., M. R. Elizondo, et al. (2009). "Normal table of postembryonic zebrafish development: staging by externally visible anatomy of the living fish." Dev. Dyn. **238**(12): 2975-3015.

Park, M. and R. T. Moon (2002). "The planar cell-polarity gene stbm regulates cell behaviour and cell fate in vertebrate embryos." Nat Cell Biol **4**(1): 20-25.

Park, T. J., R. S. Gray, et al. (2005). "Subcellular localization and signaling properties of dishevelled in developing vertebrate embryos." Current Biology : CB **15**(11): 1039-1044.

Park, T. J., S. L. Haigo, et al. (2006). "Ciliogenesis defects in embryos lacking inturned or fuzzy function are associated with failure of planar cell polarity and Hedgehog signaling." Nat. Genet. **38**(3): 303-311.

Park, T. J., B. J. Mitchell, et al. (2008). "Dishevelled controls apical docking and planar polarization of basal bodies in ciliated epithelial cells." Nat Genet **40**(7): 871-879.

Petit, C. and G. P. Richardson (2009). "Linking genes underlying deafness to hair-bundle development and function." Nature Neuroscience **12**(6): 703-710.

Rajchard, J., I. Hajek, et al. (2000). "Circadian biorhythm of melatonin level in swordtail (Xiphophorus helleri)." Czech Journal of Animal Science **45**(4): 153-160.

Ramamurthy, V. and M. Cayouette (2009). "Development and disease of the photoreceptor cilium." Clinical Genetics **76**(2): 137-145.

Ramsey, M. and B. D. Perkins (2013). "Basal bodies exhibit polarized positioning in zebrafish cone photoreceptors." The Journal of Comparative Neurology **521**(8): 1803-1816.

Randlett, O., L. Poggi, et al. (2011). "The oriented emergence of axons from retinal ganglion cells is directed by laminin contact in vivo." Neuron **70**(2): 266-280.

Raymond, P. A., L. K. Barthel, et al. (1993). "Expression of rod and cone visual pigments in goldfish and zebrafish: a rhodopsin-like gene is expressed in cones." Neuron **10**(6): 1161-1174.

Raymond, P. A., S. M. Colvin, et al. (2014). "Patterning the cone mosaic array in zebrafish retina requires specification of ultraviolet-sensitive cones." PLoS One **9**(1): e85325.

Reckel, F. and R. R. Melzer (2003). "Regional variations in the outer retina of atherinomorpha (Beloniformes, Atheriniformes, Cyprinodontiformes: Teleostei): photoreceptors, cone patterns, and cone densities." Journal of Morphology **257**(3): 270-288.

Rister, J. and C. Desplan (2011). "The retinal mosaics of opsin expression in invertebrates and vertebrates." Developmental Neurobiology **71**(12): 1212-1226.

Roberts, N. W. and M. G. Needham (2007). "A mechanism of polarized light sensitivity in cone photoreceptors of the goldfish Carassius auratus." Biophysical Journal **93**(9): 3241-3248.

Roberts, N. W., M. L. Porter, et al. (2011). "The molecular basis of mechanisms underlying polarization vision." Philosophical Transactions of the Royal Society of London. Series B, Biological Sciences **366**(1565): 627-637.

Robinson, J., E. A. Schmitt, et al. (1993). "Zebrafish ultraviolet visual pigment: absorption spectrum, sequence, and localization." Proceedings of the National Academy of Sciences **90**(13): 6009-6012.

Rock, R., S. Schrauth, et al. (2005). "Expression of mouse dchs1, fjx1, and fat-j suggests conservation of the planar cell polarity pathway identified in Drosophila." Developmental dynamics : An Official Publication of the American Association of Anatomists **234**(3): 747-755.

Rosenthal, G. G. (2007). "Spatiotemporal dimensions of visual signals in animal communication." Annual Review of Ecology, Evolution, and Systematics **38**(1): 155-178.

Rosenthal, G. G. (2013). "Individual mating decisions and hybridization." Journal of Evolutionary Biology **26**(2): 252-255.

Rosenthal, G. G., X. F. de la Rosa Reyna, et al. (2003). "Dissolution of sexual signal complexes in a hybrid zone between the swordtails Xiphophorus birchmanni and Xiphophorus malinche (Poeciliidae)." Copeia **2003**(2): 299-307.

Rosenthal, G. G. and C. S. Evans (1998). "Female preference for swords in Xiphophorus helleri reflects a bias for large apparent size." Proceedings of the National Academy of Sciences of the United States of America **95**(8): 4431-4436.

Rosenthal, G. G., T. Y. Flores Martinez, et al. (2001). "Shared preferences by predators and females for male ornaments in swordtails." The American Naturalist **158**(2): 146-154.

Rosenthal, G. G. and F. J. Garcia de Leon (2006). "Sexual behavior, genes, and evolution in Xiphophorus." Zebrafish **3**(1): 85-90.

Rosenthal, G. G., W. E. Wagner Jr, et al. (2002). "Secondary reduction of preference for the sword ornament in the pygmy swordtail Xiphophorus nigrensis (Pisces: Poeciliidae)." Animal Behaviour **63**(1): 37-45.

Ross, A. J., H. May-Simera, et al. (2005). "Disruption of Bardet-Biedl syndrome ciliary proteins perturbs planar cell polarity in vertebrates." Nature Genetics **37**(10): 1135-1140.

Rush, V. N. (1996). Visual pigment variation in the Poecilininae fishes its effect on behavior and evidience of variation at four levels: within-individuals, among

individuals, among populations and among species. Doctor of Philosophy, University of California Santa Barbara.

Ryan, M. J. and M. E. Cummings (2013). "Perceptual biases and mate choice." Annual Review of Ecology, Evolution, and Systematics **44**(1): 437-459.

Saburi, S., I. Hester, et al. (2008). "Loss of Fat4 disrupts PCP signaling and oriented cell division and leads to cystic kidney disease." Nat Genet **40**(8): 1010-1015.

Salbreux, G., L. K. Barthel, et al. (2012). "Coupling mechanical deformations and planar cell polarity to create regular patterns in the zebrafish retina." PLoS Computational Biology **8**(8): e1002618.

Sharma, N., N. F. Berbari, et al. (2008). "Ciliary dysfunction in developmental abnormalities and diseases." Current Topics in Developmental Biology **85**: 371-427.

Shashar, N., S. Johnsen, et al. (2011). "Underwater linear polarization: physical limitations to biological functions." Philosophical Transactions of the Royal Society of London. Series B, Biological Sciences **366**(1565): 649-654.

Simons, M., J. Gloy, et al. (2005). "Inversin, the gene product mutated in nephronophthisis type II, functions as a molecular switch between Wnt signaling pathways." Nature Genetics **37**(5): 537-543.

Simons, M. and M. Mlodzik (2008). "Planar cell polarity signaling: from fly development to human disease." Annu Rev Genet **42**: 517-540.

Singh, J. and M. Mlodzik (2012). "Planar cell polarity signaling: coordination of cellular orientation across tissues." Wiley Interdisciplinary Reviews. Developmental Biology **1**(4): 479-499.

Sokol, S. Y. (1996). "Analysis of Dishevelled signalling pathways during Xenopus development." Curr Biol **6**(11): 1456-1467.

Stearns, T., L. Evans, et al. (1991). "Gamma-tubulin is a highly conserved component of the centrosome." Cell **65**(5): 825-836.

Steinberg, R. H., S. K. Fisher, et al. (1980). "Disc morphogenesis in vertebrate photoreceptors." J. Comp. Neurol. **190**(3): 501-508.

Sugiyama, Y., R. J. Stump, et al. (2010). "Secreted frizzled-related protein disrupts PCP in eye lens fiber cells that have polarised primary cilia." Dev Biol **338**(2): 193-201.

Takechi, M. and S. Kawamura (2005). "Temporal and spatial changes in the expression pattern of multiple red and green subtype opsin genes during zebrafish development." The Journal of Experimental Biology **208**(7): 1337-1345.

Talcott, K. E., K. Ratnam, et al. (2011). "Longitudinal study of cone photoreceptors during retinal degeneration and in response to ciliary neurotrophic factor treatment." Investigative Ophthalmology & Visual Science **52**(5): 2219-2226.

Taylor, J., N. Abramova, et al. (1998). "Van Gogh: a new Drosophila tissue polarity gene." Genetics **150**(1): 199-210.

Tobler, M., S. W. Coleman, et al. (2010). "Reduced opsin gene expression in a cave-dwelling fish." Biol Lett **6**(1): 98-101.

Tohya, S., A. Mochizuki, et al. (2003). "Difference in the retinal cone mosaic pattern between zebrafish and medaka: cell-rearrangement model." Journal of Theoretical Biology **221**(2): 289-300.

Verzijden, M. N. and G. G. Rosenthal (2011). "Effects of sensory modality on learned mate preferences in female swordtails." Animal Behaviour **82**(3): 557-562.

Vihtelic, T. S., C. J. Doro, et al. (1999). "Cloning and characterization of six zebrafish photoreceptor opsin cDNAs and immunolocalization of their corresponding proteins." Vis. Neurosci. **16**(3): 571-585.

Vihtelic, T. S. and D. R. Hyde (2000). "Light-induced rod and cone cell death and regeneration in the adult albino zebrafish (Danio rerio) retina." Journal of Neurobiology **44**(3): 289-307.

Vinson, C. R. and P. N. Adler (1987). "Directional non-cell autonomy and the transmission of polarity information by the frizzled gene of Drosophila." Nature **329**(6139): 549-551.

Vladar, E. K., D. Antic, et al. (2009). "Planar cell polarity signaling: the developing cell's compass." Cold Spring Harb Perspect Biol **1**(3): a002964.

Wagner, H. J., D. Kath, et al. (1993). "Dark-adaptive cone elongation in the blue acara retina is triggered by green-sensitive cones." Visual Neuroscience **10**(3): 523-527.

Wallingford, J. B. (2010). "Planar cell polarity signaling, cilia and polarized ciliary beating." Current Opinion in Cell Biology **22**(5): 597-604.

Wallingford, J. B. and B. Mitchell (2011). "Strange as it may seem: the many links between Wnt signaling, planar cell polarity, and cilia." Genes Dev. **25**(3): 201-213.

Wallingford, J. B., B. A. Rowning, et al. (2000). "Dishevelled controls cell polarity during Xenopus gastrulation." Nature **405**(6782): 81-85.

Wan, J. and D. L. Stenkamp (2000). "Cone mosaic development in the goldfish retina is independent of rod neurogenesis and differentiation." The Journal of Comparative Neurology **423**(2): 227-242.

Wang, J., N. S. Hamblet, et al. (2006). "Dishevelled genes mediate a conserved mammalian PCP pathway to regulate convergent extension during neurulation." Development **133**(9): 1767-1778.

Watson, C. T., K. P. Lubieniecki, et al. (2010). "Genomic organization of duplicated short wave-sensitive and long wave-sensitive opsin genes in the green swordtail, Xiphophorus helleri." BMC Evolutionary Biology **10**: 87.

Wei, X., J. Zou, et al. (2006). "Nok plays an essential role in maintaining the integrity of the outer nuclear layer in the zebrafish retina." Experimental Eye Research **83**(1): 31-44.

Weidemann, H. L. (1966). "Der einfluss quantengleicher farblichter aut die retinomotorik dreier captentypen in der netchaut der guppy (Lebistes reticulatus Peters)." These Mathematisch - Naturwissenschattliche Facultat der George-August-Universitat Gottingen.

Westerfield, M. (1995). The zebrafish book : a guide for the laboratory use of zebrafish (Brachydanio rerio). Eugene, OR, M. Westerfield.

Willis, P. M., G. G. Rosenthal, et al. (2012). "An indirect cue of predation risk counteracts female preference for conspecifics in a naturally hybridizing fish Xiphophorus birchmanni." PLoS One **7**(4): e34802.

Wolfrum, U. (1995). "Centrin in the photoreceptor cells of mammalian retinae." Cell Motil Cytoskeleton **32**(1): 55-64.

Wong, B. B. and G. G. Rosenthal (2006). "Female disdain for swords in a swordtail fish." The American Naturalist **167**(1): 136-140.

Wong, B. B. M. (2004). "Superior fighters make mediocre fathers in the Pacific blue-eye fish." Animal Behaviour **67**(3): 583-590.

Wong, B. B. M., H. S. Fisher, et al. (2005). "Species recognition by male swordtails via chemical cues." Behavioral Ecology **16**(4): 818-822.

Wu, J. and M. Mlodzik (2008). "The Frizzled extracellular domain is a ligand for Van Gogh/Stbm during nonautonomous planar cell polarity signaling." Developmental Cell **15**(3): 462-469.

Yu, X., C. P. Ng, et al. (2008). "Foxj1 transcription factors are master regulators of the motile ciliogenic program." Nat. Genet. **40**(12): 1445-1453.

Zar, J. H. (1996). Biostatistical analysis. Upper Saddle River, N.J., Prentice-Hall.

Zaunreiter, M., H. Junger, et al. (1991). "Retinal morphology of cyprinid fishes: a quantitative histological study of ontogenetic changes and interspecific variation." Vision Research **31**(3): 383-394.

Zou, J., X. Wang, et al. (2012). "Crb apical polarity proteins maintain zebrafish retinal cone mosaics via intercellular binding of their extracellular domains." Developmental Cell **22**(6): 1261-1274.

Zou, J., X. Yang, et al. (2010). "Restricted localization of ponli, a novel zebrafish MAGUK-family protein, to the inner segment interface areas between green, red, and blue cones." Investigative Ophthalmology & Visual Science **51**(3): 1738-1746.

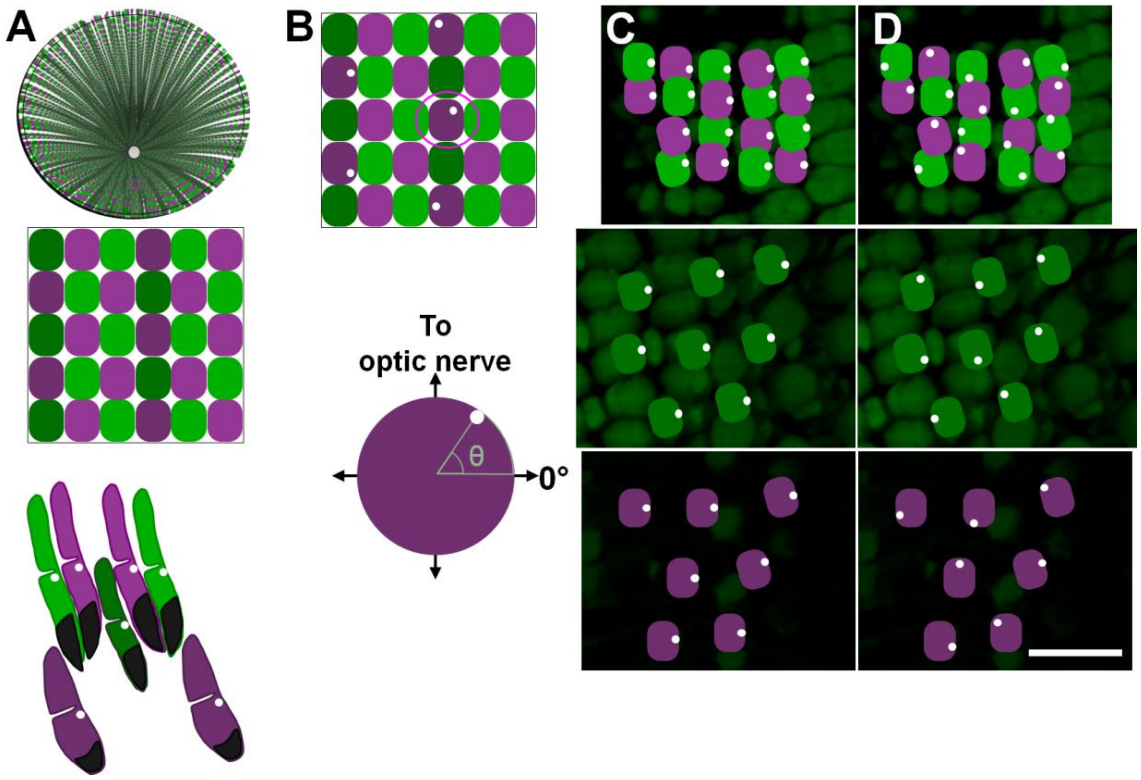

Magenta-green version of Figure 6. Basal body positioning within the zebrafish cone mosaic.

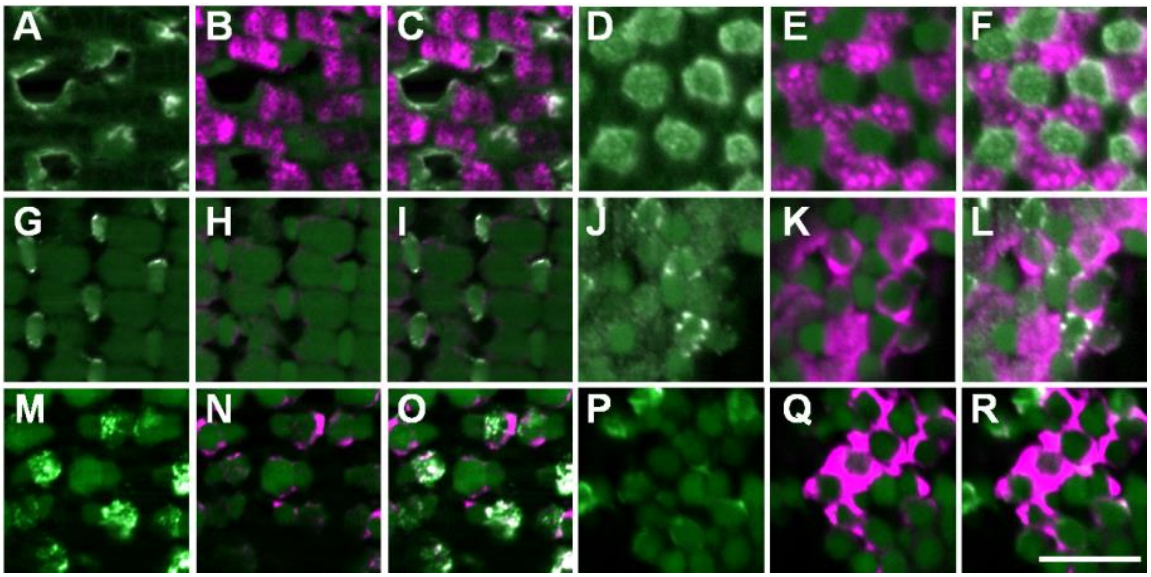

Magenta-green version of Figure 7. Cone subtypes can be identified by the vertical tiering distribution.

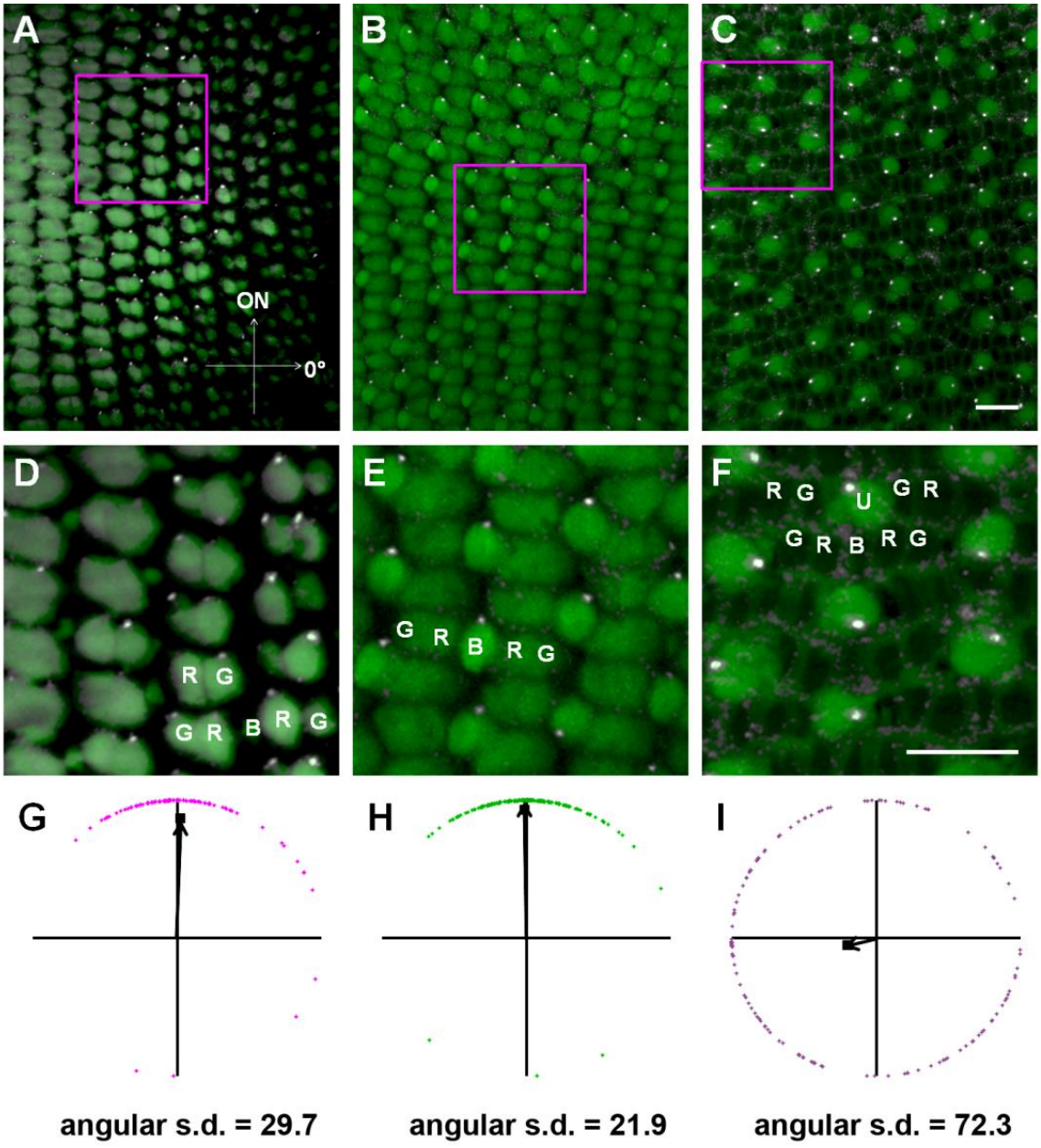

Magenta-green version of Figure 8. Basal body positioning is strongly patterned in individual fields of red-/green- and blue-sensitive cones.

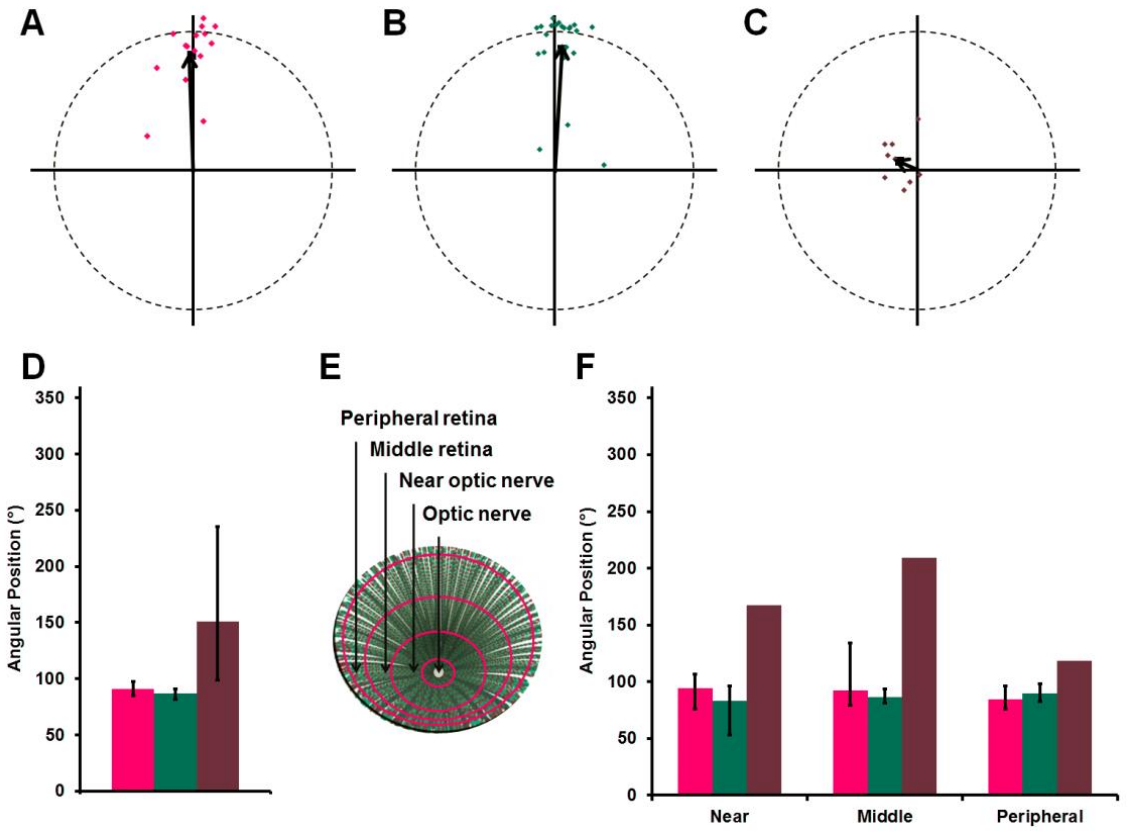

Magenta-green version of Figure 9. Basal body positioning is consistent throughout the adult retina.

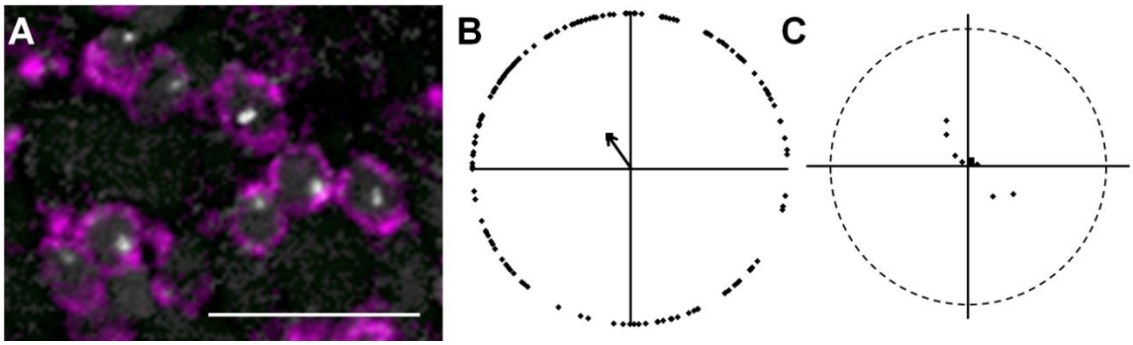

Magenta-green version of Figure 10. Rod basal bodies are randomly positioned.

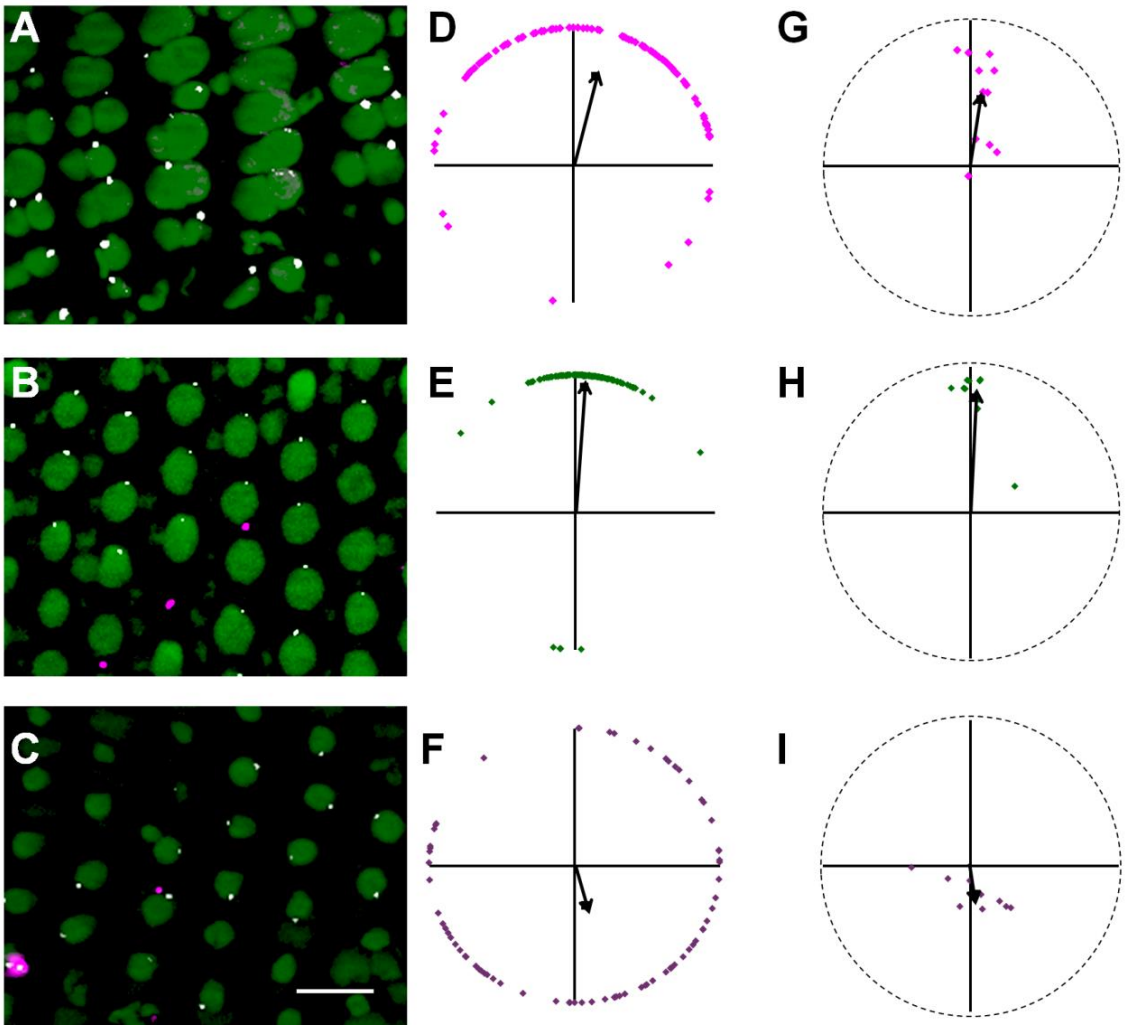

Magenta-green version of Figure 11. Loss of rods does not affect basal body positioning in cones.

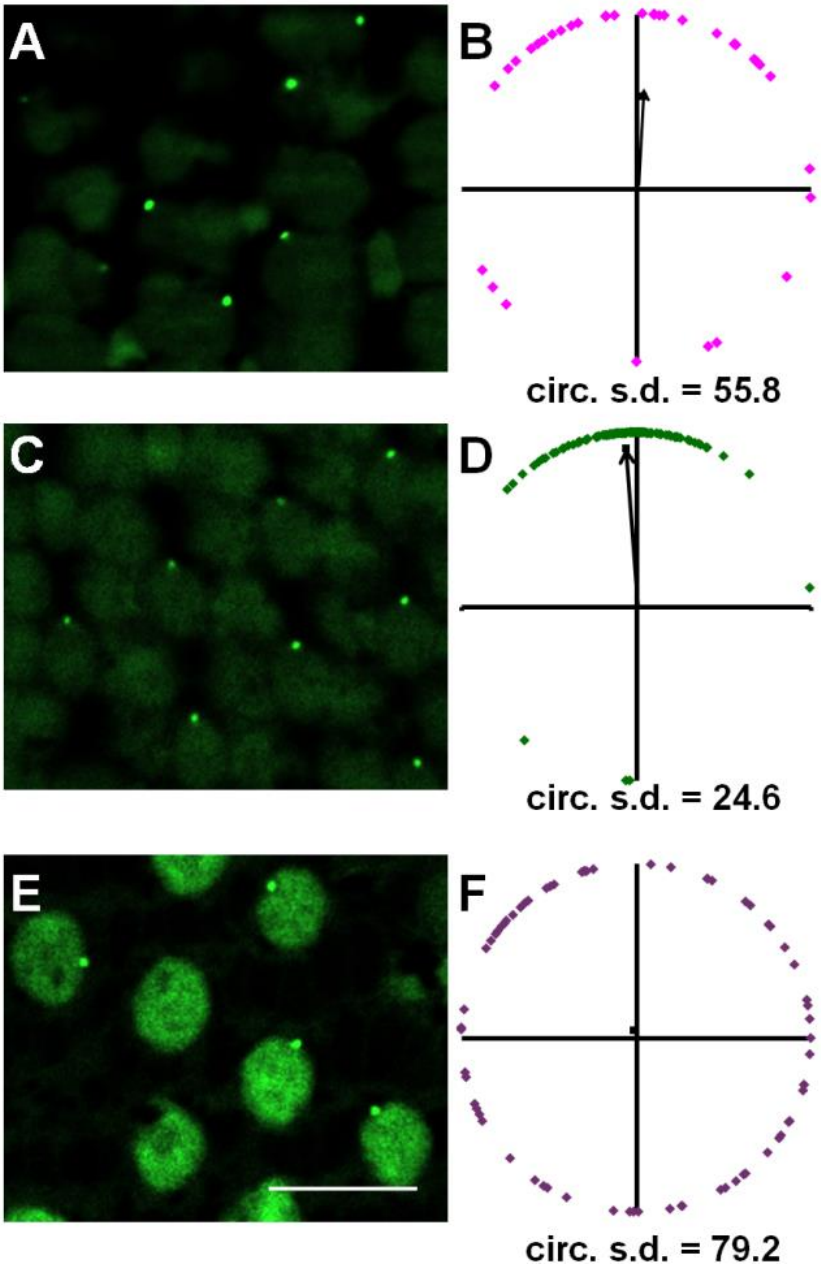

Magenta-green version of Figure 12. Centrin-GFP labels basal bodies in the retinas of adult *Tg(XlRho:gap43-CFP)*^{ucd1} transgenic zebrafish.

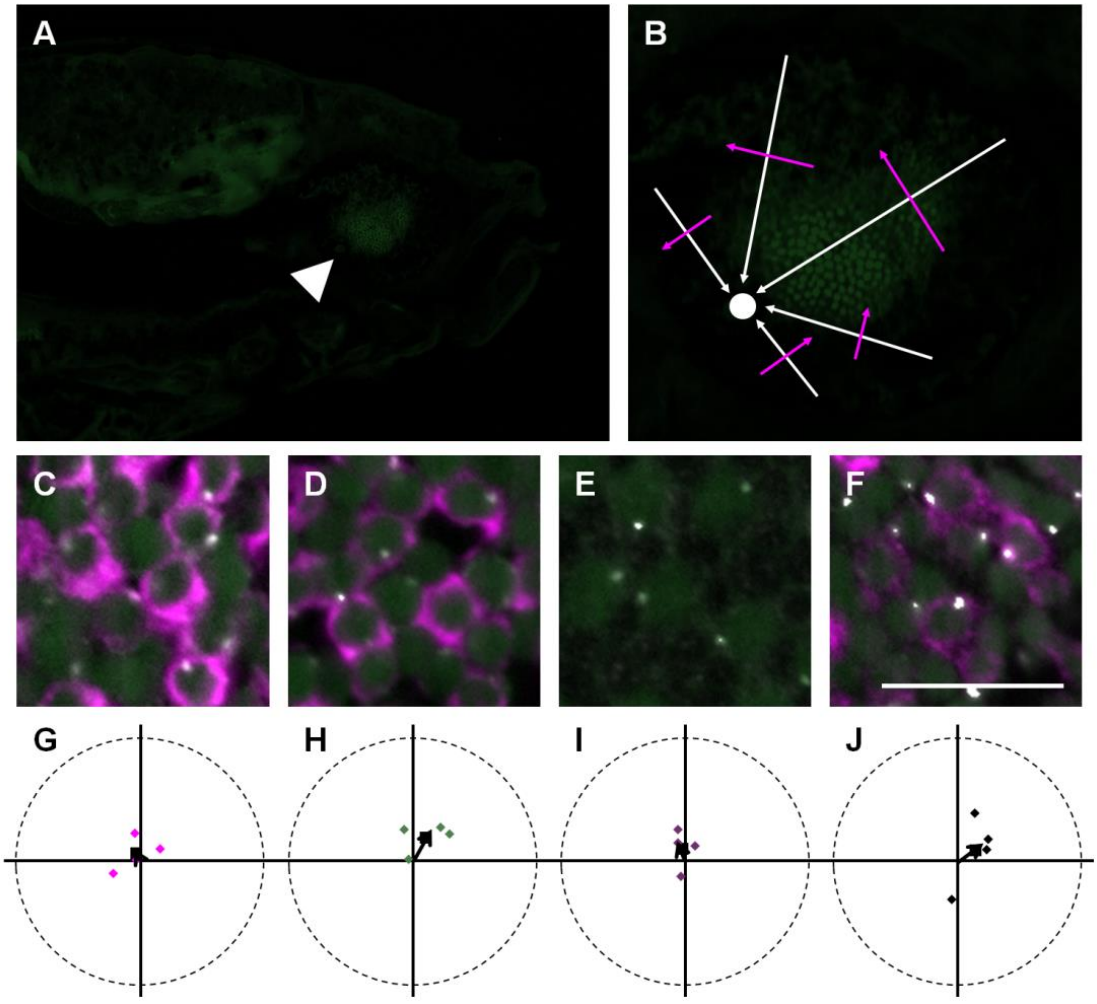

Magenta-green version of Figure 13. Larval photoreceptor basal bodies are randomly positioned.